Non-smooth Dynamical Systems and Applications

Mora, Karin

Award date:
2014

Awarding institution:
University of Bath

Non-smooth Dynamical Systems and Applications

submitted by

Karin Mora

for the degree of Doctor of Philosophy

of the

University of Bath

Department of Mathematical Sciences

October 2013

Summary

The purpose of this work is to illuminate some of the non-smooth phenomena found in piecewise-smooth continuous and discrete dynamical systems, which do not occur in smooth systems. We will explain how such non-smooth phenomena arise in applications which experience impact, such as impact oscillators, and a type of rotating machine, called magnetic bearing systems. The study of their dynamics and sensitivity to parameter variation gives not just insights into the critical motion found in these applications, but also into the complexity and beauty in their own right.

This work comprises two parts. The first part studies a general one-dimensional discontinuous power law map which can arise from impact oscillators with a repelling wall. Parameter variation and the influence of the exponent on the existence and stability of periodic orbits is presented.

In the second part we analyse two coupled oscillators that model rotating machines colliding with a circular boundary under friction. The study of the dynamics of rigid bodies impacting with and without friction is approached in two ways. On the one hand existence and stability conditions for non-impacting and impacting invariant sets are derived using local and global methods. On the other hand the analysis of parameter variation reveals new non-smooth bifurcations. Extensive numerical studies confirm these results and reveal further phenomena not attainable otherwise.

Work Done in Collaboration

Whilst substantially containing original work by myself, this Thesis also contains some work done in collaboration with Prof. Paul Glendinning (School of Mathematics, University of Manchester) and Prof. Patrick Keogh (Department of Mechanical Engineering, University of Bath).

Parts of Chapter 5 have been submitted for publication. Therefore, to maintain its form, Section 5.2 contains two paragraphs written by Prof. Keogh and these are clearly indicated using footnotes. They summarise engineering background knowledge on the applications of magnetic bearing systems that are being studied in Chapter 5. Part of the content of Section 5.6 has been produced in collaboration with Prof. Paul Glendinning but is entirely written by myself.

Acknowledgements

It begins to rain;
Two pigeons perch on a post,
Then leap into spring.

by Karin Mora and Christopher Mollison

Contents

List of Figures

CHAPTER 1

Introduction

1.1 Motivation

Some processes, behaviours or physical phenomena can be described in terms of systems that evolve in time and which experience fast changes. These changes occur so rapidly that one can assume they are instantaneous when setting up a mathematical model for them. Dynamical systems can model many of the applications that experience such a sudden change by describing the dynamics using non-smooth functions. Often these functions are smooth in general but have non-smooth transitions at certain points (they are piecewise-smooth). This type of dynamical system is then called a *piecewise-smooth dynamical system*. Piecewise smooth dynamical systems have now become an essential tool for understanding not only problems in engineering, as discussed in Section 1.2.1, but also a wide range of applications in other fields such as Biology and Ecology, which will be briefly discussed in Section 1.2.2. It is the rich and subtle dynamics of such piecewise-smooth systems, and the problems they model, which forms the basis of this Thesis.

As examples of such systems, a sudden change can occur when an object impacts another, when a switch is applied in an electric system, or when an object is sliding and experiencing friction. Such engineering applications have been and still are a driving force in developing the mathematical theory in the field of piecewise-smooth dynamical systems. One problem in mechanical engineering stands out: the problem of describing the dynamics of an object which, under external forcing, impacts an obstacle. This problem is referred to as the *single degree of freedom impact oscillator*, and has been discussed in the literature [3, 122, 97, 106, 113] at least since 1958, [3]. Often it is termed the *impact oscillator*, a name which we adopt throughout this Thesis. It has been modelled using piecewise-smooth dynamical systems which give rise to phenomena

that do not occur in smooth dynamical systems.

One such phenomenon manifests in the case of a trajectory that touches the obstacle in precisely one point tangentially with zero velocity. This phenomenon is called the *grazing event*. These phenomena are typical for piecewise-smooth dynamical systems and can also be found in more complex or higher dimensional problems. In this Thesis we will study an example of such a system arising in *magnetic bearing systems* [89, 41, 22]. A magnetic bearing system comprises a rotating beam (called the rotor), which levitates due to magnetic forces. During abnormal function it may collide with its housing (called the stator).

Applications such as these have many interesting properties and understanding how the dynamics of such systems changes under parameter variation is an essential tool for finding the overall behaviour of the system. Often the changes are smooth, but at certain parameter values, called *bifurcation points*, we see much more dramatic changes often associated with a change in stability. Bifurcation phenomena that occur in smooth systems have been well studied and documented in now-standard literature [65, 53, 55]. Similar phenomena also occur in piecewise-smooth systems. At present however, many types of bifurcations, called *discontinuity induced bifurcation (DIB)* [34], are unique to piecewise-smooth dynamical systems. There exists only a sparse literature on using piecewise-smooth dynamical systems to study magnetic bearing systems. The literature is even sparser when it comes to deriving analytical conditions to understand certain dynamics, such as periodic behaviour, or bifurcation, in such systems. These are all open questions that will be addressed in Chapters 5 and 6.

One method of studying systems with impacts is by constructing a suitable piecewise-smooth Poincaré map and then studying its dynamics. For the periodically forced impact oscillator, for example, such a map can be constructed by sampling the position and velocity at periods T of the forcing function. Then the Poincaré map, which is two-dimensional, maps position and velocity from time t_0 to time $t_0 + T$. If there are no impacts, then the map is linear. However, if an impact occurs then this has to be taken into account, and the map becomes nonlinear. In [90] Nordmark has developed a method called *discontinuity mapping*, which explicitly constructs the map and allows it to be analysed. The discontinuity mapping takes the non-impacting Poincaré map and adds a correction term, which takes into account that an impact has occurred. Such systems can exhibit many behaviours, including periodic and chaotic motions. Periodic motions (which are a cyclic and finite sequence of iterates of the map) can themselves be impacting or non-impacting and change as parameters vary. When a parameter is varied, a non-impacting limit cycle that has a grazing impact can become an impacting trajectory indicating a change in stability. This phenomenon is know as a grazing bifurcation and has been extensively studied in particular by Nordmark [90] and Whiston [123]. In [90] it is shown that near a grazing bifurcation the local Poincaré

map is the approximation of trajectories that miss the obstacle and trajectories that hit the obstacle with low impact velocity. As a direct consequence, the associated Poincaré map is continuous with a non-smooth first derivative which is approximated by a square-root term. These maps have fascinating dynamics.

Furthermore, the local two-dimensional Poincaré map can be approximated by a continuous one-dimensional piecewise-smooth map with a non-smooth point at which the first derivative is non-smooth [90, 91] (under certain assumptions described in Chapter 2). The form of this one-dimensional map is that on one side of the non-smooth point it is linear while on the other side it has the square-root term. This map is referred to as the continuous *square-root map* and has been studied in [34, 90, 91, 92, 8, 24, 17]. Other applications, for example DC-DC converters [36, 32, 126], give rise to similar piecewise-smooth one-dimensional maps where on both sides of the discontinuity the function is linear. This is referred to as the continuous *piecewise linear map* [43, 44, 95, 35]. Other piecewise-smooth maps include the discontinuous piecewise-linear map [59, 8, 9, 61, 7] and the discontinuous square-root map studied in [38, 102]. All these maps yield complex and intricate dynamics and bifurcations. In Chapter 3 we present a general one-dimensional map for which all of the above are special cases. The analysis of such a map has not been presented in the literature and it allows us both to unite the study of all the earlier problems and also to explain why certain bifurcations are observed in some maps but not in others.

In summary, the purpose of this Thesis is two-fold. Firstly we will study the dynamics and bifurcation phenomena of a one-dimensional piecewise-smooth map which can result from impact problems. Secondly we will apply this general analysis to the specific case of the magnetic bearing problem.

1.2 Applications in Engineering to Biology and Ecology

1.2.1 Applications in Engineering

In this section we motivate the Thesis by presenting other applications in engineering that have been modelled by piecewise-smooth systems. The theory of piecewise-smooth systems allows a systematic study of the dynamics of these problems.

As a first example, the rocking block model studied in [58] comprises a block on a harmonically back-and-forth tilting base. In such rocking we can see motion on one corner or the other or a combination of both. As such, in addition to the object impacting with its base inelastically, to describe the dynamics one has to monitor about which corner the block is rocking. The transient behaviour of the rocking block is rich and includes a multitude of periodic and aperiodic motions related to the non-smoothness of the system [119]. As an example, a large number of inelastic impacts can accumulate in a short period of time leading to the block coming to rest. This is

known as *chattering* and we will also observe it in the motion of the magnetic bearing problem. Depending on the harmonic forcing and the system parameters, the motion of the rocking block can be periodic or chaotic [119]. The rocking block problem has been used to model the effects of earthquakes on buildings or other slender objects, such as statues, as well as offshore problems such as shipping containers on a ship in high seas [120]. For these problems, understanding the transient behaviour of the rocking block and its potential for overturning [58] enables safety predictions to be made. Solving the shipping container problem is difficult and perhaps also unintuitive as it has been shown in [58] that blocks may not topple under high acceleration and may topple under low acceleration given the right initial conditions. The non-smoothness of the system characterises the boundary of the parameter regions that distinguish between overturning and not overturning blocks in that these boundaries appear fractal [119].

As a second example, the dynamics of gear rattle can be modelled by an impact oscillator with two impact surfaces. Basin of attraction computations showing the transition between periodic states [83] give insight into when the gears operate noisily. Furthermore Mason et al show that the global dynamics of such a system is affected by grazing bifurcations [82]. The intricate parameter dependence was revealed in [81] by studying co-dimension one, two and three bifurcations.

As a third example, the interaction of a bell and its clapper has been modelled by a double pendulum impacting a moving boundary [70]. As its phase space is four-dimensional, non-smooth quasi-periodic motion has been observed as well as typical non-smooth behaviour like chattering. In addition, synchronisation between bell and clapper plays an important roll in determining if the bell rings or not.

1.2.2 Applications in Biology and Ecology

More recently, applications of piecewise-smooth systems have been found in biological and ecological systems.

The human sleep-wake rhythm can be approximated by a slow-fast dynamical system with a switch [98]. Skeldon suggests [109] that in the sleep mode, the Phillips-Robinson model [98] resembles the impact oscillator near grazing and displays the same non-smooth dynamics such as grazing bifurcations and non-smooth bifurcation cascades.

Piecewise-linear ordinary differential equations have also been employed to study gene regulatory networks. The differential inclusion framework has been applied to show existence and stability of equilibria [19, 31] and limit cycles [42].

To model insect populations and achieve good agreement with experimental data, Varley, Gradwell and Hassel proposed a one-dimensional piecewise-smooth map [118, 57]. It has been suggested in [57] that the population growth switches its form between a constant function and a nonlinear function, depending on a population density threshold. The dynamics of this map, which is studied in [14, 15], gives rise to non-smooth bifurcation phenomena such as sudden transitions from stable periodic orbits to chaotic orbits as the bifurcation parameter is varied.

Competing algae populations have been modelled by a piecewise-smooth predator-prey model in [100]. In [100] it is assumed that the predators switch between different prey according to an optimal hunting and foraging theory giving rise to the lack of smoothness in the model.

There have also been applications of piecewise-smooth models in the study of certain heart arrhythmias [66] and of firing neurons [29, 27, 28]. The evolution of these systems is bound by thresholds which, when exceeded, leads to switching. This behaviour gives rise to the non-smoothness in the system.

1.3 Thesis Outline

This thesis comprises two main topics in piecewise-smooth dynamical systems: systems evolving in discrete time and systems evolving in continuous time. The first part, Chapters 3 and 4, is concerned with discrete time systems. In certain cases these have been shown to approximate continuous time systems, [34], but they give rise to interesting dynamics and bifurcations in their own right. The second part, Chapters 5 and 6, is concerned with the study of the impacting magnetic bearing problem and the remarkable dynamics found in such problems, deriving in part from a novel bifurcation.

Chapter 2: Piecewise-Smooth Dynamical Systems Theory

In this Chapter we introduce the basic concepts and terminology of smooth dynamical systems, which is kept brief, and also review some of the background theory of non-smooth dynamical systems. In particular, we describe the impact oscillator problem to give an introduction to impacting systems. We also show how it gives rise to one-dimensional maps which motivate Chapter 3. The numerical methods applied to the study of piecewise-smooth dynamical systems, which we will use in the later Chapters of this Thesis, are also presented. We finish with a brief introduction of magnetic bearing systems.

Chapter 3: The Piecewise Power Law Maps with Exponent $p \in [0, 1]$

In this Chapter we study the dynamics of piecewise-smooth systems described in terms of a one-dimensional map with one discontinuity. This map takes a linear form on one

side of the discontinuity and a power law form with exponent $p \in [0, 1]$ on the other side of the discontinuity. It is a general map in the sense that other well known and studied maps, such as the continuous and discontinuous linear or square-root map, represent special cases of our map. We show that both chaotic and stable periodic orbits exist depending on the bifurcation parameter. We study discontinuity induced bifurcations that give rise to a cascade of bifurcations under parameter variation. By analysing certain periodic orbits we learn about this bifurcation cascade, i.e. its structure and how it manifests. Furthermore, we identify the role of the exponent p and the discontinuity of the piecewise power law map in the bifurcation cascade as this has barely been addressed in the literature.

Chapter 4: The Piecewise Power Law Maps with Exponent $p > 1$

As in Chapter 3, we study the dynamics of piecewise-smooth systems described in terms of a one-dimensional map. We propose to study a map with one discontinuity of the same form as found in Chapter 3. The difference to the previous Chapter lies in the assumption that the exponent $p > 1$. Also in this Chapter we show that chaotic and stable periodic orbits exist. However, in the bifurcation cascades, arising from the discontinuity induced bifurcation, these periodic and chaotic orbits are organised in different structures compared to those in Chapter 3. More importantly, we identify and analyse a new route to chaos.

Chapter 5: Non-smooth Hopf Type Bifurcations in Rotating Machinery with Impact and Friction

In Chapters 5 and 6 we study an application of piecewise-smooth systems to a practical problem in engineering. We consider in particular the novel dynamics arising in the behaviour of a nonlinear rotor in a circular bearing where the rotor impacts with the wall of the bearing. This is done by investigating discontinuity induced bifurcations corresponding to collisions with the rotor housing (touchdown bearing surface interactions). The simplified Föppl/Jeffcott rotor with clearance and mass imbalance is modelled by a two degree of freedom impact-friction oscillator. Three types of motion have been observed in magnetic bearing systems: no contact, repeated instantaneous contact and continuous contact (rub). We study how these are affected by damping and stiffness present in the system using a combination of analytical and numerical methods developed for non-smooth dynamical systems. By studying the impact map, we show that all three types of motion arise at a novel non-smooth Hopf-type bifurcation from a discontinuity induced bifurcation point for certain parameter values. A local analysis of this bifurcation point allows a complete understanding of this behaviour in a general setting. The analysis identifies criteria for the existence of such smooth and non-smooth bifurcations, which is an essential step towards achieving reliable and ro-

bust controllers that can take compensating action to avoid impacts or at least reduce the effects of impacts.

(This Chapter has been submitted for publication.)

Chapter 6: Numerical Investigation of Magnetic Bearing Systems

In this Chapter we extend the local bifurcation analysis of Chapter 5 to give a more complete global understanding of the magnetic bearing system. To do this we identify and classify three types of motion: non-impacting orbits, orbits undergoing a chattering sequence and repeatedly impacting orbits which may be periodic or chaotic. We further identify new and interesting dynamics in the global analysis of such motions. Finally we compute the complex domains of attraction of each type of motion, allowing a general picture of the dynamics to be determined.

Chapter 7: Conclusions

In the final Chapter we summarise the Thesis and the main results. As the Thesis consists of two seemingly separate parts, we describe how they both fit together. Last but not least we discuss open problems and questions that still have to be addressed in future work.

New Work Contained in this Thesis

The one-dimensional piecewise-smooth maps that have been studied in the literature (continuous/discontinuous linear or square-root map) give some insight into the effects of the discontinuity and nonlinearity of the map on the map's dynamics, the discontinuity-induced bifurcations and hence the resulting bifurcation cascades. However, by studying the general maps proposed in Chapters 3 and 4 we systematically generalise present results in terms of the parameters of the map, in particular the nonlinear exponent p and the discontinuity. Analytically we prove in Chapter 3 why different dynamics, such as chaotic attractors and cascades of bifurcating periodic orbits (called *period-incrementing cascades*), are observed for certain parameter values. We show why the breakdown of the cascade occurs for the discontinuous nonlinear map but not for the continuous piecewise-smooth linear map. We explain why in certain piecewise-smooth linear maps chaotic attractors are observed while in others only coexisting stable periodic orbits make up the dynamical landscape.

In both Chapters 3 and 4 we show the existence of bifurcation cascades that have not been presented in literature. Although the mechanism of one of these cascades is well known, we show numerically that it consists of a different kind of periodic orbit than reported in literature. More importantly, we show the existence of a bifurcation

mechanism, unlike the well understood and widely published period-incrementing or period-adding cascades, first introduced in [51] for a map with nonlinear functions on both sides of the discontinuity. We show numerically that such a bifurcation cascade, called the anharmonic cascade, exists in the piecewise-power law map proposed in Chapter 4, which is nonlinear only on one side of the discontinuity.

In the study of magnetic bearing systems, piecewise-smooth dynamical systems theory has rarely been adopted to understand the system's dynamics. In fact, particular impact problems have often been considered without an analysis of possible bifurcations. This is the purpose of Chapters 5 and 6. Analytically and numerically we prove the existence and stability of impacting and non-impacting equilibria as well as limit cycles which have one impact with the boundary per period. We analytically derive the conditions of a new type of bifurcation we refer to as the non-smooth Hopf-type bifurcation, where two kinds of equilibria and two limit cycles bifurcate. Furthermore, we show numerically that typical non-smooth phenomena can be observed, such as the grazing impact and grazing bifurcation. We numerically identify the critical parameter values that can lead to repeated impact or continuous contact between the rotor and its boundary, the stator.

CHAPTER 2

Dynamical Systems Theory

A physical system is characterised by the set $X = \mathbb{R}^n$ of all its possible states, called **phase space**. The change of a state in time $t \in T$, where T is a number set, is called **evolution**. In this Thesis we will study the evolution of systems in discrete time, i.e. $T = \mathbb{Z}$, and in continuous time $T = \mathbb{R}$. The evolution of an initial state $x_0 \in X$ to a state $x_t \in X$, as time t moves on, can be described by an evolution operator ϕ parametrised by t, i.e. a family of maps given by

$$\phi^t : X \to X, \quad x_t = \phi^t(x_0).$$

2.1 Smooth Dynamical Systems

We now give the definition of a dynamical system.

Definition 2.1. *[34] A phase space X, time set T and the evolution operator ϕ^t are said to define a* ***dynamical system*** *$\{T, X, \phi^t\}$ if*

$$\phi^0(x) = x, \quad \textit{for all} \quad x \in X, \tag{2.1}$$

$$\phi^{t+s}(x) = \phi^s(\phi^t(x)) \quad \textit{for all} \quad x \in X, \quad t, s \in T. \tag{2.2}$$

Definition 2.2. *[71] An* ***orbit*** *or* ***trajectory*** *with initial condition x_0 is an ordered subset of the state space X and is the set*

$$\{x \in X : x = \phi^t(x_0), \textit{ for all } t \in T \textit{ such that } \phi^t(x_0) \textit{ is defined}\}. \tag{2.3}$$

Definition 2.3. *[71] The* ***phase portrait*** *of the dynamical system is the partitioning of the state space into orbits.*

Definition 2.4. *[34] A dynamical system $\{T, X, \phi^t\}$ is said to be **smooth of index r**, or C^r, if the first r derivatives of ϕ with respect to x exist and are continuous at every point $x \in X$.*

Definition 2.5. *[71] A subset $Y \subset X$, such that $x_0 \in Y$ implies $\phi^t(x_0) \in Y$ for all $t \in T$, is called an **invariant set** of a dynamical system $\{T, X, \phi^t\}$.*

We are interested in dynamical systems whose asymptotic state is stable, i.e. attracting. Let Y_0 be a closed (contains its own boundary) and bounded invariant set.

Definition 2.6. *[71] An invariant set Y_0 is called an **attractor** if*

1. *for any sufficiently small neighbourhood $U \supset Y_0$ there exists a neighbourhood $V \supset Y_0$ such that $\phi^t(x) \in U$ for all $x \in V$ and all $t > 0$ (Lyapunov stability); and*
2. *there exists a neighbourhood $U_0 \supset Y_0$ such that $\phi^t(x) \to Y_0$ for all $x \in U_0$, as $t \to \infty$ (asymptotic stability).*

Dynamical systems can have several attractors. The role of each attractor within the dynamics of the whole system can be understood by examining the sets on which the initial conditions of particular orbits accumulate. The attracting set of an orbit is called the basin of attraction.

Definition 2.7. *[34] The **domain of attraction** (**basin of attraction**) of an attractor Y_0 is the maximal set U^* for which $x \in U^*$ implies $\phi^t(x) \to Y_0$ as $t \to \infty$.*

We now define two types of invariant sets that describe the long-term asymptotics of a trajectory.

Definition 2.8. *[53] The ω-limit set of x, $\Lambda(x)$, and the α-limit set of x, $A(x)$, are the sets*

$$\Lambda(x) = \{y \in \mathbb{R}^n | \exists \text{ a sequence } \{t_n\} \text{ with } t_n \to \infty \text{ and } \phi^{t_n}(x) \to y \text{ as } n \to \infty\}$$

and

$$A(x) = \{y \in \mathbb{R}^n | \exists \text{ a sequence } \{s_n\} \text{ with } s_n \to -\infty \text{ and } \phi^{t_n}(x) \to y \text{ as } n \to \infty\}.$$

In this Thesis we set out to study states $x \in X \subset \mathbb{R}^n$ of dynamical systems that evolve in continuous time $t \in T = \mathbb{R}$, described by a system of ordinary differential equations (ODEs)

$$\frac{dx}{dt} \equiv \dot{x} = F(x), \quad x \in \mathcal{D} \subset \mathbb{R}^n \tag{2.4}$$

where $\mathcal{D}$ is a domain and $F : \mathbb{R}^n \to \mathbb{R}^n$ is smooth in an open region $U \subset \mathbb{R}^n$. Then, by standard theory [71], there is a unique function $x = x(t, x_0)$, $x : \mathbb{R} \times \mathbb{R}^n \to \mathbb{R}^n$, which is smooth in (t, x) and, for each initial condition $x_0 \in U$, satisfies the conditions:

1. $x(0, x_0) = x_0$, and
2. there is an interval $\mathcal{I} = (-\delta_1, \delta_2)$, where $\delta_{1,2} = \delta_{1,2}(x_0) > 0$ such that for all $t \in \mathcal{I}$,

$$\begin{aligned} y(t) &= x(t, x_0) \in U, \quad \text{and} \\ \dot{y}(t) &= f(y(t)). \end{aligned}$$

Let $\mathcal{D} = X \subset \mathbb{R}^n$ then the ODE system given by (2.4) is a continuous time dynamical system $\{T, X, \phi^t\}$ with evolution operator $\phi^t(x_0) := x(t, x_0)$. Currently, we are assuming that F depends only on the states $x \in X$ explicitly and not on time $t \in T$. Then the dynamical system $\{T, X, \phi^t\}$ is called **autonomous**.

In periodically forced systems, which form the bedrock of this Thesis, F depends on the time set T explicitly, i.e. $F(x, t)$. However, this system can be rewritten to be autonomous by setting time as the $(n+1)$-state, i.e. $x_{n+1} = t$. Thus $X = \mathbb{R}^{n+1}$ and the general theory and framework for autonomous systems applies.

We will also study states $x \in X \subset \mathbb{R}^n$ of dynamical systems that evolve in discrete time $t \in T = \mathbb{Z}$, described by a system of difference equations, also called maps,

$$\begin{aligned} x &\mapsto f(x), \quad x \in \mathcal{D} \subset \mathbb{R}^n, \\ x_{m+1} &= f(x_m), \quad m = \{0, 1, 2, \ldots\} \end{aligned} \tag{2.5}$$

where $\mathcal{D}$ is a domain and the function $f : \mathbb{R}^n \to \mathbb{R}^n$ is smooth. Let $\mathcal{D} = X \subset \mathbb{R}^n$ then the system (2.5) is a discreet-time dynamical system $\{T, X, \phi^t\}$ where the evolution operator is the m^{th} iterate of the map, i.e.

$$\phi^m(x_0) = x_m = f(x_{m-1}) = \ldots := f^{(m)}(x_0)$$

where $m \geq 0$ and f is composed with itself m times, i.e. $f^{(m)}(x_0) = f \circ f \circ \ldots \circ f(x_0)$.

The simplest type of invariant sets which are the key to the analysis presented in this Thesis are equilibria and limit cycles (or fixed points and periodic orbits).

Definition 2.9. *An **equilibrium** or **fixed point** $x^* \in X$ of a dynamical system $\{X, T, \phi^t\}$ is a point that satisfies*

$$\phi^t(x^*) = x^* \tag{2.6}$$

for all $t \in T$.

For a continuous-time dynamical system (2.4) the condition (2.6) becomes

$$F(x^*) = 0$$

and we refer to x^* as an equilibrium of the ODE system (2.4).

The equivalent condition to (2.6) for a discrete-time dynamical system is

$$f(x^*) = x^*$$

and we call x^* a fixed point of the map (2.5).

Definition 2.10. *[71] A **periodic orbit** is a nonequilibrium orbit L such that each point $x^* \in L$ satisfies*

$$\phi^{t+T^*} x^* = \phi^t x^* \tag{2.7}$$

with some $T^* > 0$, for all $t \in T$.

The period of a periodic orbit L is the smallest T^* which satisfies this definition.

Consider the continuous-time dynamical system (2.4). Then the condition corresponding to (2.7) for a periodic orbit L is given by

$$x(T^*, x^*) = x^*, \quad \text{with period } T^* > 0$$

for each $x^* \in L$. In phase space, the periodic orbit L is a closed curve. If, in the neighbourhood of L, there are no other periodic orbits, then L is termed a **limit cycle**.

Consider the discrete-time dynamical system (2.5). Then the condition corresponding to (2.7) for a periodic orbit L, sometimes referred to as a periodic point, is given by

$$f^{(m)}(x^*) = x^*, \quad \text{with period } T^* = m > 0$$

for each $x^* \in L$. Thus the period-m periodic orbit L is given by a (finite) sequence of points

$$\{x^*, f(x^*), f^2(x^*), \ldots, f^m(x^*) = x^*\}$$

for fixed $m > 0$. Other types of invariant sets exist and are discussed in [34, 71, 53], for example.

Consider a continuous-time dynamical system (2.4) which has a limit cycle L. The fate of an arbitrary value x_p on the limit cycle L can be determined by reducing a continuous-time dynamical system to a discrete-time dynamical system. This can be done by constructing an $(n-1)$-dimensional smooth cross-section Σ through the flow, such that the orbit intersects Σ transversely and x_p lies on Σ. Let $g(x) : \mathbb{R}^n \to \mathbb{R}$ be a scalar function with $g(x_p) = 0$. The section Σ, referred to as the **Poincaré section**, is defined by

$$\Sigma = \{x \in \mathbb{R}^n : g(x) = 0\}.$$

The limit cycle L must intersect the Poincaré section again, say at the point $\tilde{x}$. Thus a map P from Σ to itself can be constructed to study the intersection points.

Definition 2.11. *[71] The map $P : \Sigma \to \Sigma$, given by*

$$x_p \mapsto \tilde{x} = P(x),$$

is called a Poincaré map associated with the limit cycle L.

The advantage of such a construction is that the phase space dimension is reduced by one. Thus, the study of limit cycles corresponds to the study of fixed points of Poincaré maps.

This Thesis considers the parametrised versions of the ODE system (2.4) or the map (2.5)

$$\dot{x} = F(x, \mu) \quad \text{or} \quad x \mapsto f(x, \mu)$$

with state $x \in \mathbb{R}^n$ and parameter $\mu \in \mathbb{R}^p$. A bifurcation is the transition point between two qualitatively different dynamics of a flow (2.4) or a map (2.5), such as loss of stability or a change in the number of invariant sets. Before we make this statement more precise, we remind the reader that a homeomorphism is a continuous invertible function with a continuous inverse function.

Definition 2.12. *[71] A dynamical system $\{T, \mathbb{R}^n, \phi^t\}$ is called **topologically equivalent** to a dynamical system $\{T, \mathbb{R}^n, \psi^t\}$ if there is a homeomorphism $h : \mathbb{R}^n \to \mathbb{R}^n$ mapping orbits of the first system onto orbits of the second system, preserving the direction of time.*

We now formally define the term bifurcation.

Definition 2.13. *[71] A **bifurcation** occurs at $\mu = \mu^* \in \mathbb{R}^p$ if the phase portrait of the smooth dynamical system $\{T, X, \phi^t\}$ is not topologically equivalent as μ is varied through the value $\mu = \mu^*$.*

We adopt this concept of bifurcation in this Thesis, rather than the concept using the Implicit Function Theorem [55, 71] (i.e. a bifurcation occurs when the Implicit Function Theorem does not hold), because it is similar to the concept of non-smooth bifurcation we introduce in Section 2.2, [34].

As part of the analysis of this Thesis we will plot bifurcation and cobweb diagrams. A **one-parameter bifurcation diagram**, a state component against a parameter, illustrates stable invariant sets and their bifurcation as a parameter is varied.

A **two-parameter bifurcation diagram** illustrates one-parameter bifurcation curves as two parameters are varied.

A **cobweb diagram** is a tool for graphically iterating a one-dimensional discrete dynamical system (2.5) to determine the fate of an initial value and the stability of invariant sets. To determine the next iterate, a reflection on the main diagonal is required.

Bifurcations that occur in smooth dynamical systems can also occur in piecewise-smooth dynamical systems. As we will be studying Poincaré maps of flows, we will now discuss some bifurcations that occur in discrete systems, in particular bifurcations of fixed points and periodic orbits that have a direct analogy to flows. Many other types of bifurcations in smooth dynamical systems can be found in [71].

The birth or destruction of two fixed points is the phenomenon termed **fold bifurcation** at $\mu = \mu^*$, see Figure 2-1a. It occurs when the discrete system (2.5) has one fixed point at $\mu = \mu^*$ with eigenvalue $+1$. The analogous bifurcation in a continuous-time dynamical system is the birth or destruction of two equilibria.

The birth or destruction of a period-2 periodic orbit while coexisting with a fixed point is termed a **period-doubling bifurcation** at $\mu = \mu^*$, see Figure 2-1b. It occurs when the discrete system (2.5) has one fixed point at $\mu = \mu^*$ with eigenvalue -1. The analogous bifurcation in a continuous-time dynamical system is the birth or destruction of a period-2 periodic orbit while coexisting with an equilibrium.

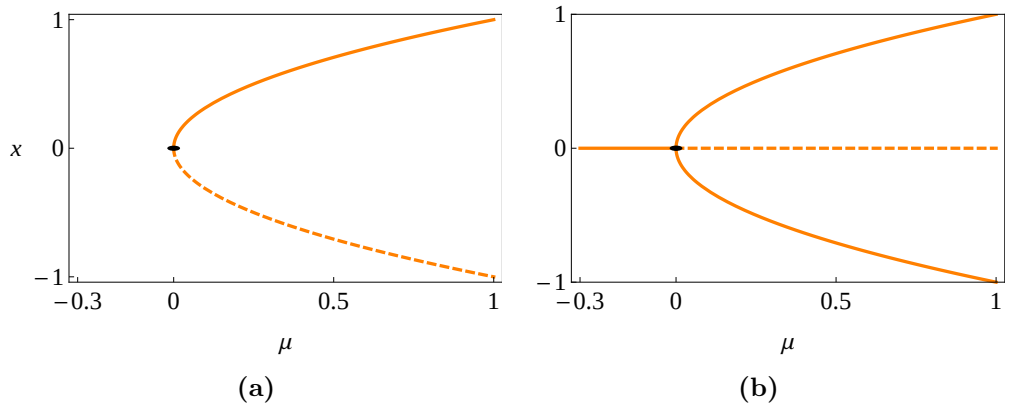

Figure 2-1: *Figure 2-1a: Smooth fold bifurcation. Figure 2-1b: Smooth period-doubling bifurcation.*

Higher period periodic orbits, other than period-2, can also undergo a period-doubling bifurcation. Consider the **logistic map** given by

$$x \mapsto \mu x(1-x), \quad x \in [0,1], \quad 0 < \mu \leq 4. \tag{2.8}$$

A bifurcation diagram of this map is presented in Figure 2-2c. There are two fixed points, $x_1^* = 0$ and $x_2^* = (\mu - 1)/\mu$ which are stable for $0 < \mu < 1$ and $1 < \mu < 3$ respectively, Figure 2-2a. The fixed point x_2^* bifurcates into a stable period-2 periodic orbit at $\mu = 3$ and loses stability, see Figure 2-2b. As μ increases further, the stable period-2 orbit loses stability and bifurcates into a stable period-4 periodic orbit. This sequence of bifurcations, which continues ad infinitum and in which the period m tends to infinity, is termed a **period-doubling cascade**, see Figure 2-2c. This cascade leads to a more complex invariant set, as μ increases from 1 and crosses the point of

accumulation. This is an aperiodic attracting set termed a **chaotic invariant set**. We now give the formal definition of such a set.

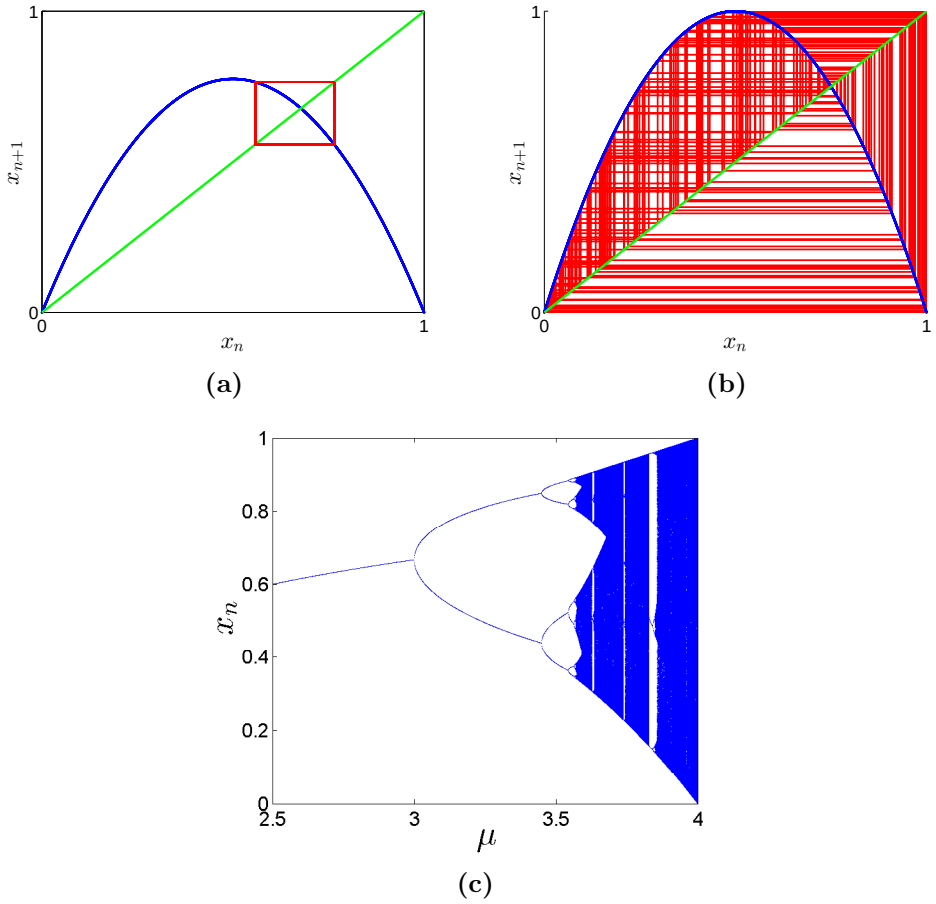

Figure 2-2: *Cobweb diagrams of the logistic map* (2.8) *with initial value* $x_0 = 0.765$ *illustrate that the map has a stable period-2 periodic orbit for* $\mu = 3.1$*, Figure 2-2a, and a chaotic attractor for* $\mu = 4$*, Figure 2-2b. The bifurcation diagram of the logistic map* (2.8)*, Figure 2-2c, shows the bifurcation structure of attracting orbits. In particular, the period-doubling cascade is observed.*

Definition 2.14. *[34] A closed and bounded invariant set* Λ *is called* ***chaotic*** *if it satisfies two additional conditions:*

1. *It has* ***sensitive dependence on the initial conditions****; i.e.:*
   There exists an $\varepsilon > 0$ *such that, for any* $x \in \Lambda$*, and any neighbourhood* $U \subset \Lambda$ *of* x*, there exists* $y \in U$ *and* $t > 0$ *such that* $|\phi^t(x) - \phi^t(y)| > \varepsilon$*.*

2. *There exists a* ***dense trajectory*** *that eventually visits arbitrarily close to every point of the attractor, i.e.:*
   There exists an $x \in \Lambda$ *such that for each point* $y \in \Lambda$ *and each* $\varepsilon > 0$ *there exists a time* t *(which may be positive or negative) such that* $|\phi^t(x) - y| < \varepsilon$*.*

In this Thesis we focus our attention on chaotic attractors. The transition of a dynamical system from a bifurcation cascade to a chaotic attractor, as a parameter is varied, is referred to as a **route to chaos** [54, 53]. Furthermore this kind of transition can be observed in piecewise-smooth dynamical systems and will be introduced in Chapters 2.2, 3 and 4. However, there exist other types of routes to chaos in smooth dynamical systems discussed in [54, 53].

2.2 Piecewise-smooth Dynamical Systems

A piecewise-smooth dynamical system is a dynamical system $\{T, X, \phi^t\}$ with a flow or map that is piecewise smooth, i.e. at the non-smooth points the flow or map may even be discontinuous. There exist several formalisms for piecewise-smooth dynamical systems which vary depending on the application they model [34].

2.2.1 Impacting Hybrid Systems

Physical systems such as impacting objects can be modelled by a combination of flows and maps [117, 33, 34, 37] termed hybrid systems. A hybrid system is a specific type of piecewise-smooth system. Before we give the formal definition, we introduce some notation that will be used throughout the Thesis. The boundary of a set S is denoted by ∂S. By the closure of a set S, denoted by $\bar{S}$, we mean that $\bar{S} = S \cup \partial S$.

Definition 2.15. *[34] Let $\mathcal{D}$ be a domain such that $\cup_i S_i = \mathcal{D} \subset \mathbb{R}^n$ and S_i has a non-empty interior. Let the parameter $\mu \in \mathbb{R}^m$ and let $i, j \in \mathbb{N}$. A **piecewise-smooth hybrid system** comprises a set of ODEs*

$$\dot{x} = F_i(x, \mu), \quad \text{if states} \quad x \in S_i, \tag{2.9}$$

*and a set of reset maps termed **reset laws***

$$x \mapsto R_{ij}(x, \mu), \quad \text{if states} \quad x \in \Sigma_{ij} := \bar{S}_i \cap \bar{S}_j. \tag{2.10}$$

*Each Σ_{ij}, termed a **discontinuity boundary**, is either an $\mathbb{R}^{(n-1)}$-dimensional manifold included in the boundary ∂S_j and ∂S_i, or is the empty set. Each F_i and R_{ij} are assumed to be smooth and well defined in open neighbourhoods around S_i and Σ_{ij} respectively.*

A hybrid dynamical system is not a unique concept and thus other formalisms and definitions exist [117]. In particular, a hybrid system modelling impacts is defined in the following way.

Definition 2.16. *[34] An **impacting hybrid system** is a piecewise-smooth hybrid*

system for which $R_{ij} : \Sigma_{ij} \to \Sigma_{ij}$, and the flow is constrained locally to lie on one side of the boundary; that is, in $\bar{S}_i = S_i \cup \Sigma_{ij}$.

The impact problems considered in this Thesis comprise a moving object under forcing which comes into contact with one rigid obstacle. Thus we study a hybrid system (2.9), (2.10) with a single discontinuity boundary Σ, which will also be referred to as an **impact surface** as it represents the obstacle. When a trajectory intersects the impact surface then we will refer to the event as an **impact event** or an **impact**.

An impact event is assumed to take zero time. This is a realistic assumption as the time and length scales at impact are several magnitudes smaller than those of the entire system [34]. The trajectory of a hybrid system (2.9), (2.10) at an impact is modelled by the reset law R, which takes the loss of energy and the change in velocity into account.

For the class of hybrid systems studied in this Thesis, the impact surface Σ can be defined in terms of a smooth scalar function $H(x) : \mathbb{R}^n \to \mathbb{R}$ such that

$$\Sigma = \{x : H(x) = 0\} \quad \text{and} \quad S_1 = \{x : H(x) > 0\}$$

where S_1 is the region to which the dynamics of a system is constrained. The reset law R prevents any trajectory from entering the region $S_2 = \{x : H(x) < 0\}$. Trajectories in S_2 are physically unrealistic as they represent the moving object entering a rigid solid body such as a wall. Thus, the impacting hybrid systems parametrised by μ, which are studied in this Thesis, take the form

$$\begin{aligned} \dot{x} &= F(x, \mu) \quad \text{if} \quad H(x, \mu) > 0, \\ x &\mapsto R(x, \mu) \quad \text{if} \quad H(x, \mu) = 0, \end{aligned} \tag{2.11}$$

with states $x \in \mathbb{R}^n$, $\mu \in \mathbb{R}$, for a smooth vector field $F : \mathbb{R}^n \times \mathbb{R} \to \mathbb{R}^n$ (which is well defined in a full neighbourhood of Σ as well as S_2) and a reset law R.

Assume that an impact takes place at a time t_0. Then the states immediately before and after the impact, which intersect Σ, x^- and x^+ respectively, are defined by

$$x^- = \lim_{t \to t_0^-} x(t) \quad \text{and} \quad x^+ = \lim_{t \to t_0^+} x(t).$$

Thus, in terms of the reset law R, x^+ is given by

$$x^+ = R(x^-, \mu). \tag{2.12}$$

The following assumptions and definitions are motivated by mechanical applications [37]. Let $v(x, \mu)$ be the normal velocity and $a(x, \mu)$ the normal acceleration of the flow

with respect to Σ given by

$$v(x,\mu) = \frac{dH}{dt} = H_x F, \tag{2.13}$$

$$a(x,\mu) = \frac{d^2H}{dt^2} = (H_x F)_x\, F = H_{xx}FF + H_x F_x F. \tag{2.14}$$

Then, we suppose that the reset law R is of the form

$$R(x,\mu) = x + W(x,\mu)\, H_x F = x + W(x,\mu)v(x,\mu) \tag{2.15}$$

for some smooth function $W : \mathbb{R}^n \to \mathbb{R}^n$. Note that if $v(x) = 0$ then $R(x,\mu)$ becomes the identity mapping.

Therefore, assuming R is of the form (2.15), the impact surface Σ consists of three separate regions, Σ^-, Σ^+ and Σ^0, depending on the normal velocity v, given by

$$\begin{aligned} \Sigma^- &= \{x \in \Sigma : v(x,\mu) < 0\}, \\ \Sigma^+ &= \{x \in \Sigma : v(x,\mu) > 0\}, \\ \Sigma^0 &= \{x \in \Sigma : v(x,\mu) = 0\}. \end{aligned} \tag{2.16}$$

Definition 2.17. *[34] The set Σ^0, given by* (2.16)*, is referred to as a* ***grazing set****.*

Accordingly, for a physically plausible flow, we require that Σ is always approached by the flow with $v \leq 0$, which corresponds to $x^- \in \Sigma^-$ termed **transversal impact** or $x^- \in \Sigma^0$ termed **grazing impact**.

We will now outline the possible flows in an impacting hybrid system described in [33, 37, 34]. Let the initial value $x(0) = x_0 \in S^1$. Then the system of ODEs (2.9) hold and give rise to a smooth flow $\phi^t(x_0)$. If $\phi^t(x_0)$ does not experience an impact then it corresponds to a smooth dynamical system. If $\phi^t(x_0)$ undergoes a transversal impact at t_0 then $x^- \in \Sigma^-$ gets mapped to $x^+ = R(x^-) \in \Sigma^+$ by (2.12) giving rise to the flow $\phi^t(x^t)$ and further impacts can follow. If the flow $\phi^t(x_0)$ experiences a grazing impact $x^- \in \Sigma^0$, in which case the reset map R given by (2.15) is the identity mapping, then the acceleration $a(x^-)$ indicates the system's evolution. If $a(x^-) > 0$ then the flow will separate instantly from the discontinuity boundary Σ into S_1. However, if $a(x^-) < 0$ then $\phi^t(x^-)$ sticks to Σ. This type of behaviour is called **sticking motion** and evolves under the sliding vector field F_s given by

$$F_s(x,\mu) = F(x,\mu) - \lambda(x,\mu)\, W(x,\mu) \tag{2.17}$$

where, to remain in the sticking region $\lambda(x,\mu) > 0$, and

$$\lambda(x,\mu) = \frac{a(x,\mu)}{(H_x F)_x\, W(x,\mu)}. \tag{2.18}$$

The definition of $\lambda(x, \mu)$ given by (2.18) is chosen to keep $H(x, \mu) = 0$ and $v(x, \mu) = 0$, [33, 37, 34].

Sticking motion is often a result of a sequence of impacts during which the impact velocity $v(x^-, \mu)$ and time length between impacts decrease. Such a sequence of impacts, Figure 2-3, termed **chattering** [18, 94, 34] or **Zeno phenomenon** [34], accumulates in finite time onto a point which marks the beginning of the sticking motion [18, 94, 34].

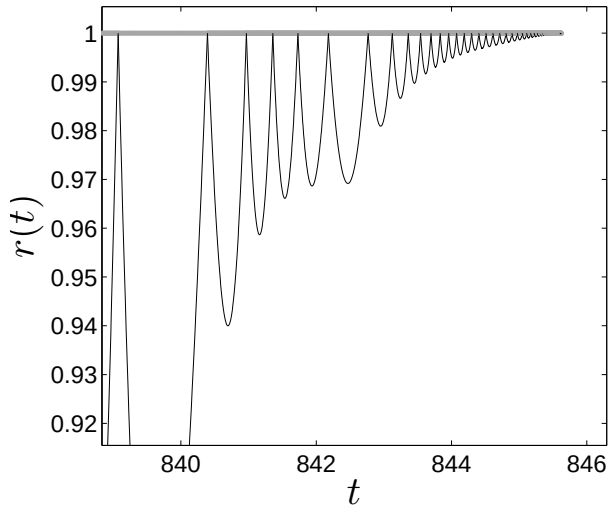

Figure 2-3: *A chattering sequence in magnetic bearing systems where $r(t)$ is the distance of the rotor centre (moving object) from the origin of the coordinates which coincides with the centre of the circular boundary (impact surface). The impact surface is located at $r = 1$. A sequence of impacts for $t \in [0, 846]$ that leads to chattering for $t \in [840, 846]$.*

Equilibria of Impacting Hybrid Systems

We will now introduce the various types of equilibria that can be identified in impacting hybrid systems.

Definition 2.18. *[33, 37, 34] A point $x^* \in \mathcal{D}$ is termed an **admissible equilibrium** of* (2.11) *if*

$$F(x^*, \mu) = 0 \quad \textit{and} \quad H(x^*, \mu) > 0.$$

Definition 2.19. *[33, 37, 34] A point $x^* \in \mathcal{D}$ is termed a **virtual equilibrium** of* (2.11) *if*

$$F(x^*, \mu) = 0 \quad \textit{and} \quad H(x^*, \mu) < 0.$$

Now, we introduce equilibria of the sticking flow.

Definition 2.20. *[33, 37, 34] A point $x^* \in \mathcal{D}$ is termed a **pseudo-equilibrium** of*

(2.11) *if it is an equilibrium of the sticking vector field* (2.17)*, i.e.*

$$F(x^*, \mu) - \lambda W(x^*, \mu) = 0,$$
$$H(x^*, \mu) = 0$$

with λ *as defined in* (2.18)*.*

Definition 2.21. *[33, 37, 34] A pseudo-equilibrium is termed* ***admissible*** *if*

$$\lambda > 0,$$

and ***virtual*** *if*

$$\lambda < 0.$$

We now define an equilibrium point which identifies when equilibria and pseudo-equilibria can coincide depending on the parameter μ.

Definition 2.22. *[33, 37, 34] A point* $x = x^* \in \mathcal{D},\ \mu = \mu^* \in \mathbb{R}$ *is termed a* ***boundary equilibrium point*** *of* (2.11) *if*

$$F(x^*, \mu^*) = 0 \quad \textit{and} \quad H(x^*, \mu^*) = 0.$$

The boundary equilibrium point also represents the boundary between admissible and virtual flows, between physically realistic and unrealistic trajectories. This will be demonstrated in Chapter 5.

Boundary Equilibrium Bifurcation

Bifurcations that occur in smooth dynamical systems, such as those introduced in Section 2.1, can also occur in piecewise-smooth dynamical systems [34]. We will refer to these as **smooth bifurcations**. In this Section we define bifurcations that are unique to piecewise-smooth systems, termed **non-smooth bifurcations**.

A bifurcation theory of a general piecewise-smooth dynamical system is still being developed [34]. In fact, there is no rigorous definition of a general non-smooth bifurcation. However, there have been advancements in the identification and classification of non-smooth bifurcations of particular systems, such as the impacting hybrid systems [33, 37, 34]. One class of such bifurcations results from the interaction of the flow with the discontinuity boundary, causing a structural instability as a parameter is varied, and is termed **discontinuity induced bifurcation (DIB)**.

We will now introduce bifurcations resulting from an equilibrium of (2.11) crossing the discontinuity boundary. Equivalent bifurcations occurring in piecewise-smooth discrete systems will be introduced in Section 2.2.2.

Definition 2.23. *[33, 37, 34] The system* (2.11) *is said to undergo a* ***boundary equilibrium bifurcation (BEB)*** *at $\mu = \mu^*$ if the system* (2.11) *has a boundary equilibrium point at $x = x^*$ and $\mu = \mu^*$ that satisfies the following conditions:*

1. *$F_x(x^*, \mu^*)$ is invertible (or equivalently $\det(F_x) \neq 0$), and*
2. *$H_\mu(x^*, \mu^*) - H_x(x^*, \mu^*)F_x^{-1}(x^*, \mu^*)F_\mu(x^*, \mu^*) \neq 0$.*

We can observe two different scenarios of regular and pseudo-equilibria branching from a boundary equilibrium bifurcation point.

Definition 2.24. *[33, 37, 34] An admissible (virtual) equilibrium and a virtual (admissible) pseudo-equilibrium that bifurcate, at a BEB point, into a virtual (admissible) equilibrium and an admissible (virtual) pseudo-equilibrium, respectively, is termed* ***persistence****.*

Definition 2.25. *[33, 37, 34] At a BEB point, the birth or destruction of two admissible equilibria, one regular and one pseudo, which turn into two virtual equilibria respectively, is termed a* ***non-smooth fold.***

Theorem 2.26. *[34, 37] Assume that $x = x^*, \mu = \mu^*$ is a boundary equilibrium bifurcation point of* (2.11) *such that*

$$H_x(x^*, \mu^*)F_x^{-1}(x^*, \mu^*)W(x^*, \mu^*) \neq 0.$$

1. ***Persistence*** *is observed at the boundary equilibrium bifurcation point $x = x^*, \mu = \mu^*$ if*
$$H_x(x^*, \mu^*)F_x^{-1}(x^*, \mu^*)W(x^*, \mu^*) > 0.$$
2. *A* ***non-smooth fold*** *is observed at the boundary equilibrium bifurcation point $x = x^*, \mu = \mu^*$ if*
$$H_x(x^*, \mu^*)F_x^{-1}(x^*, \mu^*)W(x^*, \mu^*) < 0.$$

More complex invariant sets can bifurcate from a BEB point and general results have been proven for hybrid systems with phase space $X \subset \mathbb{R}^2$ [33, 37]. Only a few results have been obtained for higher dimensional systems. The magnetic bearing system studied in Chapters 5 and 6 gives rise to a novel and complex bifurcation at the BEB point, where a regular equilibrium, a pseudo-equilibrium and two limit cycles bifurcate. This result contributes to the ongoing classification of non-smooth bifurcations.

In this Section we have introduced bifurcations that result from the interaction of equilibria with the discontinuity boundary. Other intricate bifurcations can result from limit cycles interacting with the discontinuity boundary, called a **grazing bifurcation**. These will be introduced in the context of the impact oscillator. In Chapter 6 we will show that they also occur in magnetic bearing systems.

2.2.2 Piecewise-smooth Maps

We will now give the definition of *piecewise-smooth maps* and the associated terminology. We will also introduce the non-smooth bifurcations that occur in piecewise-smooth maps.

Definition 2.27. *[34] Let $\mathcal{D} \subset \mathbb{R}^n$ be a domain, S_i a non-empty interior for finite $i \in \mathbb{N}$ such that $\cup_i S_i = \mathcal{D}$. A* ***piecewise-smooth map*** *is a finite set of smooth maps*

$$x \mapsto F_i(x, \mu), \quad \textit{for} \quad x \in S_i \tag{2.19}$$

where $F_i : \mathbb{R}^n \times \mathbb{R}^m \mapsto \mathbb{R}^n$.

Definition 2.28. *[34] The intersection $\Sigma_{ij} = \bar{S}_i \cap \bar{S}_j$ is termed* ***discontinuity boundary****.*

Throughout this Thesis we consider piecewise-smooth maps with a single discontinuity boundary $\Sigma = \Sigma_{12}$. This being the case, it is more convenient to introduce a smooth scalar function $H(x) : \mathbb{R}^n \to \mathbb{R}$ to identify on which side of the discontinuity boundary a point x lies. The sets S_1, S_2 and Σ can be defined as

$$\begin{aligned} S_1 &= \{x \in \mathcal{D} : H(x, \mu) < 0\}, \\ S_2 &= \{x \in \mathcal{D} : H(x, \mu) > 0\}, \\ \Sigma &= \{x \in \mathcal{D} : H(x, \mu) = 0\}. \end{aligned}$$

Thus, according to Definitions 2.27 and 2.28, the form of the general map on a domain $\mathcal{D}$ with interiors S_1 and S_2 is

$$x \mapsto f(x, \mu) = \begin{cases} F_1(x, \mu), & \text{if } x \in S_1 \\ F_2(x, \mu), & \text{if } x \in S_2 \end{cases} \tag{2.20}$$

where $x \in \mathcal{D} \subset \mathbb{R}^n$, $\mu \in \mathbb{R}^m$ and the functions F_1 and F_2 are smooth in $\mathcal{D}$.

One-dimensional maps where the functions $F_1, F_2 : \mathbb{R} \mapsto \mathbb{R}$ are of a certain form have been studied extensively in the literature, see [34] for an outline. We now introduce some of those maps that will be important in Chapter 3.

Assume F_1 and F_2 are linear functions with $F_1 = F_2$. If $H(x, \mu) = 0$ then the map (2.20) is termed a **piecewise-linear continuous map** [43, 44, 95, 35]. However, if $F_1 \neq F_2$ when $H(x, \mu) = 0$ then the map (2.20) is termed a **piecewise-linear discontinuous map** [59, 8, 9, 61, 7].

Assume F_1 is a linear function and F_2 is a nonlinear function of the form $F_2(x, \mu) = \sqrt{x} + \mu$, such that $F_1 = F_2$ if $H(x, \mu) = 0$. Then the map (2.20) is termed a **continuous square-root map**, [34, 90, 91, 92, 8, 24, 17]. If $F_1 \neq F_2$ when $H(x, \mu) = 0$ then the map (2.20) is termed a **discontinuous square-root map** [102, 38].

If (2.20) is a discontinuous map then either F_1 or F_2 has to be defined on the discontinuity boundary Σ. However, the dynamics is not affected by this choice ([34], p.72).

We will now define the various types of fixed points of a system (2.20).

Definition 2.29. *[34] We say that a point $x = x^*$ is an **admissible fixed point** of (2.20) if*

$$\begin{aligned} x^* &= F_1(x^*, \mu) \quad \text{if} \quad x^* \in S_1 \\ \text{or} \quad x^* &= F_2(x^*, \mu) \quad \text{if} \quad x^* \in S_2. \end{aligned}$$

Definition 2.30. *[34] We say that a point $x = x^*$ is a **virtual fixed point** of (2.20) if*

$$\begin{aligned} x^* &= F_1(x^*, \mu) \quad \text{if} \quad x^* \in S_2 \\ \text{or} \quad x^* &= F_2(x^*, \mu) \quad \text{if} \quad x^* \in S_1. \end{aligned}$$

As for smooth discrete systems, we denote the composition of a piecewise-smooth function f with itself n times by $f^n(x) = f \circ f \circ \ldots \circ f(x)$.

Definition 2.31. *[34] Let $f : \mathbb{R} \to \mathbb{R}$ be a piecewise-smooth function. We say that a set of points*

$$L = \{x^*, f(x^*), f^2(x^*), \ldots, f^{n-1}(x^*)\}$$

*is termed an **admissible period-n periodic orbit** if each $x \in L$ is an admissible fixed point of $f^n(x)$, i.e. $x = f^n(x)$. A **virtual period-n periodic orbit** exists if there is $x \in L$ such that x is a virtual fixed point of $f^n(x)$.*

As with flows, an orbit of (2.20) is said to cross Σ transversally at $x = \bar{x}$ and $\mu = \bar{\mu}$ when $H(\bar{x}, \bar{\mu}) = 0$ if

$$H_x(\bar{x}, \bar{\mu}) F_{i,\mu}(\bar{x}, \bar{\mu}) \neq 0 \quad \text{for} \quad i = 1 \text{ or } 2.$$

We now turn to defining the non-smooth bifurcation that occurs in a piecewise-smooth map (2.20), called a border-collision bifurcation. Without loss of generality, we assume such a bifurcation occurs at parameter value $\mu = 0$.

Definition 2.32. *[34] We say a fixed point x^* undergoes a **border-collision (BC) bifurcation** at $\mu = 0$ if there exists an interval $(-\varepsilon, \varepsilon)$, with ε small, such that:*

1. *x^* is admissible for $\mu \in (-\varepsilon, 0)$,*
2. *x^* is virtual for $\mu \in (0, \varepsilon)$,*
3. *$x^* \in \Sigma$ for $\mu = 0$,*

4. x^* *crosses* Σ *transversally for* $\mu \in (-\varepsilon, \varepsilon)$,

5. the first derivatives of (2.20) *satisfy*

$$\frac{\partial F_1}{\partial x}(x^*, \mu)\Big|_{\mu=0} \neq \frac{\partial F_2}{\partial x}(x^*, \mu)\Big|_{\mu=0},$$

i.e. are discontinuous at $x = x^*, \mu = 0$.

The border-collision bifurcation of a fixed point is the simplest type of DIB in piecewise-smooth maps and is equivalent to the BEB in flows. As with piecewise-smooth flows, this bifurcation can give rise to the persistence and non-smooth fold bifurcation scenarios in n-dimensional piecewise-linear maps [43, 35, 44]. However, these scenarios will not be investigated in this Thesis. Instead, in Chapters 3 and 4, we will show how the border-collision of a fixed point of (2.20) gives birth to more complex invariant sets such as chaotic attractors.

Piecewise-smooth maps with discontinuities in several locations have been discussed in literature. For example, in [116] it has been shown that piecewise linear maps with two discontinuity points also exhibit a period-adding scenario at the border-collision bifurcation.

2.2.3 Numerical Methods

The analysis of piecewise-smooth dynamical systems via analytical methods can be limited as the associated expressions and equations are often nonlinear due to the system's lack of smoothness, as has been described in [90, 91, 34] and as we also demonstrate in Chapters 3 (example of piecewise-smooth maps) and 5 (example of impacting hybrid systems). Hence numerical methods can provide an important insight into the dynamical system through its numerical simulation and the numerical study of parameter effects on it.

There are currently two prevalent methods to simulate a non-smooth dynamical system: the *event-driven* [34] and the *time-stepping* [2] scheme.

As the name indicates, the event-driven scheme, which will be employed in this Thesis, is based on accurately computing the event, i.e. the time at which a trajectory crosses the discontinuity boundary Σ. It is assumed that the solution between events is differentiable enabling the use of standard numerical integration techniques such as the subroutines provided by MATLAB® [84] which are used throughout this Thesis. Once such an event has been detected and treated, i.e. the transition rules have been applied, the system is re-initialised at that instance. Hence without the clear definition of all discontinuity boundaries and transition laws this scheme cannot be applied.

The time-stepping scheme, which will not be employed in this Thesis, is a time-discretisation method that evolves the system as a whole and checks whether the sys-

tem's constraints are satisfied at each time step. Consequently, uniqueness and existence of a flow are determined at each time step while the actual event is ignored. The evolution of an impacting system from one step to the next requires a different formulation to the hybrid system [2, 1].

The choice of the numerical scheme depends very much on the application. The event-driven scheme is fast and accurate for low dimensional systems with few discontinuity boundaries (up to 10 according to [34]). Due to the re-initialisation process it can be computationally expensive, even infeasible, when the number of events is large. This can happen in two ways:

Case 1 The system experiences an infinite accumulation of impacts in a finite time, called chattering, or

Case 2 The system has many colliding particles.

The second case does not pose an issue as the phase space of impacting hybrid systems X studied in this Thesis is at most in R^4 (Chapters 5 and 6).

Although the time-stepping scheme is capable of dealing with both cases in addition to a large number of other constraints, it can miss certain dynamics that depend on the precise computation of the event, such as grazing events [34]. Furthermore, alternative methods have been developed for event-driven schemes (sometimes called extended event-driven schemes) that can detect, handle and progress the simulation of Case 1 type behaviour. In [94] Nordmark and Piiroinen have established conditions that detect if such dynamics is about to occur using the most recently obtained recorded events during a simulation. Then, using an asymptotically derived map, the limit of this accumulation can be approximated and hence the subsequent dynamics, such as sticking or sliding, can be determined by the algorithm.

Chattering in the magnetic bearing system will be studied in Chapter 6. We will determine when it occurs but not what happens post accumulation point. Thus, the method devised by Nordmark and Piiroinen [94] will not be used.

These simulations can be further utilised to understand the qualitative changes in a dynamical system when a parameter is varied. In this Thesis we compute a brute-force type of bifurcation diagram called a **Monte Carlo bifurcation diagram** [34] to study the attracting invariant sets once the transients have subsided.

We now give a rough explanation of the algorithm.

1. Fix the bifurcation parameter value.

2. Generate a random set of initial conditions.

3. Compute the piecewise-smooth orbit for each initial value until transient behaviour has subsided and the orbit has converged to an attractor. For piecewise-

smooth maps we have chosen 5000 iterations. For the impacting hybrid system in this Thesis, i.e. magnetic bearing system, we have chosen 1000 impacts.

4. Compute and record the piecewise-smooth orbit for another 1000 iterations or 100 impacts.

5. Plot the recorded states against the bifurcation parameter.

6. Vary the bifurcation parameter slightly and repeat this process.

This quick and accurate method is suited to pick up the most likely dynamics and indicate coexistence of attractors. Furthermore, a priori knowledge of the set of initial conditions is not necessary. Finally, note that this method is not adapted to follow unstable periodic orbits. More details on other piecewise-smooth dynamical systems and their numerical simulation can be found in [2, 1, 34].

2.3 Impact Oscillator

The one degree of freedom impact oscillator is central to the work presented in this Thesis as, on the one hand, it gives rise to the type of one dimensional piecewise-smooth map studied in Chapter 3 and, on the other hand, it is a prime example of an impacting hybrid system. The methods and concepts introduced in this Section will be used to study the magnetic bearing system which is modelled by a two degrees of freedom impact oscillator with friction. We now show how to model the impact oscillator using impacting hybrid systems introduced in Chapter 2.2.

When we refer to the one degree of freedom impact oscillator we mean a spring-damper system that impacts a rigid obstacle. The physical model comprises a particle which is attached to a linear spring and dashpot, its movement externally forced by a function $u(t)$, and an obstacle which is positioned at $x = \sigma$, see Figure 2-4. Let t denote time. Away from the obstacle the equation of motion for the position of the centre of mass $x(t)$ is given by

$$\ddot{x}(t) + 2\zeta\dot{x}(t) + x(t) = u(t) \quad \text{if} \quad x(t) < \sigma \tag{2.21}$$

where ζ is the damping ratio and the natural frequency has been scaled to unity. Here we assume the forcing is periodic and sinusoidal, i.e. $u(t) = \cos(\omega t)$ with period $T^* = 2\pi/\omega$. Note that (2.21) can be written in the form $\dot{x} = F(x)$.

We define the impact surface $\Sigma := \{(t, x, \dot{x}) : H(x) := x - \sigma = 0\}$. An impact occurs at time $t = t_0$ when the particle arrives at the position $x(t_0) = \sigma$ with velocity $\dot{x}(t_0)$. Any subsequent impact times are denoted by t_i with $i \in \mathbb{N}$. We assume that the energy at impact in this system dissipates in zero time and this is modelled by the reset law that maps pre-impact state $(-)$ to the post-impact state $(+)$. At impact time

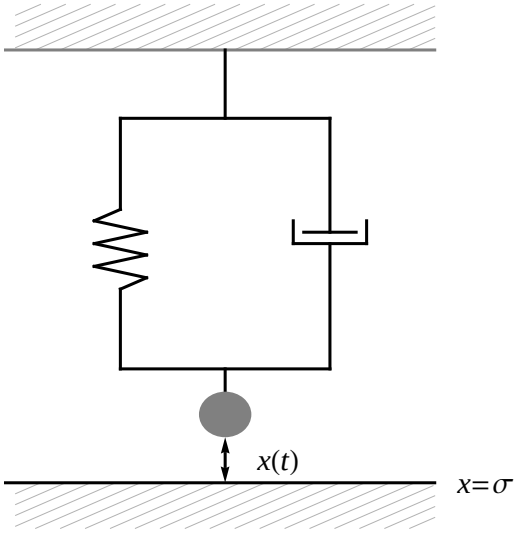

Figure 2-4: *The impact oscillator with damping and stiffness. The particle (grey disk) with position $x(t)$ impacts with a fixed obstacle when $x(t) = \sigma$.*

$t = t_i$ the position x remains the same but the velocity $\dot{x}$ changes direction and reduces in magnitude to take energy dissipation into account, i.e.

$$(x^+(t_i), \dot{x}^+(t_i)) = (x^-(t_i), -r\dot{x}^-(t_i)) \quad \text{if} \quad x = \sigma \tag{2.22}$$

where r is **Newton's coefficient of restitution**, with $r \in (0, 1)$. Although not considered here, the impact oscillator with the coefficient of restitution taking the value $r = 1$ [73], called elastic impact, or $r = 0$ [105], called completely dissipative impact, have been studied. Generally, the appropriate value for the coefficient of restitution depends on the application and hence on the material properties, geometry of the impacting objects and relative impact velocity [34]. Although it would be more realistic to assume that r is not a constant and depends, for example, on relative velocity, it has been shown that such a simple model is a good approximation, i.e. the dynamics predicted by the model agree with experimental results [96, 99]. This is briefly elaborated in Section 2.3.1.

Furthermore, note that the ODE (2.21) and reset law (2.22) are linear but due to the effect of one on the other, the system as a whole is nonlinear [34].

As briefly indicated in the introduction, hybrid dynamical systems are typically studied by taking a Poincaré section to define a Poincaré map and investigating this map, which is induced by the piecewise-smooth flow.

The impact surface can be adopted as a Poincaré section. Then the Poincaré map $P_I : \Sigma \to \Sigma$, termed **impact map**, can be defined. The impact map maps one impact

event to the next and is given by

$$(t_{i+1}, \dot{x}^+(t_{i+1})) = P_I(t_i, \dot{x}^+(t_i)), \tag{2.23}$$

as the position $x(t_i) = \sigma$ for all $i \in \mathbb{N}$. This method is used to study simple periodic orbits with (high) impact velocity, for example, a periodic orbit with one impact per period T. This periodic orbit, which impacts with the same velocity $\dot{x}^+(t_i)$ at each t_i, corresponds to a fixed point of the impact map P_I, and its existence condition is given by

$$t_{i+1} = t_i \mod T \quad \text{and} \quad \dot{x}^+(t_{i+1}) = \dot{x}^+(t_i). \tag{2.24}$$

This method is applied as it allows (to an extent) the analytical study of such limit cycles in the impact oscillator [46] or rotating machines [86] (Chapter 5).

A Poincaré section Σ_S can be defined in terms of the forcing period T^*, i.e. we measure position x and velocity $\dot{x}$ after T^* time has passed. Then we can define the Poincaré map $P_S : \Sigma_S \to \Sigma_S$, termed **stroboscopic map**, given by

$$(x(t + T^*), \dot{x}(t + T^*)) = P_S(x(t), \dot{x}(t)). \tag{2.25}$$

This method is typically used to study orbits with low impact velocity.

We now discuss some of the motions observed in impact oscillators. High impact velocity orbits can die down via many impacts in finite time. This is called chattering or Zeno phenomenon, introduced in Chapter 2.2.1. If the chattering sequence is infinite then the impacts accumulate on a point where the impact velocity $\dot{x}^-$ becomes zero. If the acceleration is pointing into the obstacle then the particle will stick to it and enter sticking motion. The particle will only move away from it once the acceleration changes sign. For the impact oscillator, Budd and Dux [18] use the impact map P_I to find an expression for the point of accumulation. A detailed study of this geometry near such a point is presented in [23]. Chattering can be part of complex dynamics. For example, it can be part of periodic motion where the following trajectories and sequence of events are repeated exactly, ad infinitum: high velocity impacts following a certain pattern are followed by a chattering sequence which accumulates at one point. Such motion has been reported in [18] and [4].

Low velocity impacts can lead to trajectories with grazing impacts (Chapter 2.2.1); these touch the impact surface Σ at precisely one point at which the normal impact velocity is zero, and are termed **grazing trajectories**. This means that the orbit lies tangential to Σ and any small perturbation nearby gives rise to orbits that completely miss the impact surface or have a low velocity impact. To understand this local phenomenon and study its effects on the system's dynamics, a Poincaré map can be derived. One option is to use the impact map P_I (2.23), which has been shown to be discontinuous at a grazing event [72, 73]. Nordmark [90] applied the strobo-

scopic map P_S to derive a normal form map for the trajectories near grazing, called **zero-time discontinuity mapping (ZDM)**. The stroboscopic map of non-impacting orbits is smooth. This is not the case for impacting orbits, i.e. it is piecewise-smooth [90, 91, 92, 123]. The ZDM, which takes into account all orbits, impacting or non-impacting, near a grazing trajectory, makes a correction for this *error*. Nordmark [90] and Whiston [123] have shown that this map contains a square-root term, which gives rise to complex dynamics [90, 91, 92, 123, 48, 99, 24, 17, 85, 82]. The square-root term results from the Taylor series approximation of the orbit's evolution in time and its correction, [90, 34].

Furthermore, in [90] Nordmark has shown that grazing trajectories have a destabilising effect on the dynamics of the system, in particular if a parameter is varied. Consider a limit cycle which does not interact with Σ. If, as a parameter is varied, it undergoes a grazing event, we term this a **grazing bifurcation**. The analysis of the ZDM gives an insight into what the limit cycle bifurcates.

Although we do not give the full details here of how to obtain the ZDM, we note that a nonlinear change of coordinates described in [90, 85] from position $x(t)$ and velocity $\dot{x}(t)$ to the coordinates x_n and y_n is necessary to obtain the map defined below by (2.26) and (2.27). We emphasize that the x_n does not refer to position $x(t)$. The ZDM is given by

$$\begin{aligned} x_{n+1} &= \lambda x_n + y_n + \mu \\ y_{n+1} &= -\gamma x_n \end{aligned} \tag{2.26}$$

if $x_n < 0$, i.e. no impact occurs, and

$$\begin{aligned} x_{n+1} &= -\sqrt{x_n} + y_n + \mu \\ y_{n+1} &= -\gamma r^2 x_n \end{aligned} \tag{2.27}$$

otherwise, i.e. an impact takes place. This map is termed a **two-dimensional continuous square-root map**.

Consider the parameter γ which depends on damping ratio ζ and forcing period T^*, i.e. $\gamma = e^{-2\zeta T^*}$. Assume that the term ζT^* is large, i.e. $\zeta T^* \gg 1$. Then $\gamma \approx 0$ and the two-dimensional piecewise-smooth map given by (2.26) and (2.27) can be approximated by a one-dimensional map given by

$$x_{n+1} = \begin{cases} \lambda x_n + \mu, & \text{if } x_n < 0 \\ -\sqrt{x_n} + \mu - \ell, & \text{if } x_n > 0 \end{cases} \tag{2.28}$$

where $\ell = 0$ and which is known as the **continuous square-root map**. Both the one- and two-dimensional continuous square-root maps have been studied in great detail in [91, 24, 34] and [90, 92, 24, 34], respectively.

Assume that the obstacle is imparting a repelling impulse onto the impacting object.

This impulse, which occurs in addition to Newton's law of restitution, is assumed to be a constant b. Then the reset law is given by

$$(x^+(t_i), \dot{x}^+(t_i)) = (x^-(t_i), -r\dot{x}^-(t_i) + b), \quad \text{if} \quad x = \sigma. \tag{2.29}$$

The impact oscillator (2.21) with reset law (2.29) has been studied by Pring and Budd in [102]. They have shown that its ZDM can also be approximated by a one-dimensional map which is of the form (2.28) with $\ell > 0$. This map is know as the **discontinuous square-root map**.

The dynamics of the continuous square-root map (2.28) (where $\ell = 0$) is briefly introduced now and expanded upon in Chapter 3. Assume $\lambda \in (0, 1)$ and $\mu \in \mathbb{R}$. Then the map (2.28) (where $\ell = 0$) has a stable fixed point x_L for $\mu < 0$. This fixed point undergoes a border-collision bifurcation at $\mu = 0$ when $x_L = 0$. As a parameter is varied, this fixed point x_L can bifurcate into another fixed point in a persistence scenario as elaborated in Chapter 2.2.2. The fixed point x_L can bifurcate into a large period periodic orbit which leads to a bifurcation cascade [34], similar to the one observed in the logistic map (Chapter 2.1, Figure 2-2c). Finally, the fixed point x_L of a piecewise-smooth map can bifurcate into a chaotic attractor as the bifurcation parameter is varied [34]. The sudden transition from a fixed point to a large period periodic orbit or a chaotic attractor is a characteristic feature of piecewise-smooth dynamical systems.

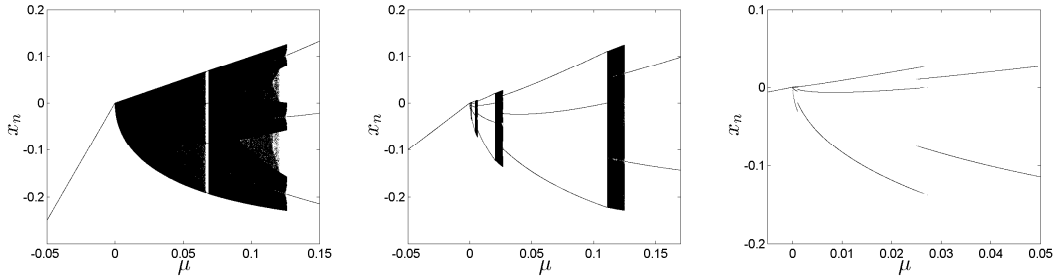

Figure 2-5: *The bifurcation structure of the continuous square-root map* (2.28) *(where $\ell = 0$). For $\mu < 0$ we observe the stable fixed point. This fixed point undergoes a border-collision bifurcation at $x = 0$, $\mu = 0$. Three qualitatively different bifurcation scenarios can be observed for $\mu > 0$: robust chaos ($\lambda = 0.8$) in Figure 2-5a, the period-incrementing cascade with chaotic windows ($\lambda = 0.5$) in Figure 2-5b, and the period-incrementing cascade with coexisting periodic orbits ($\lambda = 0.2$) in Figure 2-5c.*

The bifurcation cascades that have been observed in piecewise-smooth dynamical systems as a parameter is varied include:

- **the period-incrementing cascade** (Figures 2-5b and 2-5c): A cascade of periodic orbits, where a period-N orbit bifurcates into a period-$(N + 1)$ orbit as the bifurcation parameter, μ, is increased (or decreased) towards μ^*, [6],

- **the period-adding cascade** (also called a Farey Tree): The periodic orbits of this cascade are organised such that at the parameter values between two neighbouring periodic orbits, say of period-N and period-M, there exists a period-$(N + M)$ orbit. This concatenation of neighbouring periodic orbits can continue ad infinitum [34],

- **robust chaos** (Figure 2-5a): A chaotic attractor, which is uninterrupted by windows of stable periodic orbits, exists over an open interval of parameter values of μ close to μ^*, [10].

Now we are in the position to give a brief outline of some of the bifurcation scenarios of a fixed point of the map x_L that undergo a border-collision bifurcation at $\mu = 0$. Three qualitatively different bifurcation scenarios have been reported in literature for small $\mu > 0$ depending on the parameter λ:

- if $2/3 < \lambda < 1$, robust chaos is observed, Figure 2-5a,

- if $1/4 < \lambda < 2/3$, a period-incrementing cascade with chaotic windows is observed, Figure 2-5b, and

- if $0 < \lambda < 1/4$, a period-incrementing cascade with coexisting periodic orbits is observed, Figure 2-5c.

By chaotic window we mean that there exists an interval of the bifurcation parameter, between two periodic orbits, in which a chaotic attractor exists.

2.3.1 Experimental Validation of Non-smooth Systems

In this Section we discuss more recent developments in experimentally validating non-smooth models. The approximation of these mechanical systems by a simple model such as the impact oscillator (2.21) with reset law (2.22) has been validated in recent experiments. Piiroinen et al's [99] experimental set-up comprises a forced pendulum impacting a fixed obstacle with low velocity so that the pendulum is near grazing. Their comparison of the experimental data with simulations of the ODE model (2.21) and (2.22), as well as with the square-root normal form map derived by applying the discontinuity mapping, shows good qualitative agreement. In particular, non-smooth phenomena observed and predicted by the map include the sudden transition from a periodic orbit to chaos as well as the period-incrementing cascade. Furthermore, good quantitative agreement has been shown between the numerical simulation and the square-root map.

Similar good correspondence between model and experiment has been observed for more complicated impacting systems. Ing et al [60] present the impact oscillator with an elastic obstacle near grazing. They find sudden transitions from periodic orbits to

chaos. However, they focus on comparing periodic orbits predicted numerically and periodic orbits observed experimentally for the same system set-up. The two data sets, the numerical and the experimental, of the same periodic orbit agree well with each other.

Alzate et al consider the cam-follower system [4], an impact oscillator where the obstacle is in motion as well. The non-smooth phenomena observed here is chattering and aperiodic behaviour.

Davis and Virgin [30], who also investigate an impact oscillator with a moving obstacle, a rigid pendulum driven by a rotating obstacle, present a more realistic impact law. As the energy at impact is also converted into heat, sound and vibration, they argue that the resulting uncertainty in the measurement of the coefficient of restitution should be taken into account by including a random component. The investigation of high velocity impacts leads to corresponding experimental and numerical data.

2.4 Magnetic Bearing Systems

We will now give a brief introduction into the engineering application, called **magnetic bearing systems**, which will be studied in Chapters 5 and 6. Following the introduction of the basic set up to model a magnetic bearing system, we outline the possible motion in such a system.

A magnetic bearing system, Figure 2-6, consists of a cylindrical shaft, also referred to as a **rotor**, which is attached to a motor at one end and is free at the other. The motor spins the rotor at a constant speed Ω. The shaft is supported by magnetic bearings, which form a circular boundary, called a **stator**. In this Thesis we assume that the stator is fixed and rigid. The support from magnetic forces is three fold: it keeps the rotor levitating, it provides control and it stabilises the rotor motion [22, 41, 89].

In Chapters 5 and 6 we study a two-dimensional cross section of the systems at the free end, Figure 2-6. The rotor is a disk with mass m and radius R and the fixed and rigid stator is the impact surface in the shape of a circle. The imbalance in the disk is represented by the eccentricity radius e_c, which is the distance between the rotor's centre and the rotor's centre of mass and the eccentricity angle ϕ, Figure 2-6. The clearance disk with radius c_r denotes the area in which the rotor has free motion. The position of the rotor centre will be expressed either in Cartesian coordinates $(\tilde{x}, \tilde{y})$, in polar coordinates $(\tilde{r}, \tilde{\theta})$ or in complex coordinates $z = \tilde{x} + i\tilde{y}$.

The normal operational mode occurs when the rotor does not come into contact with the stator, i.e. in free motion, also referred to as non-contacting motion, which is frictionless. The effect of the mass imbalance on the rotor motion gives rise to a trajectory that is contained within the clearance circle. We say that the rotor's motion

is **synchronous** if the angular velocity (at the rotor centre) is the same as the rotational speed Ω.

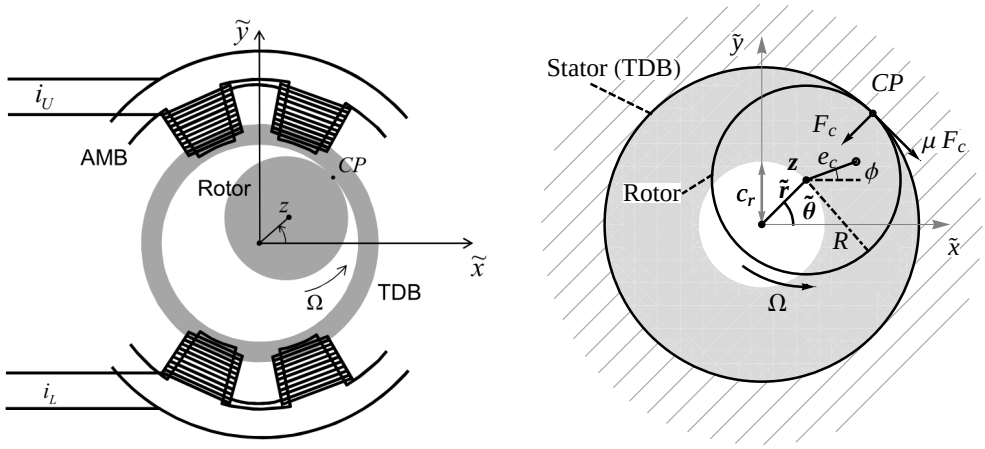

Figure 2-6: *Fixed Frame: (2-6a) The active magnetic bearing (AMB) currents, i_U and i_L, are shown in the vertical axis only. With appropriate control, these determine the AMB stiffness and damping characteristic. (2-6b) The rotor-touchdown bearing (TDB) impact at the contact point CP, contact force F_c and frictional force μF_c are acting. The rotor centre is shown in both complex coordinate z and polar coordinates $(\tilde{r}, \tilde{\theta})$. In free flight its motion is constrained to be within the clearance disk (white). The rotor is affected by mass imbalance with eccentricity e_c and phase angle ϕ.*

An impact between rotor and stator can occur if there is a power failure or some other type of electrical fault in one of the components. If, as a result, the magnets do not support the rotor any longer, then this fault is referred to as **delevitation**, [22, 41, 89, 50]. This motion will not be investigated in this Thesis. Other faults can include mass loss, i.e. additional mass imbalance arises due to a change in mass of the rotor or stator [22, 41, 89, 50].

We assume that if an impact occurs, the magnetic bearing system remains operational, i.e. the motor spins the rotor which is still fully supported by magnetic forces. An impact can lead to further instantaneous impacts which in turn can lead to continuous contact via a chattering sequence [34]. Chattering sequences are investigated in Chapter 6.

Continuous contact is referred to as **rubbing** [89, 50], which can be in a forward sense if the tangential velocity is positive, called **forward rubbing**, or in a backward sense if the tangential velocity is negative, called **backward rubbing** [89, 50]. Continuous contact can be pure sliding, a combination of rolling and sliding, or pure rolling. Pure rolling in a backward sense is referred to as **backward whirl rubbing** [11, 89, 50]. In Chapters 5 and 6 we mainly study instantaneous impacts and briefly look at synchronous forward rubbing.

CHAPTER 3

The Piecewise Power Law Maps with Exponent $p \in [0, 1]$

Analysing and describing the intricate dynamics of applications that are modelled by piecewise-smooth ODEs or hybrid systems can often be achieved by approximating them by a piecewise smooth one-dimensional map, [34], parametrised by μ. Such applications arise in electrical [34], mechanical [90] or biological [16] systems as discussed in Chapter 2. Two maps of that kind have been studied in great detail in the literature, i.e. the piecewise-linear map and the square-root map. The continuous and discontinuous linear maps are well understood now, see for example [7, 6, 59, 34, 101] and the references therein. Similarly, the continuous square-root map has been studied in great detail, [90, 91, 24]. In summary, these findings conclude that in the vicinity of a border-collision bifurcation at $\mu = \mu^*$ (as defined in Chapter 2: When a fixed point of the map intersects a discontinuity boundary) these maps, continuous or discontinuous, have a qualitatively different dynamic behaviour of great complexity for certain parameters. Such dynamic behaviour, which was already introduced in Chapter 2.3 and repeated here for clarity, can include

- *the period-incrementing cascade*: a cascade of periodic orbits where a period-N orbit bifurcates into a period-$(N + 1)$ orbit as the bifurcation parameter, μ, is increased (decreased) towards μ^*, [6],
- *the period-adding cascade* (also called a Farey Tree): The periodic orbits of this cascade are organised such that at the parameter values between two neighbouring periodic orbits, say of period-N and period-M, there exists a period-$(N+M)$ orbit. This concatenation of neighbouring periodic orbits can continue ad infinitum [34],

- *robust chaos*: a chaotic attractor, which is uninterrupted by windows of stable periodic orbits, exists over an open interval of parameter values of μ close to μ^*, [10].

We see examples of all three types in Figures 3-2 and 3-11.

In our analysis of such maps we will distinguish between regimes of the bifurcation parameter where stable periodic orbits can coexist, and regimes where the range of values of μ, for which different stable periodic orbits exist, are separated by bands of chaos. In our study the existence of chaotic attractors (and hence ranges of chaotic windows or robust chaos) is shown by finding trapping regions for the map and then by proving that no periodic orbit is stable in this region for the same parameter value.

Piecewise-smooth one-dimensional maps of linear and square-root form were originally introduced in the study of grazing phenomena [90, 91, 92, 123, 47, 48].

More recently attention has shifted to studying the parametrised discontinuous square-root map which arises, for example, when considering impacts of a mass with a repelling wall near grazing as Pring and Budd [102] have shown. As described in Chapter 2 they apply the *zero-time discontinuity mapping* to derive an appropriate two-dimensional map and furthermore, by assuming that the system has high damping, they reduce this to a one-dimensional discontinuous map. A novel dynamical feature has been shown to exist, [38, 102], where for certain parameter values the period-incrementing cascade is interrupted by a window of chaos. By that we mean that stable periodic orbits of low and high period exist but orbits with intermediate period cease to be stable. For example, period-N orbits are stable if $2 \leq N \leq 5$ and $N \geq 8$, but unstable if $6 \leq N \leq 7$. Banerjee and Dutta [38] refer to this scenario as a *breakdown of period-incrementing cascade*. For the same parameters only robust chaos is observed for the continuous square-root map. This emphasizes that the interplay of the map's nonlinearity, discontinuity and other parameters needs to be investigated in more detail to obtain a clear picture of the dynamics and bifurcation structure. In this Chapter we will do this by studying a general map for which all the previous maps are special cases. New general conditions are derived which identify for what parameters the characteristic dynamic behaviour mentioned above occurs.

Let H be a smooth function $H : \mathbb{R} \mapsto \mathbb{R}$ given by

$$H(x) = x.$$

Throughout this Chapter we will consider a piecewise-smooth map with one discontinuity boundary $\Sigma = \{x : H(x) = 0\}$ where the LHS is linear and the RHS has local

power law form x^p given by

$$x_{n+1} = f(x_m; p, \ell) = \begin{cases} f_L(x_n) = \lambda x_n + \mu, & \text{if } H(x_n) < 0 \\ f_R(x_n) = -\eta x_n^p + \mu - \ell, & \text{if } H(x_n) > 0 \end{cases} \tag{3.1}$$

where we assume in this Chapter that $p \in [0,1]$, $\lambda \in (0,1)$, $\mu \in \mathbb{R}$, $\eta > 0$ and that the discontinuity $\ell \in \mathbb{R}$. This map (see Figure 3-1), which we will refer to as the **piecewise power law map (PPL map)**, is continuous for $\ell = 0$ and discontinuous otherwise. Furthermore, the RHS derivative, df_R/dx given by

$$df_R/dx = -p\eta x_n^{p-1}$$

becomes unbounded as x_n tends to zero from the right if $p \in (0,1)$. This results in significant stretching of f_R for small x_n, i.e. the slope of f_R is very steep. In contrast the LHS derivative given by

$$df_L/dx = \lambda$$

is bounded and lies in the interval $(0,1)$ for any negative x_n.

Since this system contains four different parameters it is usual practice to scale out one of them. However, we refrain from this as it makes comparisons to any of the past results on the continuous and discontinuous piecewise linear or square-root maps, e.g. in [34], very simple.

Another aim of this Chapter is to generalise the conditions under which the period-incrementing cascade arises in the map (3.1). We will show how these conditions depend on the exponent of (3.1), p, and on the size of the discontinuity of (3.1), ℓ. Further, we investigate why certain dynamics such as the breakdown of the period-incrementing cascade can be found only in particular maps. We present results for both a positive and a negative discontinuity. The latter case could arise when analysing impacts with an attracting wall, as might result, for example, in systems with electrostatic or magnetic attraction.

The analysis of the map (3.1) is undertaken by studying admissible period-N periodic orbits, given by the finite sequence $\{x_n\}_{n=1}^N$ with $N \in \mathbb{N}$. Equivalently, this sequence can be described by a finite symbolic sequence using the letters $\mathcal{L}$ and $\mathcal{R}$. Label a point x_n of the period-N periodic orbit by

$$\mathcal{L} \quad \text{if} \quad x_n < 0 \qquad \text{and} \qquad \mathcal{R} \quad \text{if} \quad x_n > 0$$

where $n \in \{1, 2, 3, \ldots, N\}$. The order of the letters $\mathcal{L}$ and $\mathcal{R}$ corresponds to the order of the points x_n with $n = \{1, \ldots, N\}$. As an example, consider the period-4 periodic orbit illustrated in Figure 3-1 with corresponding symbolic sequence $\mathcal{LLLR}$ or $\mathcal{L}^3\mathcal{R}$. This orbit is cyclic if and only if $x_5 \equiv x_1$ and exists provided the points x_n (with

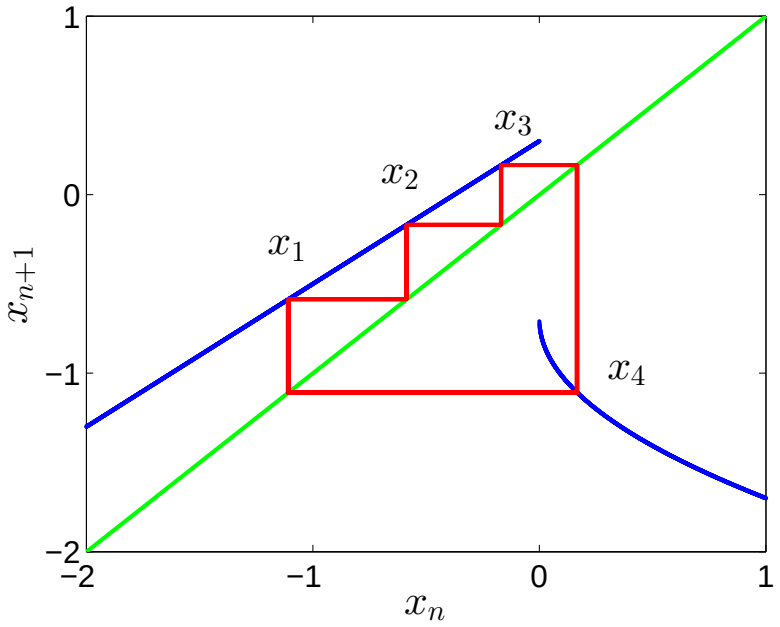

Figure 3-1: *Piecewise-smooth map with parameters $\lambda = 0.8$, $\mu = 0.3$, $\eta = 1$ and $\ell = 1$ (in blue). The intersections of the red line with the map depicts a period-4 periodic orbit of the form $\mathcal{L}^3\mathcal{R}$, i.e. three intersections with f_L and one intersection with f_R.*

$n \in \{1, 2, 3, 4\}$) satisfy the existence condition given by

$$x_1 < x_2 < x_3 < 0 < x_4 \tag{3.2}$$

where the points of the sequence $\{x_n\}_{n=1}^4$ are given by

$$x_1 = f_R(x_4) \quad \text{and} \quad x_n = f_L(x_{n-1}) \quad \text{for} \quad n \in \{2, 3, 4\}.$$

If any of the inequalities in (3.2) do not hold then the periodic orbit does not exist. Moreover, these symbolic sequences are shift invariant, i.e. $\mathcal{L}^3\mathcal{R} \equiv \mathcal{L}^2\mathcal{R}\mathcal{L} \equiv \mathcal{L}\mathcal{R}\mathcal{L}^2$. In general, periodic orbits can have many different symbolic sequences. We will now introduce two particular sequences that will be studied in more detail in this and the next Chapter.

Definition 3.1. *A period-N periodic orbit given by the symbolic sequence $\mathcal{L}^{N-M}\mathcal{R}^M$ exists with $N, M \in \mathbb{N}$ if and only if the points x_n of the sequence $\{x_n\}_{n=1}^N$ satisfy*

$$x_1 < x_2 < \ldots < x_{N-M} < 0 < x_{N-M+1} < \ldots < x_N \quad \textit{with} \quad x_1 = x_{N+1}$$

where the iterates x_n are given by

$$x_1 = f_R(x_N), \quad x_n = f_L(x_{n-1}) \quad \textit{for} \quad n = \{2, \ldots, N - M + 1\} \quad \textit{and}$$
$$x_n = f_R(x_{n-1}) \quad \textit{for} \quad n = \{N - M + 2, \ldots, N\}.$$

Periodic orbits of this form have been shown to be present in period-adding cascades of piecewise linear maps [34, 101, 7, 8] and of the more general map (3.1) as we will show in this and the next Chapter.

Definition 3.2. *A period-N orbit corresponding to the symbolic sequence $\mathcal{L}^{N-1}\mathcal{R}$ is called a* ***maximal periodic orbit****.*

The maximal periodic orbit exists if and only if the points x_n of the sequence $\{x_n\}_{n=1}^{N}$ satisfy

$$x_1 < x_2 < \ldots < x_{N-1} < 0 < x_N \tag{3.3}$$

where the iterates x_n are given by

$$x_1 = f_R(x_N) \quad \text{and} \quad x_n = f_L(x_{n-1}) \quad \text{for} \quad n = \{2, 3, \ldots, N - 1\}. \tag{3.4}$$

Period-incrementing cascades have been shown to be composed of maximal periodic orbits in piecewise linear maps [34, 6, 7, 5, 8, 9, 16, 59, 31], in square-root maps [34, 90, 91, 92, 38, 8, 102, 24, 17], and for the map (3.1) as we will see later in this Chapter.

We will show that when the discontinuity takes the form $\ell > 0$, independent of any other parameter values, then the period N of stable maximal periodic orbits tends to infinity as the bifurcation parameter μ tends to zero from above. However, this is not the case when $\ell \leq 0$, as we will also show in this Chapter. Analytically we show that when $\ell = 0$, the maximal period orbits cease to exist near $\mu = \mu^* \equiv 0$ and instead we see robust chaos. When $\ell < 0$, then numerical results indicate the existence of other periodic orbits with symbolic sequences $\mathcal{LR}^{2N}$ and $\mathcal{LR}^{2N-1}$. $\mathcal{LR}^{2N}$ orbits are organised in a period-incrementing cascade-like structure, by which we mean that the period increases incrementally by two and not one, while $\mathcal{LR}^{2N-1}$ orbits are organised in a period-adding scenario. To obtain analytical results when $\ell < 0$ we will study a simplified version of the map (3.1), where we assume that the LHS multiplier $\lambda = 0$.

The remainder of this Chapter is organised in the following way. We analyse the dynamic behaviour of the continuous PPL map ($\ell = 0$) in Section 3.1. Then we move on to studying the discontinuous PPL map with $\ell > 0$ in Section 3.2 and with $\ell < 0$ in Section 3.3. A comparison of the dynamics of the various maps (linear, nonlinear, continuous and discontinuous) is presented towards the end of each Section.

3.1 The Continuous PPL Map: $\ell = 0$

Throughout this Section we consider the map $f(x_n; p, \ell)$ given by (3.1) with $\ell = 0$, which we will refer to as the continuous power law map $f(x_n; p, 0)$. The square-root map [34] is a special case of this map, i.e. the continuous map $f(x_n; 1/2, 0)$, given by (3.1) with $p = 1/2$ and $\ell = 0$, and has been discussed in literature extensively [34, 90, 91, 92, 24, 17]. In Chapter 2 the three qualitatively different bifurcation scenarios have been summarised, i.e.

- robust chaos,
- period-incrementing cascade with chaotic windows, and
- period-incrementing cascade with coexisting periodic orbits.

We will show in this Section that these bifurcation scenarios are also found in the continuous PPL map and we derive the parameter conditions under which they occur. Moreover, the intricate and until now unknown dependence of the bifurcation scenarios on the exponent p is revealed.

We assume initially that

$$\lambda \in (0, 1), \quad p \in (0, 1), \quad \eta > 0, \quad \text{and that} \quad \mu < 0. \tag{3.5}$$

In this case the continuous PPL map $f(x_n; p, 0)$ (3.1) has exactly one admissible fixed point at $x = x_L$ given by

$$x_L = \mu/(1 - \lambda) < 0. \tag{3.6}$$

The orbit in (3.6) is stable as the corresponding eigenvalue λ lies in the interval $(0, 1)$. If μ is increased then at the parameter value

$$\mu \equiv \mu^* = 0$$

the fixed point $x = x_L \equiv 0$ undergoes a border-collision bifurcation (as defined in Chapter 2), i.e. it collides with the discontinuity boundary Σ. For $\mu > 0$ the fixed point x_L becomes virtual and we observe complex dynamics for μ close to $\mu^* = 0$. In this dynamics we see periodic orbits and possibly windows of chaotic behaviour of the various forms described at the beginning of this Chapter. The resulting dynamics for $\mu > 0$ depends on the exponent, p, and the left eigenvalue, λ, and is presented in the following Theorem.

Theorem 3.3. *Consider the map $f(x_n, p, 0)$ given by (3.1), with $\ell = 0$ and exponent p, where $0 < p < 1$. Let $N \in \mathbb{N}$, $\lambda \in (0, 1)$, $\eta > 0$ and define the parameters λ_1 and λ_2*

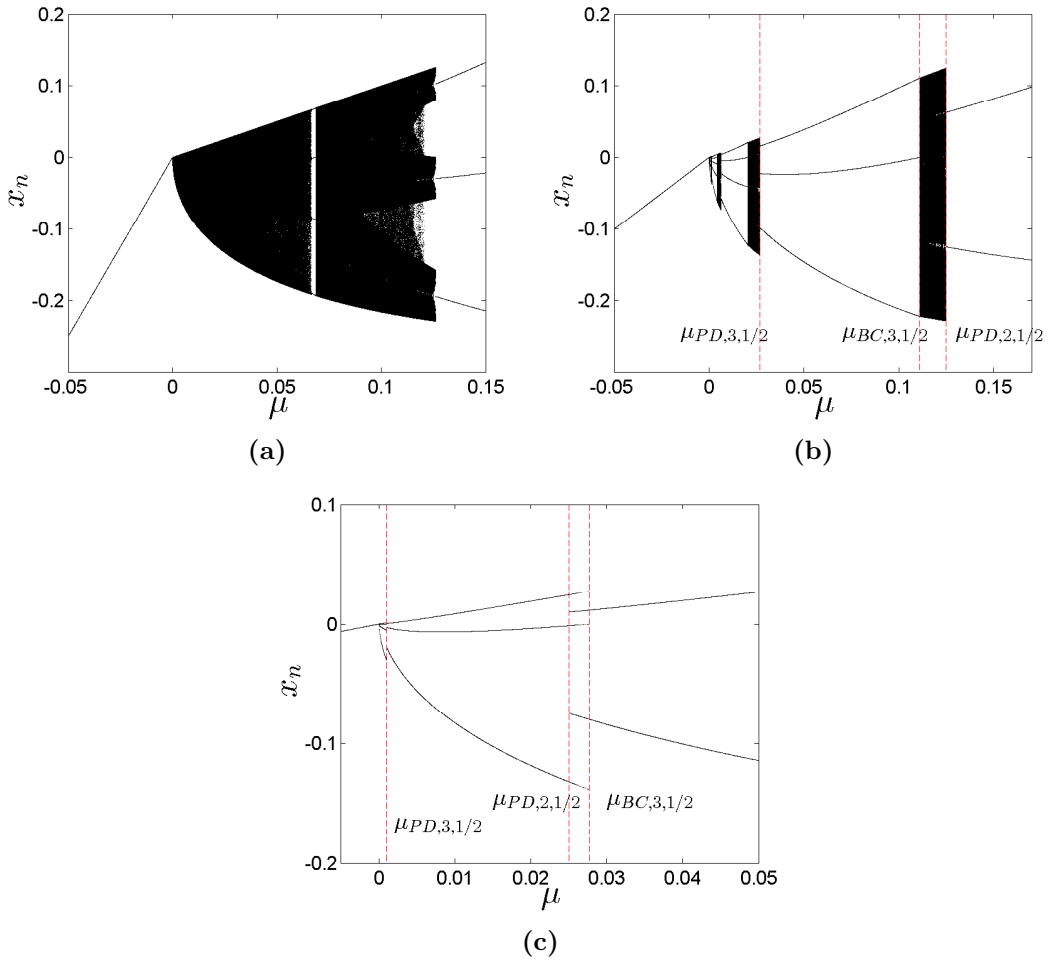

Figure 3-2: *The bifurcation structure of the continuous PPL map $f(x_n; 1/2, 0)$ with $\eta = 1$. For $\mu < 0$ we observe the stable fixed point x_L given by (3.6). This fixed point undergoes a border-collision bifurcation at $x^* = 0$, $\mu^* = 0$. By Theorem 3.3 three qualitatively different bifurcation scenarios can be observed for $\mu > 0$: the weakly stable case ($\lambda = 0.8$) in Figure 3-2a, the intermediate case ($\lambda = 0.5$) in Figure 3-2b, and the strongly stable case ($\lambda = 0.2$) in Figure 3-2c. The period-doubling $\mu_{PD,N,1/2}$ and border-collision $\mu_{BC,N,1/2}$ bifurcation values of the period-N periodic orbits with $N = 2, 3$ and $N = 2$, respectively, are shown.*

to be

$$\lambda_1 := \frac{1}{1+p} \quad \textit{and} \quad \lambda_2 := 1 - p(1+p)^{(1-p)/p}, \tag{3.7}$$

respectively, and the parameters $\mu_{PD,N,p}$ *and* $\mu_{BC,N,p}$ *to be*

$$\mu_{PD,N,p} := (1+p)(1-\lambda)\left(p^p \eta \lambda^{N-1}\right)^{\frac{1}{1-p}}, \tag{3.8}$$

$$\mu_{BC,N,p} := \left(\eta(1-\lambda)\lambda^{N-2}\right)^{\frac{1}{1-p}}, \tag{3.9}$$

respectively. Then the bifurcation scenario, for small $\mu > 0$*, which depends on* λ*,* p *and* $\eta > 0$*, takes three qualitatively different forms:*

I The weakly stable case *if* $\lambda_1 < \lambda < 1$

for which robust chaos is observed for $\mu \in (0, \mu_1)$*.*

II The intermediate case *if* $\lambda_2 < \lambda < \lambda_1$

for which a period-incrementing cascade consisting of maximal periodic orbits of the form $\mathcal{L}^{N-1}\mathcal{R}$ *is observed. As* $\mu \to 0^+$ *the period* $N \to \infty$*. The stable period-*N *maximal periodic orbit exists for* $\mu \in (\mu_{PD,N,p}, \mu_{BC,N,p})$ *for* N *large, i.e. the unstable orbit gains stability in a period-doubling bifurcation at* $\mu = \mu_{PD,N,p}$ *and ceases to exist in a border-collision bifurcation at* $\mu = \mu_{BC,N,p}$*. Note that for large* N *the existence interval boundary points are scalable, i.e.*

$$\frac{\mu_{BC,N+1,p}}{\mu_{BC,N,p}} = \frac{\mu_{PD,N+1,p}}{\mu_{PD,N,p}} = \lambda^{1/(1-p)}.$$

A chaotic attractor is observed for $\mu \in (\mu_{BC,N+1,p}, \mu_{PD,N,p})$ *for all* N *large.*

III The strongly stable case *if* $0 < \lambda < \lambda_2$*.*

This case is very similar to the intermediate case *with the exception that no chaotic attractor exists for* $\mu > 0$*. Instead the neighbouring maximal periodic orbits with period-*N *and* $(N+1)$ *coexist for* $\mu \in (\mu_{PD,N,p}, \mu_{BC,N+1,p})$ *and* N *large.*

These bifurcation scenarios are illustrated in Figure 3-2. Furthermore, we plot the boundary points of these bifurcation scenarios, i.e. λ_1 and λ_2, against the exponent p. This shows that if $p \in (0,1)$ then all three bifurcation scenarios can occur depending on λ, whereas if $p = 0$ then only the strongly stable case can occur for all $\lambda \in (0,1)$. If $p = 1$ then both the weakly stable case and the intermediate case are possible but not the strongly stable case. This will be discussed in more detail following the proof.

Proof. To prove this result we will generalise a similar argument to the ones presented in [34] (§4.3.1), [91] and [17] where the conditions for the equivalent bifurcation scenarios of the square-root map have been derived. The main idea is to construct an interval V

in a rescaled variable and a discontinuous map $F : V \to V$. F maps V back to itself under the iteration of f, i.e. several of the iterations lie on the linear side of f ($x < 0$) while exactly one iteration lies on its nonlinear side ($x > 0$). We refer to the map F as an induced map and V as a trapping region. When the number of iterates on the linear side is large then F can be approximated by a function G. We will show that by exploiting the invariance of the function G under the rescaling

$$\mu \to \lambda^{\frac{1}{1-p}}\mu$$

the study of the fixed points of G and hence F can be simplified. Thus enabling us to determine periodic orbits of $f(x_n; p, 0)$ given by (3.1) and their role in the creation of a period-incrementing cascade.

Consider the continuous PPL map (3.1) with $\ell = 0$, $0 < p < 1$, $\lambda \in (0,1)$, $\eta > 0$ and small $\mu > 0$. Define the interval W, given by

$$W = \{x : 0 < x \leq \mu\},$$

and let the initial value $x_0 \in W$. In the interval W, $|f_R'(x)|$ is large for small enough μ and hence

$$x_1 = f(x_0) = -\eta\, x_0^p + \mu < 0.$$

At the same time the slope of $f_L(x)$ lies in the interval $(0,1)$. Consequently, a large number of iterates of the continuous map, say up to $m(x_0, \mu)$, can lie on the linear part f_L of the piecewise smooth map f, where these iterates x_n with $1 \leq n \leq m-1$ are given by

$$x_n = \frac{1-\lambda^n}{1-\lambda}\,\mu - \eta\,\lambda^{n-1}x_0^p < 0.$$

We define x_m to be the first such iterate which lies again in W which must exist as $\lambda < 1$. This shows that W is in fact a trapping region, i.e. it is mapped to itself by the iterations of the map f. When $x_0 = \mu$ then $m(x_0, \mu)$ attains its maximum $N(\mu)$. As x_0 decreases towards zero, $N(\mu)$ decreases.

Assume that $x_0 \in W$ and consider the following change in coordinates

$$y_0 = 1 - x_0(1-\lambda)/\mu.$$

Thus the corresponding trapping region to W is V which is given by

$$V = \{y_0 : \mu\,\lambda \leq \mu\big(1 - y_0(1-\lambda)\big) < \mu\}$$

and the iterate corresponding to x_m is y_m which is given by

$$y_m = \lambda^m \mu + \eta(1-\lambda)\lambda^{m-1}\mu^p\Big(\frac{1-y_0}{1-\lambda}\Big)^p.$$

We now define the induced map $F : V \to V$ given by

$$\begin{aligned} F(y_0) &= y_m \\ &\equiv \lambda^m \mu + \eta(1-\lambda)\lambda^{m-1}\mu^p\Big(\frac{1-y_0}{1-\lambda}\Big)^p, \end{aligned} \tag{3.10}$$

which is induced by consecutive actions of the function f. The map F has N continuous branches. If m is constant then the map F, given by (3.10), is continuous in the interval V_N denoted by

$$V_m = \{y_0 : \mu\,\lambda \le F(y_0) < \mu\}.$$

At the point where m increases or decreases F is discontinuous. To study the structure of F we approximate it by a simpler function G for large m. To do this, let $y_0 = \lambda$, or equivalently $x_0 = \mu$, then $F(\lambda)$ which is given by

$$F(\lambda) = \eta(1-\lambda)\lambda^{N-1}\mu^p + \lambda^N\mu \tag{3.11}$$

which corresponds to branch N. Then consider the following expression

$$\Big(\frac{\lambda}{F(\lambda)/\mu}\Big)^{\frac{1}{1-p}} = \Big(\frac{\lambda}{\eta(1-\lambda)\lambda^{N-1}\mu^{p-1} + \lambda^N}\Big)^{\frac{1}{1-p}}. \tag{3.12}$$

For large N the expression (3.12) is approximated by

$$\Big(\frac{\lambda}{\eta(1-\lambda)\lambda^{N-1}\mu^{p-1}}\Big)^{\frac{1}{1-p}} = \frac{\mu}{(\eta(1-\lambda)\lambda^{N-2})^{\frac{1}{1-p}}}.$$

Define the parameter s to be this approximation, i.e.

$$s = \frac{\mu}{(\eta(1-\lambda)\lambda^{N-2})^{\frac{1}{1-p}}} \approx \Big(\frac{\lambda}{F(\lambda)/\mu}\Big)^{\frac{1}{1-p}} \tag{3.13}$$

for large N. Observe the strong self-similarity of s under the rescaling

$$\mu \to \lambda^{\frac{1}{1-p}}\mu. \tag{3.14}$$

By that we mean that the parameter s remains the same if we increase the period N by one, i.e. $N \to N+1$, and substitute μ with (3.14). This is the crucial property that enables the analysis of the scaling behaviour of the periodic orbits as we vary the parameter.

Next we show that, $s \in (\lambda^{1/(1-p)}, 1]$. As F is continuous on V_M and

$$\lambda\mu \leq F(y_0) < \mu,$$

then it follows that this inequality also holds if $y_0 = \lambda$ and if $m = N$ with N large. Hence, by (3.13)

$$\lambda\mu \leq F(\lambda) \approx \frac{\lambda}{s^{1-p}} < \mu,$$

where $F(\lambda)$ is given by (3.11). Solving this inequality for s we obtain $s \in (\lambda^{1/(1-p)}, 1]$.

Finally, we can approximate the function F by a simpler function G. To avoid confusion in later notation let $z = y_0$. Set $k = N - m$, where $k \in \mathbb{N}_0$, and consider

$$\begin{aligned}\frac{F(z)}{\mu} &= \eta(1-\lambda)\lambda^{N-k-1}\mu^{p-1}\Big(\frac{1-z}{1-\lambda}\Big)^p + \lambda^{N-k} \\ &= \frac{\lambda^{1-k}}{\lambda}\Big(\frac{1-z}{1-\lambda}\Big)^p \frac{F(\lambda)}{\mu} + \lambda^{N-k}\Big(1 - \Big(\frac{1-z}{1-\lambda}\Big)^p\Big) \\ &\approx \lambda^{1-k}s^{p-1}\Big(\frac{1-z}{1-\lambda}\Big)^p =: G(z,s) \end{aligned} \tag{3.15}$$

where in the last step we assumed that N is large in comparison to $k \geq 0$. Then, the function $G(z,s)$, as defined in (3.15), is an approximation of $F(z)/\mu$ and defined for all $k \geq 0$. Like the map F, the map G is discontinuous. But whereas F has a finite number of branches, N, the map G has infinitely many, i.e. $k \geq 0$ which is illustrated in Figure 3-3. Along these branches the number k is constant as shown in Figure 3-3. Let us now consider the first derivative of G, which is given by

$$G_z(z,s) = -\frac{p\lambda^{1-k}s^{p-1}}{1-\lambda}\Big(\frac{1-z}{1-\lambda}\Big)^{p-1}. \tag{3.16}$$

We will now show that as z increases $G_z(z,s)$ decreases. As

$$\lambda \leq z < 1 \quad \Rightarrow \quad \frac{1-z}{1-\lambda} \leq 1 \quad \Rightarrow \quad \Big(\frac{1-z}{1-\lambda}\Big)^{p-1} \geq 1 \tag{3.17}$$

and $-\lambda^{1-k} \leq -\lambda$ it follows that

$$G_z(z,s) < G_z(\lambda,s) = -\frac{p\lambda s^{p-1}}{1-\lambda}. \tag{3.18}$$

Hence the slope of each branch of G decreases as z, or equivalently k, increases, see Figure 3-3. Therefore, each branch k of the map G has a unique fixed point. Let z_k denote the fixed point of the k^{th} continuous branch of the map G, i.e. z_k satisfies the

equation

$$G(z_k, s) \equiv \lambda^{1-k} s^{p-1} \Big(\frac{1 - z_k}{1 - \lambda} \Big)^p = z_k. \tag{3.19}$$

Obviously, as $G(z_k, s)$ has infinitely many branches, it has infinitely many fixed points $z = z_k$. The most likely stable fixed point is z_0 by (3.16) and (3.18).

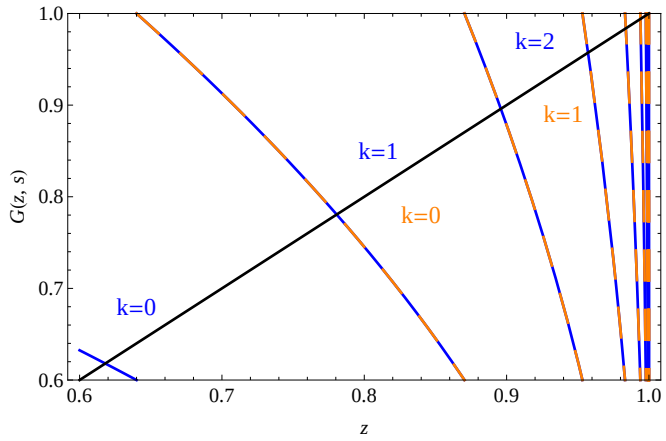

Figure 3-3: *The discontinuous induced map G given by* (3.15) *with $p = 1/2$, $\eta = 1$, $\lambda = 0.6$ and $s = 0.9$ (blue) as well as with $s = \lambda^{1/(1-p)}\, 0.9$ (orange, dashed). It has k branches, where $k \geq 0$, and each branch intersects the identity line (black) yielding a fixed point. The blue and orange branches are identical as G remains the same when s is scaled according to* (3.14) *and k is increased by one.*

Using (3.19), $G_z(z, s)$ can be rewritten such that it only depends on the fixed point z_k, i.e.

$$G_z(z_k, s) = -\frac{p z_k}{1 - z_k}. \tag{3.20}$$

We will now make predictions about the dynamics of the map G which also hold for the map F, for large N in comparison to k, and for the map $f(x_n; p, 0)$ given by (3.1). The stability of these fixed points give rise to three topologically different dynamics.

I The weakly stable case: Assume that $\lambda_1 < \lambda < 1$ where λ_1 is defined in (3.7). Then, it follows that

$$-p < -\frac{1 - \lambda}{\lambda}. \tag{3.21}$$

Above, we have shown that $s \in (\lambda^{\frac{1}{1-p}}, 1]$, then

$$-s^{p-1} < -1. \tag{3.22}$$

Hence, by using (3.18) we conclude that the first derivative

$$\begin{aligned} G_z(z_k, s) &< -\frac{p\lambda s^{p-1}}{1 - \lambda}, \qquad \forall z_k \in [\lambda, 1) \\ &< -1, \qquad \text{by (3.21) and (3.22).} \end{aligned}$$

Thus the map G, given by (3.15), has no stable fixed points and hence the map F, given by (3.10), has no stable fixed points. We can now make use of the fact that, in one-dimensional maps only two types of attractors exist, i.e. stable periodic orbits or chaotic attractors. Thus, we have shown that for $\mu > 0$ and large m the continuous power law map $f(x_n; p, 0)$ given by (3.1) has a chaotic attractor and no stable periodic orbits. By definition, this is robust chaos, which lies in the interval

$$\Big(\mu - \eta\,\mu^p\,, \mu\Big).$$

The intermediate case: Assume that $\lambda_2 < \lambda < \lambda_1$, where λ_1 and λ_2 are defined in (3.7). If $z_k < \lambda_1 \equiv 1/(1+p)$ then by (3.20)

$$-1 < G_z(z_k, s) < 0, \quad \forall k \geq 0$$

for at least one value of $k \geq 0$. We recall that by definition $z_k \in [\lambda, 1)$. Therefore, there exists a stable fixed point z_k for at least one value of $k \geq 0$ if $z_k \in [\lambda, 1/(1+p))$.

We now consider the leftmost fixed point z_0 and explain for which parameters λ and s it exists and is stable. Assume that s is close to one. Then from (3.19) it follows that z_0 is close to λ. Therefore, if $\lambda < \lambda_1$ and $s = 1$ then the fixed point $z_0 = \lambda$ exists and is stable. Assume further that $\lambda_2 < \lambda < \lambda_1$ and that s decreases from one. Then, by (3.19) with $k = 0$, z_0 increases and by (3.18) $G_z(z_0, s)$ decreases until the fixed point loses stability in a period-doubling bifurcation at $z_0 = \lambda_1$ and $s = s_{PD,0}$, i.e. $G_z(z_0, s_{PD}) = -1$, where

$$s_{PD,0} = (1+p)\,\lambda^{\frac{1}{1-p}}\,\Big(\frac{p}{1-\lambda}\Big)^{\frac{p}{1-p}}. \tag{3.23}$$

Moreover, if $\lambda > \lambda_2$ then $s_{PD,0} > \lambda^{1/(1-p)}$. Therefore, if $\lambda \in (\lambda_2, \lambda_1)$ and $s \in (s_{PD,0}, 1] \subset (\lambda^{(1/1-p)}, 1]$ then the fixed point $z_0 \in (\lambda, \lambda_1)$ exists and is stable. For $s \in (\lambda^{(1/1-p)}, s_{PD,0})$ there exists chaotic attractor and we discuss below why that is. In Figure 3-4 we depict the boundary points of s and their dependence on λ which visualises the regions of qualitatively different dynamics. Note that this Figure also includes results from *The weakly stable case* and from *The strongly stable case*.

The fixed point z_0 of the map G corresponds to a period-N maximal periodic orbit with N large and symbolic sequence $\mathcal{L}^{N-1}\mathcal{R}$ of the map $f(x_n; p, 0)$ given by (3.1). Assume that μ is small, then we can derive its values that are equivalent to $s \in (s_{PD,0}, 1]$ by using (3.13). Corresponding to $s = s_{PD,0}$ the maximal periodic

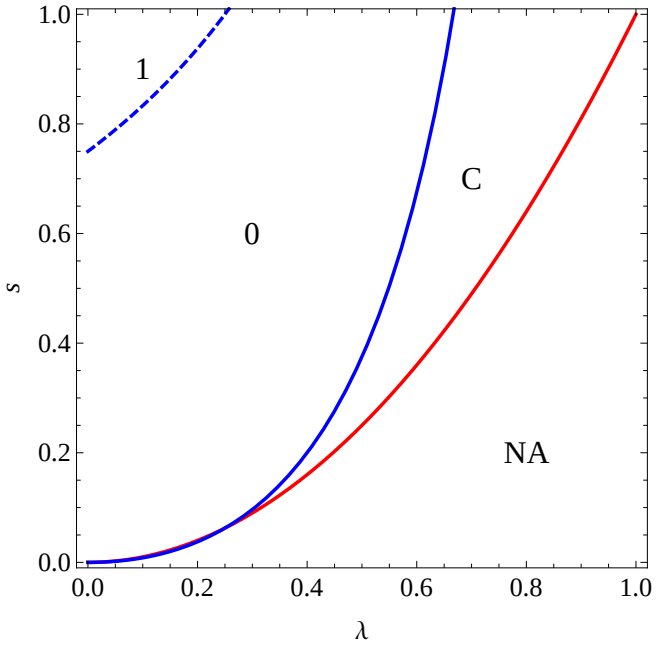

Figure 3-4: *Existence and stability of the fixed points z_k as the parameters s and λ are varied for $p = 1/2$. The curves represent the period-doubling value $s_{PD,1}$ for z_1 (blue dashed), the period-doubling value $s_{PD,0}$ for z_0 (blue), and the lower bound for s, i.e. $\lambda^{1/(1-p)}$ (red). In the region NA the parameter s lies outside the admissible interval $(\lambda^{1/(1-p)}, 1]$. In region C there exists a chaotic attractor. In region 0 the stable fixed point z_0 exists. In region 1 the stable fixed point z_1 exists.*

orbit undergoes a period-doubling bifurcation at $\mu = \mu_{PD,N,p}$, where

$$\mu_{PD,N,p} = (1+p)(1-\lambda)(p^p \eta\, \lambda^{N-1})^{\frac{1}{1-p}}. \tag{3.24}$$

The upper bound of s, $s = 1$, corresponds to a border-collision bifurcation at $\mu = \mu_{BC,N,p}$ where

$$\mu_{BC,N,p} = \left(\eta(1-\lambda)\lambda^{N-2}\right)^{\frac{1}{1-p}}. \tag{3.25}$$

Hence, the period-N maximal periodic orbit with bifurcation parameter μ exists and is stable for $\mu \in (\mu_{PD,N,p}, \mu_{BC,N,p})$ if $\lambda \in (\lambda_2, \lambda_1)$. Increasing the period N by one gives rise to the period-$N+1$ maximal periodic orbit. Note that $\mu_{BC,N+1,p} < \mu_{PD,N,p}$ for all $N \geq 2$ and hence the period-N and $N+1$ orbits do not coexist. In fact, no stable maximal periodic exists in that interval and hence we observe a chaotic attractor if $\mu \in (\mu_{BC,N+1,p}, \mu_{PD,N,p})$. This μ-interval corresponds to $s \in (\lambda^{(1/1-p)}, s_{PD,0})$.

It is straightforward to see that N tends to infinity as μ tends to zero from the right. This gives rise to a period-incrementing scenario, i.e. the period N of maximal periodic orbits increases by one as μ decreases.

Moreover, the boundary points of the existence and stability interval scale with

$\lambda^{1/(1-p)}$, i.e.

$$\frac{\mu_{BC,N+1,p}}{\mu_{BC,N,p}} = \frac{\mu_{PD,N+1,p}}{\mu_{PD,N,p}} = \lambda^{1/(1-p)}.$$

The strongly stable case: Assume that $0 < \lambda < \lambda_2$ then $s_{PD,0} < \lambda^{1/(1-p)}$ and hence s lies outside the permissible interval $(\lambda^{1/(1-p)}, 1]$. Therefore, the fixed point z_0 does not undergo a period-doubling bifurcation. As a result the fixed point z_1 on the following branch $k = 1$ is stable for μ close to one. We proceed with the stability analysis of z_1 as we did with z_0 in the *intermediate case*. Decrease μ from one, then the fixed point z_1 loses stability at a period-doubling bifurcation at the point $s = s_{PD,1}$ where

$$s_{PD,1} = (1+p)\left(\frac{p}{1-\lambda}\right)^{\frac{p}{1-p}}. \tag{3.26}$$

The value $s_{PD,1}$ has been obtained by making use of the self-similarity of s under the rescaling (3.14). Thus we can conclude that if $\lambda \in (0, \lambda_2)$ the two stable fixed points z_0 and z_1 coexist for $s \in (s_{PD,1}, 1)$, see Figure 3-4. As in the *intermediate case* the fixed points z_0 and z_1 of the map G correspond to maximal periodic orbits of period-N and $(N+1)$, respectively, of the map f. We are now able to derive the existence and stability boundary points in terms of the bifurcation parameter μ. The stable period-$N+1$ maximal periodic orbit exists for $\mu \in (\mu_{PD,N+1,p}, \mu_{BC,N+1,p})$ for all N large, where $\mu_{PD,N+1,p}$ and $\mu_{BC,N+1,p}$ are given by (3.24) and (3.25), respectively, by replacing N by $N+1$. Note that, $\mu = \mu_{PD,N+1,p}$ and $\mu = \mu_{BC,N+1,p}$ correspond to $s = s_{PD,1}$ and $s = 1$ with $k = 1$, respectively.

Similarly, corresponding to $s = 1$ with $k = 0$ the period-N maximal periodic orbit undergoes a border-collision bifurcation at $\mu = \mu_{BC,N,p}$ which is given by (3.25). However, unlike the corresponding fixed point z_0, the stable period-N maximal orbit does lose stability in a period-doubling bifurcation at $\mu = \mu_{PD,N,p}$ which is given by (3.24). We conclude this from the fact that the stable period-$(N+1)$ orbits exist for all N large within the permissible parameter interval as explained above. Finally, the period-N and $(N+1)$ maximal periodic orbits coexist for $\mu \in (\mu_{PD,N,p}, \mu_{BC,N+1,p})$.

□

In the next Section in Theorem 3.5 we will show that the lower and upper bound of the μ existence and stability interval, i.e. $\mu_{PD,N,p}$ and $\mu_{BC,N,p}$ respectively, can be computed exactly and not just for a large period N.

Now, we explain what can be deduced from Theorem 3.3 about piecewise-linear maps, i.e. as $p = 0$ or $p = 1$. Let $p = 0$. Then the map under investigation, $f(x_n; 0, 0)$ given by (3.1), is discontinuous and piecewise-linear with discontinuity $-\eta$ where f_L is

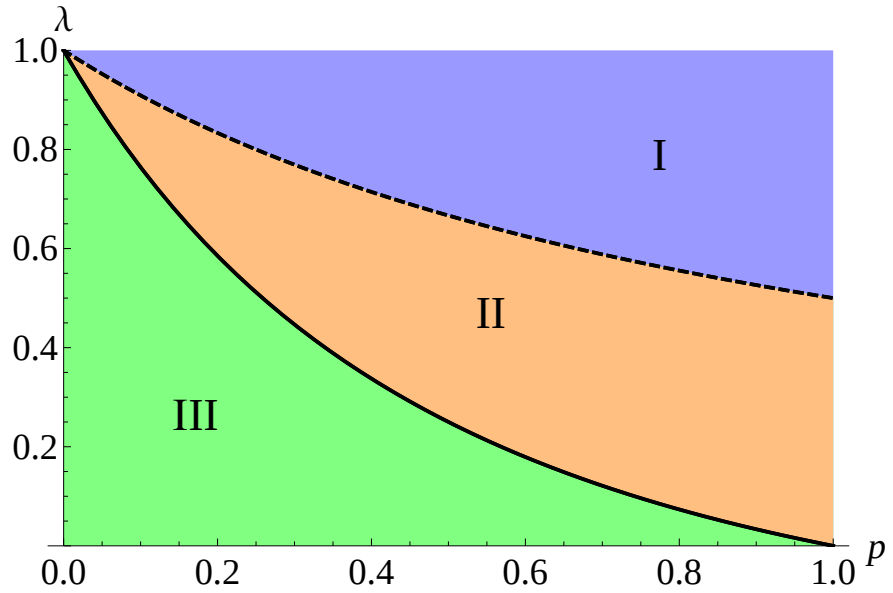

Figure 3-5: *The boundary values λ_1 (dashed) and λ_2 (black), given by* (3.7)*, against the exponent p. As described in Theorem 3.3 these boundary values separate the regions I-III in which qualitatively different bifurcation scenarios arise in the PPL map $f(x_n; p, 0)$. For the values λ and p in region I we observe* the weakly stable case*, in region II we observe* the intermediate case*, and in region III we observe* the strongly stable case.

a linear function and f_R is a constant. This map has been studied in [6]. According to Theorem 3.3 the only characteristic stable dynamics for $\mu > 0$ is the strongly stable case if $\lambda \in (0, 1)$, i.e. a period-incrementing cascade with coexisting periodic orbits (Figure 3-5). As the bifurcation parameter μ decreases towards zero, the stable period-N maximal periodic orbit is created in a border-collision bifurcation at $\mu = \mu_{BC,N,0}$ given by (3.9) for N large. Furthermore, the orbit loses stability at $\mu = \mu_{\mu PD,N,0}$ given by (3.8). Although the value of this bifurcation is predicted correctly its type is not, i.e. it is not a period-doubling bifurcation but a border-collision bifurcation. Therefore, the stable period-N maximal period orbit exists for $\mu \in (\mu_{BC2,N,0}, \mu_{BC,N,0})$ where

$$\mu_{BC2,N,0} = \frac{1-\lambda}{1-\lambda^N}\,\eta\lambda^{N-1} \equiv \mu_{PD,N,0}\,, \tag{3.27}$$

$$\mu_{BC,N,0} = \frac{1-\lambda}{1-\lambda^{N-1}}\,\eta\lambda^{N-2}. \tag{3.28}$$

We give reason for this in the next Section, when discussing the extension of the Theorem 3.3 to discontinuous maps. Moreover, neither chaotic windows nor robust chaos can arise within the parameter region that was assumed at the beginning. In other words, there exists no λ that can satisfy the other two cases, the weakly stable and the intermediate case, as both λ_1 and λ_2 are one if $p = 0$. Theorem 3.3 holds for $p = 0$ and predicts the results obtained in literature, such as [34] (pp 184-5), [7].

Let $p = 1$. Then the map under investigation, $f(x_n; 1, 0)$ given by (3.1), is continuous and piecewise-linear where both f_L and f_R are linear functions. This map has been studied by [] and its dynamics can also be predicted by Theorem 3.3. If $p = 1$ then λ_1 and λ_2, both given by (3.7), are $1/2$ and 0 respectively. By Theorem 3.3 two qualitatively different bifurcation scenarios can arise for $\mu > 0$ and N large: the weakly stable case if $\lambda \in (1/2, 1)$ and the intermediate case if $\lambda \in (0, 1/2)$. Hence there exists no $\lambda \in (0, 1)$ that satisfies the strongly stable case and therefore maximal periodic orbits never coexist. Let $\lambda \in (0, 1/2)$ and define

$$\eta_{PD,N} = \frac{1}{\lambda^{N-1}} \quad \text{and} \quad \eta_{BC,N} = \frac{1 - \lambda^{N-1}}{(1 - \lambda)\lambda^{N-2}}. \tag{3.29}$$

If $\eta < \eta_{PD,N,1}$ then $\mu_{PD,N,1}$ tends to zero as p tends to one. Furthermore, if $\eta > \eta_{BC,N}$ then $\mu_{BC,N,1}$ tends to infinity as p tends to one. Therefore, by Theorem 3.3 the stable period-N maximal periodic orbit exists for $\mu \in (0, \infty)$ for N large. This result can be better explained in terms of the parameter η. Choose η to be the bifurcation parameter. If $\lambda \in (1/2, 1)$ then for $\eta > 0$ the weakly stable case is observed. If $\lambda \in (0, 1/2)$ then for $\eta > 0$ the intermediate case is observed. It follows that a stable periodic orbit of the form $\mathcal{L}^{N-1}\mathcal{R}$ exists and is stable for $\eta \in (\eta_{BC,N}, \eta_{PD,N})$ where the boundary values are given by (3.29). With a little additional work we have shown that Theorem 3.3 also holds for $p = 1$ and agrees with results obtained in literature, such as [34] (p 146), [7] and [56].

To further support our results we now consider a special case - the map (3.1) with $p = 1/2$ which is the well understood continuous square-root map. The following example demonstrates that by applying Theorem 3.3 to this map the description of the dynamics is consistent with those in [91, 17], [34] (pp 188 - 93) and the references therein.

Example 3.4. The square-root map*: Let $p = 1/2$, $\eta = 1$ then the discrete system* (3.1) *is called the square-root map. By Theorem 3.3 its qualitatively different dynamics for $\mu > 0$ is described by the strongly stable case if $0 < \lambda < 1/4$, the intermediate case if $1/4 < \lambda < 2/3$ and the weakly stable case if $2/3 < \lambda < 1$ (Figures 3-2 and 3-5). Its stable maximal periodic orbits of the form $\mathcal{L}^{N-1}\mathcal{R}$ exist for $\mu \in (\mu_{PD,N,p}, \mu_{BC,N,p})$ where the bifurcation points are given by*

$$\mu_{PD,N,1/2} = \frac{3}{4}\lambda^{2(N-1)} \qquad \textit{and}$$
$$\mu_{BC,N,1/2} = (1 - \lambda)\lambda^{2(N-2)}.$$

3.2 The Discontinuous PPL Map I: $\ell > 0$

In the following we will analyse the dynamics of the map (3.1) when the discontinuity parameter $\ell > 0$. As in the case of the continuous map this has a stable fixed point if $\mu < 0$ which has a border-collision bifurcation at $\mu = 0$. For $\mu > 0$ complex dynamics exist. We will show that in this case, for small $\mu > 0$, we always observe a period-incrementing cascade consisting of maximal periodic orbits of the form $\mathcal{L}^{N-1}\mathcal{R}$ with large period N. Moreover period-N and period-$(N+1)$ maximal periodic orbits coexist. However, for certain values of the left multiplier λ, small values ℓ and small but finite period N the orbits are unstable and we observe a breakdown in the period-incrementing cascade, as described for the square-root map in [102] and [38]. Note that in the following Theorem the expressions for λ_1 and λ_2 are the same as in the previous Section, i.e. given by (3.7). For clarity we will restate them in the following Theorem.

Theorem 3.5. *Consider the discontinuous map* (3.1) *with discontinuity* $\ell > 0$*, exponent* $p \in (0,1)$ *and* $\eta > 0$*. Let* $N \in \mathbb{N}$*,* $\lambda \in (0,1)$ *and define the parameters* λ_1 *and* λ_2 *to be*

$$\lambda_1 := \frac{1}{1+p} \quad \text{and} \quad \lambda_2 := 1 - p(1+p)^{(1-p)/p}, \tag{3.30}$$

respectively, and the parameter $\mu_{PD,N,p}$ *to be*

$$\mu_{PD,N,p} := \frac{1-\lambda}{1-\lambda^N}\left(\lambda^{N-1}\ell + \left(p^p\eta\lambda^{N-1}\right)^{\frac{1}{1-p}}(p+1)\right). \tag{3.31}$$

The parameter $\mu_{BC,N,p}$ *cannot be defined explicitly but it is the unique solution* $\mu = \mu_{BC,N,p}$ *of the order* p *algebraic equation*

$$\left(\frac{1-\lambda^{N-1}}{1-\lambda}\right)\mu - \eta\lambda^{N-2}\mu^p - \lambda^{N-2}\ell = 0. \tag{3.32}$$

Finally, define the parameters ℓ_1 *and* ℓ_2 *to be*

$$\ell_1 := \frac{(1+p)\lambda - 1 - p\lambda^N}{1-\lambda}\left(\eta p^p\lambda^{p(N-1)}\right)^{\frac{1}{1-p}}, \tag{3.33}$$

$$\ell_2 := \frac{(1+p)(\lambda - 1 + p(1+p)^{\frac{1-p}{p}}(1-\lambda^N))}{1-\lambda}\left(\eta p^p\lambda^{p(N-1)}\right)^{\frac{1}{1-p}}, \tag{3.34}$$

respectively. Then the bifurcation scenario, for $\mu > 0$*, depends on* λ*,* p*,* η *and* ℓ *and takes three qualitatively different forms.*

Case I *if* $\lambda \in (\lambda_1, 1)$ *and* $\ell \in (0, \max_N \ell_1)$

for which there exists a finite set $N_k = \{N_1, \ldots, N_m\}$ *with*

$$3 \le N_1 < N_2 < \ldots < N_m$$

such that each $N \in N_k$ satisfies the inequality

$$\ell < \ell_1, \quad \forall N \in N_k.$$

Then robust chaos exists for $\mu \in (\mu_{PD,N_1-1,p}, \mu_{BC,N_m+1,p})$. Furthermore, there exists a finite set $N_b = \{N_{m+1}, N_{m+2}, \ldots, N_s\}$ with

$$N_m < N_{m+1} < N_{m+2} < \ldots < N_s$$

such that each $N \in N_b$ satisfies the inequality

$$\ell < \ell_2, \quad \forall N \in N_b.$$

Then stable period-N maximal periodic orbits exist for $\mu \in (\mu_{PD,N,p}, \mu_{BC,N,p})$ for all $N \geq N_m + 1$. If $\ell \in (\ell_1, \ell_2)$ then the maximal periodic orbits of period-N and $(N+1)$ are separated by a chaotic attractor which exists for $\mu \in (\mu_{BC,N+1,p}, \mu_{PD,N,p})$ for all $N \in N_b$.
If $N \geq N_s + 1$ then the period-N and $(N+1)$ maximal periodic orbits coexist for $\mu \in (\mu_{PD,N,p}, \mu_{BC,N+1,p})$.

Case II *if*

$$\lambda \in (\lambda_2, \lambda_1) \quad \textit{and} \quad \ell \in (0, \max_N l_2) \quad \textit{or} \tag{3.35}$$

$$\lambda_1 < \lambda < 1 \quad \textit{and} \quad \ell \in (\max_N \ell_1, \max_N \ell_2) \tag{3.36}$$

for which a period-incrementing cascade consisting of stable period-N maximal periodic orbits is observed. These orbits exist for $\mu \in (\mu_{PD,N,p}, \mu_{BC,N,p})$ for all $N \geq 2$. There exists a finite set $N_a = \{N_1, N_2, \ldots, N_\alpha\}$ with $3 \leq N_1 < N_2 < \ldots < N_\alpha$ such that $N \in N_\alpha$ satisfies the inequality

$$0 < \ell < \ell_2$$

if (3.35) *holds or*

$$\max_N \ell_1 < \ell < \ell_2$$

if (3.36) *holds. Then the maximal periodic orbits of period-N and $(N+1)$ are separated by a chaotic attractor which exists for $\mu \in (\mu_{BC,N+1,p}, \mu_{PD,N,p})$ for all $N \in N_a$.*
If $N \geq N_\alpha + 1$ then the period-N and $(N+1)$ maximal periodic orbits coexist for $\mu \in (\mu_{PD,N,p}, \mu_{BC,N+1,p})$.

Case III *if $\lambda \in (0,1)$ and $\ell > \max_N \ell_2$ for which a period-incrementing cascade con-*

sisting of stable period-N maximal periodic orbits is observed. The stable period-N maximal periodic orbits exist for $\mu \in (\mu_{PD,N,p}, \mu_{BC,N,p})$ for all $N \geq 2$. Furthermore, period-N and period-$(N+1)$ orbits coexist for $\mu \in (\mu_{PD,N,p}, \mu_{BC,N+1,p})$ for all $N \geq 2$.

The bifurcation scenarios of cases II and III are illustrated in Figures 3-8b and 3-8a, respectively. In Figure 3-6 we plot the functions $\max_N \ell_1$ and $\max_N \ell_2$, where ℓ_1 is given by (3.33) and ℓ_2 by (3.34), against the parameter λ for fixed parameters p and η. Finally, we plot the border-collision bifurcation value $\mu = \mu_{BC,N,p}$ and the period-doubling bifurcation value $\mu = \mu_{PD,N,p}$ against ℓ for $N = 2, ..., 28$ and while keeping the other parameters η and p fixed for the bifurcation scenario of case I. This illustrates how, for certain μ robust chaos, chaotic windows and coexisting periodic orbits arise in case I of this Theorem. Furthermore, the bifurcation scenario described in case I has been termed *breakdown in period-incrementing cascade* in [38].

Proof. Consider the discontinuous power law map (3.1) with $\lambda \in (0,1)$, $\eta > 0$, $p \in (0,1)$, $\mu > 0$ and $\ell > 0$. We will first derive the conditions for which a period-N maximal periodic orbit exists. Then we will find the conditions for which it is stable. From these conditions we will show when the cases I-III hold.
Consider the period-N maximal periodic orbit of the form $\mathcal{L}^{N-1}\mathcal{R}$ with the sequence $\{x_n\}_{n=1}^N$ of the map f given by (3.1). This orbit exists if and only if its iterates x_n satisfy (3.3) such that (3.4) holds. Note that (3.3) is equivalent to showing that

$$x_N > 0 \quad \text{and} \quad x_n < 0 \quad \text{for} \quad n = \{1, 2, \ldots, N-1\},$$

and that (3.3) can be expressed explicitly by

$$x_1 = -\eta x^p + \mu - \ell, \tag{3.37}$$

$$x_n = \lambda x_{n-1} + \mu \quad \text{for} \quad n = \{2, \ldots, N\}. \tag{3.38}$$

To show that these conditions are satisfied by the iterates x_n for $n = \{1, \ldots, N\}$, it is sufficient to show that $x_{N-1} < 0$. This follows by induction, i.e. if $x_{N-1} < 0$ then

$$x_{N-1} = \lambda x_{N-2} + \mu \quad \Rightarrow \quad x_{N-2} = \frac{x_{N-1} - \mu}{\lambda} < 0$$

as $\lambda \in (0,1)$ and $\mu > 0$. Hence, by induction, $x_n < 0$ for $n = \{1, \ldots, N-1\}$. Furthermore, if $x_1 < 0$ then

$$x_1 = -\eta x_N^p + \mu - \ell \quad \Rightarrow \quad x_N = \Big(\frac{x_1 - \mu + \ell}{\eta}\Big)^{\frac{1}{p}} > 0$$

as μ and $\ell > 0$ and if $x_1 < \mu - \ell$. Note that $\mu - \ell < 0$ for positive small μ. When

this does not hold true then we derive the necessary boundaries for ℓ. Thus we can show that $\mathcal{L}^{N-1}\mathcal{R}$ exists if $x_{N-1} < 0$. From (3.38) it can be seen that as μ increases so do x_{N-1} and x_{N-2} for fixed λ. Hence, the iterate x_{N-1} undergoes a border-collision bifurcation at $x_{N-1} = 0$ and $\mu = \mu_{BC,N,p}$. Equivalently, the period-N maximal periodic orbit exists, i.e. $x_{N-1} < 0$, if $\mu < \mu_{BC,N,p}$. Now we determine the border-collision bifurcation value $\mu_{BC,N,p}$ in terms of the other parameters λ, ℓ, N and p.
Consider the largest negative iterate x_{N-1} which satisfies

$$\begin{aligned} x_{N-1} &= f_L^{N-2} \circ f_R \circ f_L(x_{N-1}) \\ &= -\eta\lambda^{N-2}(\lambda x_{N-1} + \mu)^p - \lambda^{N-2}\ell + \mu\frac{1-\lambda^{N-1}}{1-\lambda} =: h_1(x_{N-1}). \end{aligned} \tag{3.39}$$

Rearranging (3.39) and applying the inequality $x_{N-1} < 0$ gives

$$\begin{aligned} -\lambda^{N-2}\ell + \mu\frac{1-\lambda^{N-1}}{1-\lambda} &= x_{N-1} + \eta\lambda^{N-2}(\lambda x_{N-1} + \mu)^p \\ &< \eta\lambda^{N-2}\mu^p. \end{aligned} \tag{3.40}$$

Set $x_{N-1} = 0$ into (3.39) then

$$\eta\lambda^{N-2}\mu^p - \frac{1-\lambda^{N-1}}{1-\lambda}\mu + \lambda^{N-2}\ell = 0. \tag{3.41}$$

The solution of this equation yields the border-collision value $\mu = \mu_{BC,N,p}$. This equation can be solved exactly for $p = 1/2$, as shown in [102]. However, for other values of p the border-collision bifurcation value $\mu_{BC,N,p}$ has to be computed numerically for prescribed values of η, ℓ, λ, N and p.

Next we consider the positive iterate x_N given by

$$\begin{aligned} x_N &= f_L^{N-1} \circ f_R(x_N) \\ &= -\eta\lambda^{N-1}x_N^p - \lambda^{N-1}\ell + \mu\frac{1-\lambda^N}{1-\lambda} =: h_2(x_N) \end{aligned} \tag{3.42}$$

The first derivative of $h_2(x_N)$ is negative and hence the corresponding orbit $\mathcal{L}^{N-1}\mathcal{R}$ is stable if

$$\frac{\partial(h_2(x_N))}{\partial x_N} = -p\eta\lambda^{N-1}x_N^{p-1} > -1 \tag{3.43}$$

requiring that

$$x_N > \left(p\eta\lambda^{N-1}\right)^{\frac{1}{1-p}}. \tag{3.44}$$

Hence the period-N orbit $\mathcal{L}^{N-1}\mathcal{R}$ loses stability in a period-doubling bifurcation at

$\mu = \mu_{PD,N,p}$. The value $\mu_{PD,N,p}$ is determined from (3.42) by collecting all terms involving x_N on the RHS, then applying (3.44) to it and finally solving for μ. Hence the period-N maximal periodic orbit is stable if

$$\mu > \frac{1-\lambda}{1-\lambda^N}\left(\lambda^{N-1}\ell + \left(p^p\eta\lambda^{N-1}\right)^{\frac{1}{1-p}}(p+1)\right) =: \mu_{PD,N,p}\,.$$

Therefore, a stable maximal periodic orbit exists for $\mu \in (\mu_{PD,N,p}, \mu_{BC,N,p})$. As $\mu_{BC,N,p}$ cannot be computed explicitly another condition needs to be derived to ensure that $\mu_{PD,N,p} < \mu_{BC,N,p}$. For that purpose consider the first derivative of the map $h_1(x_{N-1})$ given by (3.39)

$$\frac{\partial(h_1(x_{N-1}))}{\partial x_{N-1}} = -p\eta\lambda^{N-1}(\lambda x_{N-1}+\mu)^{p-1}. \tag{3.45}$$

This derivative is negative and if

$$x_{N-1} > \frac{1}{\lambda}\left(\left(\eta p\lambda^{N-1}\right)^{\frac{1}{1-p}} - \mu\right) =: \nu\,. \tag{3.46}$$

Then the maximal periodic orbit is stable, i.e. the derivative of $h_1(x_{N-1})$ is greater than -1. At the same time, the existence condition, $x_{N-1} < 0$, must be satisfied. This is the case if and only if

$$\mu > \left(\eta p\lambda^{N-1}\right)^{\frac{1}{1-p}} =: \mu_1. \tag{3.47}$$

This property says that if $x_{N-1} = \nu$ and $x_{N-1} = 0$ then the period-N maximal periodic orbit undergoes a period-doubling and a border-collision bifurcation at $\mu = \mu_1$, i.e.

$$\mu_1 \equiv \mu_{BC,N,p} \equiv \mu_{PD,N,p}. \tag{3.48}$$

Now, if $\ell = \ell_1$ given by (3.33) then (3.48) holds. Therefore if $\ell > \ell_1$ given (3.33) then there exists a $\mu = \mu_{PD,N,p}$ such that $\mu > \mu_1$. Hence $x_{N-1} < 0$ and $\partial h_1(x_{N-1})/\partial x_{N-1} > -1$. Therefore the stable period-N maximal periodic orbit of the form $\mathcal{L}^{N-1}\mathcal{R}$ exists for $\mu \in (\mu_{PD,N,p},\, \mu_{BC,N,p})$ and $\mu_{BC,N,p} > \mu_{PD,N,p}$ where $\mu_{PD,N,p}$ is given by (3.31) and $\mu_{BC,N,p}$ can be computed by solving (3.32).

Now we will discuss the properties of the parameter ℓ_1 that are necessary for cases I-III. As N tends to infinity ℓ_1 tends to zero from the right and hence all stable maximal orbits with large period N exist for any fixed $\ell > \ell_1 \approx 0$. The derivative with respect to N of $\ell_1 = \ell_1(N)$ defined in (3.33) is given by

$$\frac{d\ell_1}{dN} = \frac{p(\eta\lambda^{(N-1)p}p^p)^{\frac{1}{1-p}}\left(-1+(1+p)\lambda-\lambda^N\right)\log(\lambda)}{(1-p)(1-\lambda)}\,.$$

The parameter $\ell_1(N)$ has a maximum at $N = N^*$ where

$$N^* = \frac{\ln\left((1+p)\lambda - 1\right)}{\ln(\lambda)}, \tag{3.49}$$

which is defined if $\lambda > \lambda_1$. As N increases, $\ell_1(N)$ increases up to $N = N^*$ and then decreases. Hence if $\ell > \max_N \ell_1 = \ell_1(N^*)$, then the stable periodic orbit $\mathcal{L}^{N-1}\mathcal{R}$ exists for all N and $\mu \in (\mu_{PD,N,p},\, \mu_{BC,N,p})$, see Figure 3-7 for an example. Next, we turn our attention to deriving the condition for which period-N and period-$(N+1)$ orbits can coexist. Consider the border-collision bifurcation value of $\mathcal{L}^{N-1}\mathcal{R}$, i.e. $\mu = \mu_{BC,N+1,p}$. It can be computed from (3.41) by substituting $N+1$ for N. Then define this RHS by F_{CEx} i.e.

$$F_{CEx}(\mu) := \frac{1-\lambda^N}{1-\lambda}\mu - \lambda^{N-1}\ell - \eta\lambda^{N-1}\mu^p\,. \tag{3.50}$$

We will show that if $\ell > \ell_2$ then $F_{CEx}(\mu_{PD,N,p}) < 0$. This means that $\mu_{BC,N+1,p} > \mu_{PD,N,p}$ and that the stable maximal periodic orbits with period-N and $(N+1)$ coexist for $\mu \in (\mu_{PD,N,p},\, \mu_{BC,N+1,p})$. Note that if $F_{CEx}(\mu_{PD,N,p}) = 0$ then $\mu_{PD,N,p} = \mu_{BC,N+1,p}$ and the period-N and $(N+1)$ maximal periodic orbits coincide at precisely that value.
Consider

$$F_{CEx}(\mu_{PD,N,p}) = \\ (1+p)\left(\eta p^p \lambda^{N-1}\right)^{\frac{1}{1-p}} - \eta\lambda^{N-1}\left(\frac{1-\lambda}{1-\lambda^N}\left(\lambda^{N-1}\ell + \left(p^p\eta\lambda^{N-1}\right)^{\frac{1}{1-p}}(p+1)\right)\right)^p.$$

Then applying the inequality $\ell > \ell_2$ where ℓ_2 is given by (3.34) and simplifying the negative term yields

$$\begin{aligned} F_{CEx} &< (1+p)\left(\eta p^p \lambda^{N-1}\right)^{\frac{1}{1-p}} - \eta\lambda^{N-1}\left(\frac{1-\lambda}{1-\lambda^N}(1+p)^{\frac{1}{p}}\left(\eta p\lambda^{N-1}\right)^{\frac{1}{1-p}}\frac{1-\lambda^N}{1-\lambda}\right)^p \\ &= (1+p)\left(\eta p^p \lambda^{N-1}\right)^{\frac{1}{1-p}} - (1+p)\left(\eta p^p \lambda^{N-1}\right)^{\frac{1}{1-p}} \\ &= 0\,. \end{aligned}$$

As F_{CEx} satisfies (3.40) for period-$(N+1)$ orbit, it follows that $\mu_{PD,N,p} < \mu_{BC,N+1,p}$. Hence period-$N$ and period-$(N+1)$ maximal periodic orbits coexist for

$$\mu \in (\mu_{PD,N,p}, \mu_{BC,N+1,p}).$$

We now discuss the properties of the parameter ℓ_2 which are necessary for proving cases I-III. The parameter ℓ_2 tends to zero from the right as $N \to \infty$ and hence all maximal orbits with large period coexist for any fixed $\ell > 0$. The derivative with

respect to N of $\ell_2 = \ell_2(N)$ defined in (3.34) is given by

$$\frac{d\ell_2}{dN} = \frac{p(p+1)(\eta\lambda^{(N-1)p}p^p)^{\frac{1}{1-p}}(-1+\lambda+(p-\lambda^N)(1+p)^{\frac{1-p}{p}})\log(\lambda)}{(1-\lambda)(1-p)}.$$

The parameter $\ell_2(N)$ has a maximum at $N = \hat{N}$ where

$$\hat{N} = \frac{\log[(1+p)^{\frac{p-1}{p}}(-1+\lambda+p(1+p)^{\frac{1-p}{p}})]}{\log(\lambda)}$$

which is defined if $\lambda > \lambda_2$. As N increases, $\ell_2(N)$ increases up to $N = \hat{N}$ and then decreases. Hence if a fixed $\ell > \max_N \ell_2 = \ell_2(\hat{N})$ then the stable period-N and $(N+1)$ maximal periodic orbits coexist for all N and $\mu \in (\mu_{PD,N,p}, \mu_{BC,N+1,p})$, see Figure 3-7 for an example. We are now able to identify the cases I-III and their respective parameter regions that give rise to three topographically different dynamics.

Case I: Let $\lambda \in (\lambda_1, 1)$ and choose $\ell \in (0, \max_N \ell_1)$. Then there exists a finite set $N_k = \{N_1, \ldots, N_m\}$ with

$$3 \leq N_1 < N_2 < \ldots < N_m$$

such that each $N \in N_k$ satisfies the inequality

$$\ell < \ell_1, \quad \forall N \in N_k.$$

Therefore $\mu = \mu_{PD,N,p}$ does not satisfy the condition (3.47), i.e. $\mu < \mu_1$. This means that although the orbit $\mathcal{L}^{N-1}\mathcal{R}$ exists it is not stable for $\forall N \in N_k$. Hence the only attractor possible is chaotic as this is a one-dimensional map. We can conclude that for $\mu \in (\mu_{PD,N_1-1,p}, \mu_{BC,N_m+1,p})$ we observe robust chaos.
Increasing N from N_m decreases ℓ_1 and ℓ_2 and so there exists a finite set $N_b = \{N_{m+1}, N_{m+2}, \ldots, N_s\}$ with

$$N_m < N_{m+1} < N_{m+2} < \ldots < N_s$$

such that each $N \in N_b$ satisfies the inequality

$$\ell < \ell_2 \quad \forall N \in N_b.$$

As a result of this the condition (3.47) now holds for $\mu = \mu_{PD,N,p}$. But as $\ell < \ell_2$ it follows that F_{CEx}, defined in (3.50), is greater than zero and we conclude that period-N and $(N+1)$ maximal periodic orbits do not coexist. As the period-N maximal periodic orbit loses stability before the period-$(N+1)$ orbit is created in a border-collision bifurcation, we observe a chaotic attractor for

$\mu \in (\mu_{BC,N+1,p}, \mu_{PD,N,p})$ for all $N \in N_b$. As N increases from $N_s + 1$, the parameters ℓ_1 and ℓ_2 decrease. Then both the existence condition, $\mu > \mu_1$, and the stability condition, $F_{CEx} < 0$, are satisfied for the period-N maximal orbit with $N \geq N_s + 1$. Thus period-N and $(N+1)$ maximal periodic orbits coexist for $\mu \in (\mu_{PD,N,p}, \mu_{BC,N+1,p})$.

Case II: Assume 3.35 and 3.36. Then $\ell_1 < 0$ and the stable $\mathcal{L}^{N-1}\mathcal{R}$ orbit exists for $\mu \in (\mu_{PD,N,p}, \mu_{BC,N,p})$ for all $N \geq 2$. There exists a finite set $N_a = \{N_1, N_2, \ldots, N_\alpha\}$ with $3 \leq N_1 < N_2 < \ldots < N_\alpha$ such that $N \in N_\alpha$ satisfies the inequality

$$0 < \ell < \ell_2$$

if (3.35) holds or

$$\max_N \ell_1 < \ell < \ell_2$$

if (3.36) holds. For fixed ℓ in these intervals the coexistence condition does not hold, i.e. $F_{CEx} > 0$. Thus by the same argument as in the previous case, a chaotic attractor exists for $\mu \in (\mu_{BC,N+1,p}, \mu_{PD,N,p})$ for all $N \in N_a$. Increasing N beyond N_a+1 results in a decrease in the parameter ℓ_2 and now the coexistence condition, $F_{CEx} < 0$, holds as well. Therefore period-N and $(N+1)$ maximal periodic orbits coexist for $\mu \in (\mu_{PD,N,p}, \mu_{BC,N+1,p})$ for all $N \geq N_\alpha + 1$.

Case III: Assume $\lambda \in (0,1)$ and $\ell > \max_N \ell_2$. Then both the existence condition, $\mu > \mu_1$, and the coexistence condition, $F_{CEx} < 0$, are satisfied for all $N \geq 2$. Hence stable $\mathcal{L}^{N-1}\mathcal{R}$ orbits exist for $\mu \in (\mu_{PD,N,p}, \mu_{BC,N,p})$ and period-N and $(N+1)$ maximal periodic orbits coexist for $\mu \in (\mu_{PD,N,p}, \mu_{BC,N+1,p})$.

□

The fixed point x_L, given by (3.6), of f_L is the same for the continuous ($\ell = 0$) and discontinuous map ($\ell \neq 0$). By Theorem 3.5 it bifurcates into a period-N maximal periodic orbit of the form $\mathcal{L}^{N-1}\mathcal{R}$, with $N \to \infty$, in a border-collision bifurcation at $\mu = 0$ for all $\lambda \in (0,1)$, $\ell > 0$, $\eta > 0$ and $p \in (0,1)$. This is clearly different to the three bifurcation scenarios of the continuous PPL map described in Theorem 3.3. In the case of the discontinuous PPL map, the more complex dynamics is observed as μ increases from zero which is described by Theorem 3.5.

The approach taken to prove Theorem 3.5 is well suited for studying maximal periodic orbits of the form $\mathcal{L}^{N-1}\mathcal{R}$ for all periods N. If we would have chosen to use the induced map method as in Theorem 3.3 to study the existence and stability of periodic orbits of the discontinuous map (3.1) we would have only been able to demonstrate that if $\ell > 0$, maximal periodic orbits are stable and coexist if their period N is large. By taking a direct approach, i.e. computing smooth and non-smooth bifurcation values,

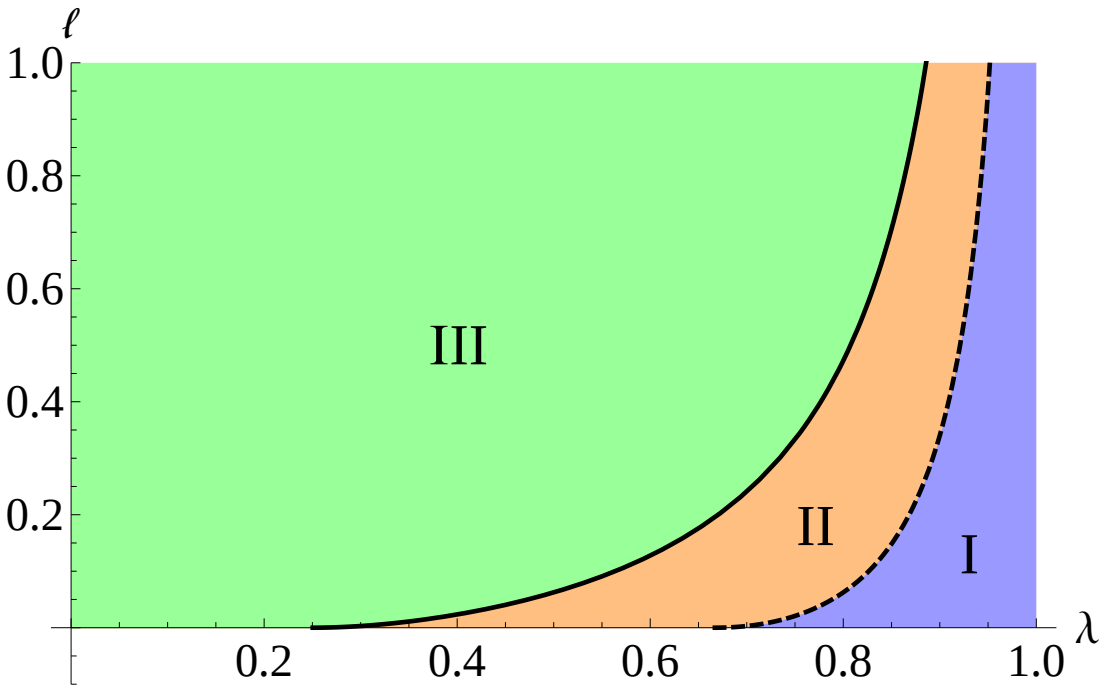

Figure 3-6: *The boundary values* $\max_N \ell_1$ *(dashed) and* $\max_N \ell_2$ *(black), where* ℓ_1 *and* ℓ_2 *are given by 3.33 and 3.34, against* λ*, where* $p = 1/2$ *and* $\eta = 1$*. As described in Theorem 3.5, these boundary values separate the regions I-III in which qualitatively different bifurcation scenarios arise in the PPL map* $f(x_n; p, \ell)$*. For the values of* ℓ *and* λ *in region I we observe case I, in region II we observe case II and in region III we observe case III.*

$\mu_{BC,N,p}$ and $\mu_{PD,N,p}$, we are able to compute the existence and stability conditions for all periods-N periodic orbits.

From Theorem 3.5 we can deduce the effects the discontinuity ℓ and the exponent p have on the map (3.1) and its dynamics.

Although Theorem 3.3 for the continuous PPL map ($\ell = 0$) is not included within Theorem 3.5 it can be easily deduced from this proof. Assume that $\ell = 0$, then for large N condition $\ell < \ell_1$ holds if $\lambda < \lambda_1$. Then stable maximal periodic orbits exist (*intermediate case*); otherwise, if $\lambda \in (\lambda_1, 1)$, all orbits are unstable and robust chaos is observed, *weakly stable case*. Similarly, two neighbouring orbits coexist if $0 = \ell > \ell_2$. Hence for large enough N the parameter $\lambda \in (0, \lambda_2)$ which is consistent with the *strongly stable case*.

Furthermore, we observe robust chaos in the continuous PPL map for $\lambda > \lambda_1$ because then $\ell_1 \to 0^+$ as N tends to infinity, i.e. ℓ_1 approaches zero but never becomes zero, Figure 3-7. This implies that the maximal periodic orbits do not regain stability for $\ell = 0$. However, if $\lambda < \lambda_1$ then $\ell_1 \to 0^-$ and so all stable maximal periodic orbits exist. A similar case can be made for coexisting orbits of period-N and period-$(N+1)$ by analysing the limit of ℓ_2 as N tends to infinity, Figure 3-7.

Both continuous ($\ell = 0$) and discontinuous ($\ell > 0$) PPL maps give rise to the

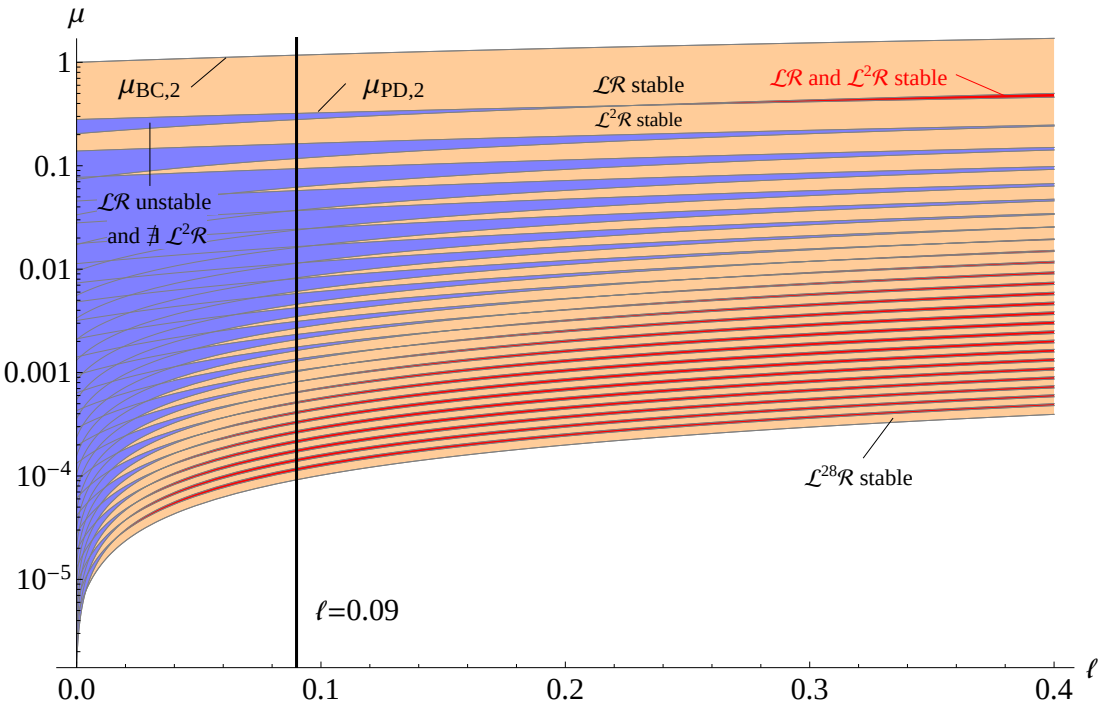

Figure 3-7: *Semi-log plot of μ against ℓ. As μ decreases towards zero the period-N orbit $\mathcal{L}^{N-1}\mathcal{R}$ is created in a border-collision bifurcation at $\mu = \mu_{BC,N,p}$ and loses stability in a period-doubling bifurcation at $\mu = \mu_{PD,N,p}$. We plot $\mu_{BC,N,p}$ and $\mu_{PD,N,p}$, as defined in* (3.31) *and* (3.32) *against the discontinuity ℓ for $N = 2, \ldots, 28$, (where $p = 1/2$, $\lambda = 0.825$, $\eta = 1$). Here we see when the periodic orbit $\mathcal{L}^{N-1}\mathcal{R}$ is stable (orange), unstable (blue) and when neighbouring period-N and $(N + 1)$ orbits coexist (red). For $\ell > 0.1$ the maximal periodic orbits are stable for all N, whereas for $\ell < 0.1$ robust chaos is possible. The white space is due to uncomputed periodic orbits, i.e. where period-N periodic orbits lie with $N \geq 29$.*

same creation and destruction mechanism of maximal periodic orbits $\mathcal{L}^{N-1}\mathcal{R}$ in the period-incrementing cascade, i.e. for $p \in (0, 1)$ an orbit is created in a border-collision bifurcation at $\mu = \mu_{BC,N,p}$ and loses its stability in a period-doubling bifurcation at $\mu = \mu_{PD,N,p}$ as μ is decreasing towards zero. As we have seen in the previous Section 3.1, this is not the case for discontinuous linear map $f(x_n; 0, 0)$ (3.1) with $p = 0$ and $\ell = 0$. In fact, $\mu = \mu_{PD,N,p} = \mu_{BC2,N,0}$, given by (3.27), another border-collision bifurcation point, for $p = 0$. To give evidence, we consider the derivative in (3.43) which is zero if $p = 0$. Hence the only restriction that needs to be imposed to ensure existence and stability of maximal periodic orbits is (3.44), i.e. $x_N > 0$, with boundary value $x_N = 0$ which is a border-collision bifurcation point.

Set $p = 0$ and let $\ell > 0$. Then the resulting map $f(x_n; 0, \ell)$ in (3.1) is the same linear discontinuous map $f(x_n; 0, 0)$ in (3.1) that was discussed in the previous Section 3.1 with the exception of its discontinuity. The only difference is that the discontinuity of $f(x_n; 0, 0)$ is η and of $f(x_n; 0, \ell)$ is $\eta + \ell$. Hence the same dynamics, a strongly stable period-incrementing cascade, results. Further, the bifurcation points $\mu = \mu_{PD,N,0} \equiv$

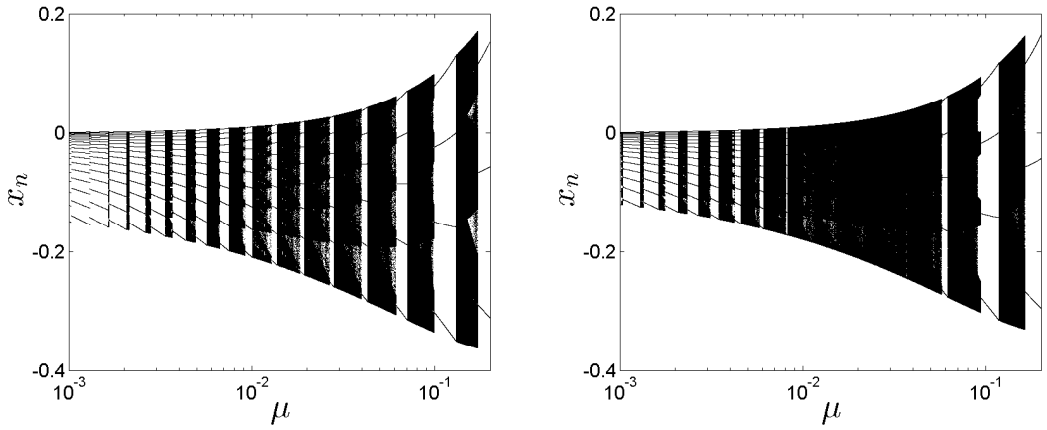

Figure 3-8: *The bifurcation structure of the discontinuous PPL map $f(x_n; p, \ell)$ with $p = 1/2, \eta = 1$ and $\lambda = 0.825$. By Theorem 3.5 we observe a period-incrementing cascade with chaotic windows for $\ell = 0.11$ (Figure 3-8a), whereas for $\ell = 0.9$ (Figure 3-8b), we observe robust chaos for $\mu \in (0.008, 0.05)$ (equivalent to black line in Figure 3-7).*

$\mu_{BC2,N}$ and $\mu_{BC,N,0}$ agree with (3.27) if we substitute $\eta + \ell$ for η.

Finally, set p to one, then the resulting map $f(x_n; 1, \ell)$ (3.1) is a discontinuous linear map. For $\mu > 0$ case III applies as both ℓ_1 and ℓ_2 are zero if p is one. Thus no ℓ exists that satisfies the other two cases, I and II. We restrict our attention to $\eta \in (0, 1)$ as then by Theorem 3.5 the maximal periodic orbits of all periods-N exist and are stable for $\mu \in (\mu_{PD,N,1}, \mu_{BC,N,1})$ given by

$$\begin{aligned}\mu_{PD,N,1} =& \frac{1-\lambda}{1-\lambda^N}\,\lambda^{N-1}\ell,\\ \mu_{BC,N,1} =& \frac{(1-\lambda)\lambda^{N-2}\ell}{1-\lambda^{N-1}-\eta\lambda^{N-2}(1-\lambda)} > 0.\end{aligned}$$

This agrees with the dynamics of the maps that are special cases of 3.1 presented in the literature [34, 6].

3.3 The Discontinuous PPL Map II: $\ell < 0$

We will show in this Section that also in the case of negative discontinuity, i.e. $\ell < 0$, the dynamics of the PPL map is intricate. First we will demonstrate that periodic orbits of the form $\mathcal{L}^{N-1}\mathcal{R}$ cease to exist for ℓ small enough. However, other periodic orbits can be observed, e.g. Figure 3-9. For a better understanding of these dynamical features, at the end of this Section we will briefly consider the piecewise linear map ($p = 1$) and nonlinear map (3.1) when the multiplier λ is zero.

Proposition 3.6. *Assume that $0 < \lambda < 1$, $\eta > 0$, $N \geq 2$ and $\ell < 0$. Consider the*

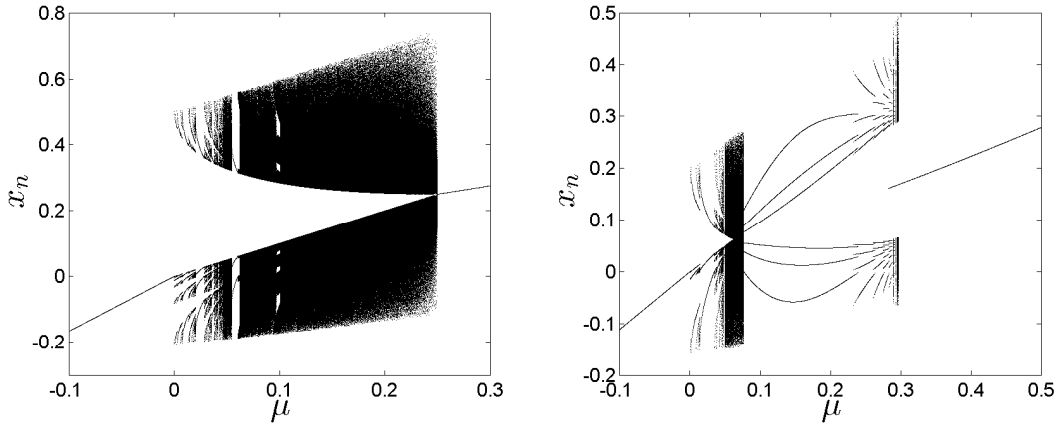

(a) **(b)**

Figure 3-9: *Bifurcation plots illustrating Case 2 of Proposition 3.6. Figure 3-9a: (where $\lambda = 0.4$, $\ell = -0.5$, $\eta = 1$, $p = 0.5$) Period-adding cascade close to $\mu = 0$ and chaotic attractor. No maximal periodic orbits. Figure 3-9b: (where $\lambda = 0.1$, $\ell = -0.2$, $\eta = 0.8$, $p = 0.5$) Period-adding cascade and period-incrementing cascade of $\mathcal{LR}^{2N-1}$.*

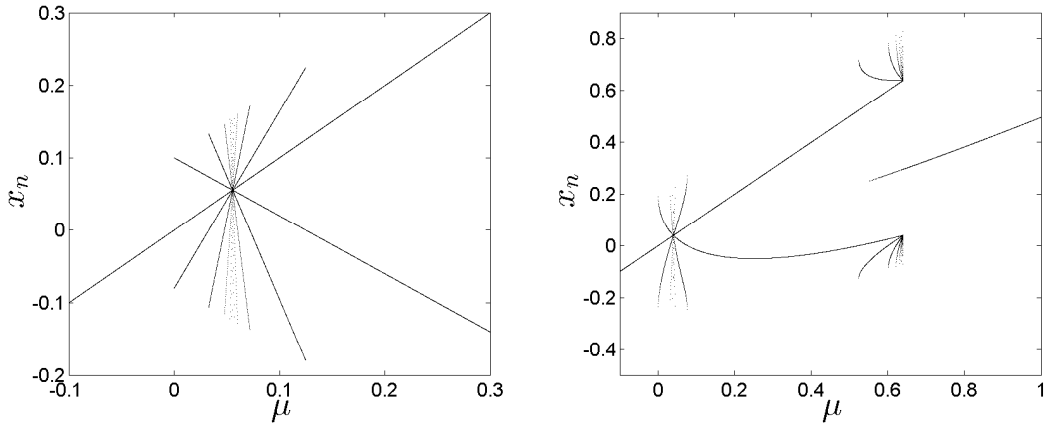

(a) **(b)**

Figure 3-10: *Piecewise-linear map ($\lambda = 0$). Figure 3-10a: As μ increases through zero we observe stable periodic orbits $\mathcal{LR}^{2N}$ which accumulate in a stable fixed point x_{FP} followed by stable periodic orbits $\mathcal{LR}^{2N-1}$. (Parameters: $\ell = -0.1$, $\eta = 1.8$ and $p = 1$). Figure 3-10b PPL map with $p = 1/2$: As μ increases through zero we observe the same type of stable periodic orbits. Further, we have an additional point of accumulation, $\mathcal{R}^2$ which is followed by a stable fixed point. The latter is not present in the piecewise linear map. (Parameters: $\ell = -0.2$, $\eta = 1$ and $p = 0.5$).*

discontinuous map $f(x_n; p, \ell)$ *in* (3.1). *Suppose there exists* ℓ_1 *is given by* (3.33) *and* ℓ_2 *given by*

$$\ell_2 := \eta(p-1)\left(\frac{\eta p \lambda^{N-2}(1-\lambda)}{1-\lambda^{N-1}}\right)^{\frac{p}{1-p}} < 0,$$

which is negative for all parameters involved. Suppose further, that there exists $\mu_{PD,N,p}$ *given by* (3.31) *and* $\mu_{BC,N,p}$ *given by* (3.32).

Then we observe the following cases:

Case 1 *: Period-incrementing cascade does not exist for all periods* N.

- *If* $\lambda^M > 2\lambda - 1$ *and* $\ell \in (\ell_2, 0)$, *or*
- *if* $2\lambda - 1 > \lambda^M > ((1+p)\lambda - 1)/p$ *and* $\ell \in (\ell_1, 0)$

then periodic orbits of the form $\mathcal{L}^{N-1}\mathcal{R}$ *are stable for* $2 \leq N \leq M$. *The closer* ℓ *is chosen to zero the larger* M *is.*
Further, if $2\lambda - 1 > \lambda^M > ((1+p)\lambda - 1)/p$ *and* $\ell_2 < \ell < \ell_1$, *then these periodic orbits exist but are unstable.*

Case 2 *: No Existence.*
If $0 < \lambda < 1$ *and* $\ell < \ell_2|_{N=2}$ *then periodic orbits of the form* $\mathcal{L}^{N-1}\mathcal{R}$ *do not exist.*

Further, period-N *orbits of the form* $\mathcal{L}^{N-1}\mathcal{R}$ *are stable in the interval* $(\mu_{PD,N,p}, \mu_{BC,N,p})$.

Proof. Similar to Theorem 3.5.

□

Therefore, the closer ℓ is to zero the more maximal periodic orbits exist and are stable but never for all N, i.e. period-incrementing is not robust.

We return to the piecewise linear map ($p = 1$). It has been documented in e.g. [34] that for $0 < \lambda < 1$, $\eta < 1$ and $\ell = -1$ two fixed points are observed which coexist in the discontinuity region. However, for $\eta > 1$ we obtain two kinds of period-incrementing cascades, see Figure 3-10. As μ increases through zero we observe stable periodic orbits of the form $\mathcal{L}\mathcal{R}^{2N}$ and their period increases by two as μ increases. Moreover, these orbits accumulate in a stable fixed point

$$x_{FP,p} \equiv \mu_{FP,p} = \left(\frac{-\ell}{\eta}\right)^{1/p}$$

and are followed by stable periodic orbits of form $\mathcal{L}\mathcal{R}^{2N-1}$ whose period decreases by two as μ increases.

Similar dynamical behaviour occurs for the nonlinear map ($0 < p < 1$). As μ increases through zero we observe the same types of stable periodic orbits. Further, $\mathcal{L}\mathcal{R}^{2N-1}$ accumulates in the periodic orbit $\mathcal{R}^2$. The orbit $\mathcal{R}^2$ is given by the iterates

$x_{R1} = f_e(x_{R2}) > 0$ and $x_{R2} = f_R(x_{R1}) > 0$. Hence $x_{R1} = f(f(x_{R1}))$ and $x_{R2} = f(f(x_{R2}))$. The accumulation occurs if $x_{R1,p} = \mu_{FP,p}$ and $x_{R2,p} = \mu_{R2,p}$ where $\mu_{R2,p}$ satisfies

$$\mu_{R2,p} - \eta\mu_{R2,p}^p - \ell - \left(\frac{-\ell}{\eta}\right)^{\frac{1}{p}} = 0. \tag{3.51}$$

For the square-root map ($p = 1/2$) this equation can be solved exactly and we obtain

$$\mu_{R2,1/2} = \left(\eta + \frac{\ell}{\eta}\right)^2. \tag{3.52}$$

In the case when $\ell > -\eta^2/2$ it follows that $\mu_{R2,1/2} > \mu_{R1,1/2}$ and both accumulation points are stable, see Figure 3-10b. Otherwise, the fixed point is unstable and the only stable periodic orbits are $\mathcal{LR}^{2N}$ which accumulate in the periodic orbit $\mathcal{R}^2$, see Figure 3-9a.

We can see from the results shown in Figure 3-10 that there is a coexistence of periodic orbits accumulating at a stable $\mathcal{R}^2$ orbit.

Numerical results, e.g. a comparison of Figure 3-9 with 3-10, show that the left multiplier λ introduces chaos into the dynamical system and introduces a Farey tree structure to the periodic orbits of the form $\mathcal{LR}^{2N}$. These periodic orbits become stable in a period-doubling bifurcation and are destroyed in a border-collision, in contrast to the periodic orbits $\mathcal{LR}^{2N-1}$ which are stabilised and destroyed in a border-collision bifurcation. It is notable that these are not the only stable periodic orbits that can be observed. But numerically they don't appear to be stable for $N \to \infty$, see Figure 3-11. Finally, it is noteworthy that for $\ell < 0$ there is an incredible variety of stable periodic orbits which is not the case for $\ell > 0$ or for the continuous map for that matter. As can be seen in Figure 3-11 there are still other periodic orbits that we have not mentioned yet. However, these will have to be the subject of future investigations.

3.4 Conclusions

In this Chapter we have considered the piecewise power law map (3.1). We assumed that its linear LHS function has increasing slope λ less than one. Thus its stable fixed point undergoes a border-collision bifurcation at the point $x = 0$ and $\mu = 0$. For $\mu > 0$ the map's dynamics is complex and depends on the eigenvalue λ, and the parameters of the nonlinear RHS function, in particular the exponent $p \in (0, 1)$ and the discontinuity ℓ. We have distinguished between three cases that show qualitatively different bifurcation scenarios depending on the discontinuity ℓ. The three cases are $\ell = 0$, $\ell > 0$ and $\ell < 0$. In the first case, $\ell = 0$, we have shown that, depending

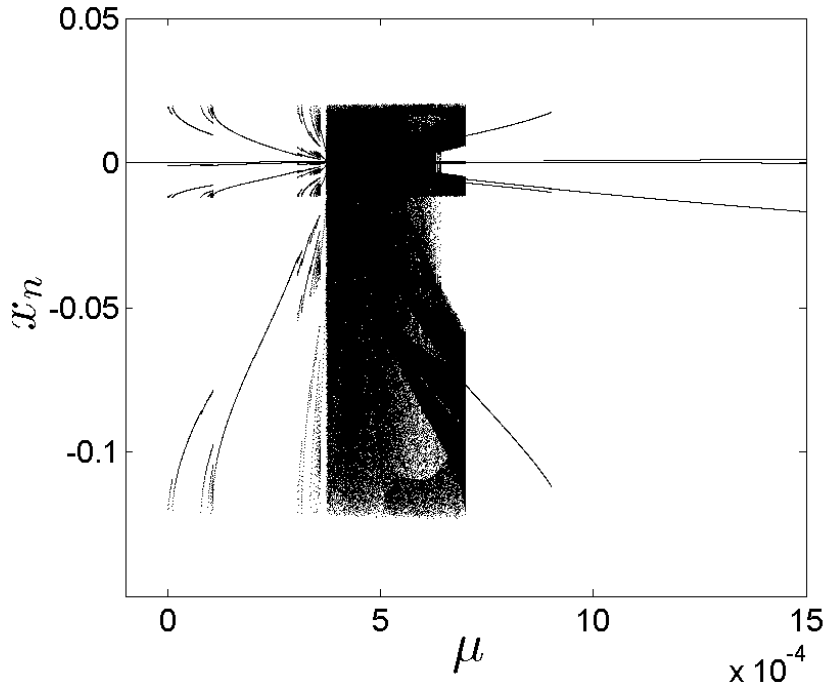

Figure 3-11: *Bifurcation diagram for square-root map with $\lambda = 0.1$, $\ell = -0.02$, $\eta = 1$. Period-adding cascade near border-collision bifurcation point $x = 0$, $\mu = 0$. As μ is increased from $\mu = 0$ we observe a chaotic attractor and a period-incrementing cascade.*

on the given parameters, we observe robust chaos, a period-incrementing cascade of maximal periodic orbits which are separated by chaotic windows or which coexist. This dynamics is observed for $\mu > 0$ and close to the border-collision bifurcation value $\mu = 0$. The general conditions we have derived show that the exponent of the nonlinear term p influences the size of the regions where these dynamics occur but not the general features.

In the second case, $\ell > 0$, we have shown that the dynamics is more stable than for the continuous map (3.1). By that we mean that for $\mu > 0$ and close to the border-collision value $\mu = 0$, a stable periodic-incrementing cascade exists for any $\ell > 0$. Other dynamics such as robust chaos and chaotic attractors are still found in the map but away from the border-collision value $\mu = 0$.

For all the cases, we have derived general existence and stability conditions for maximal periodic orbits of the form $\mathcal{L}^{N-1}\mathcal{R}$. We have shown that the maximal periodic orbit is the prevalent feature of the map's dynamics if $\ell \geq 0$ and that it is the building block of the period-incrementing cascade. If $\ell < 0$ then cascades of periodic orbits exist but these do not contain the maximal periodic orbit for large periods N. Instead we have seen periodic orbits with at least two iterates on the RHS. Furthermore, for $\ell < 0$ we have numerically observed period-adding cascades, which do not feature in the map's dynamics if $\ell \geq 0$.

We have also found good agreement results on maps presented in the literature, which are special cases of the piecewise power law map (3.1). These special cases include the piecewise-linear map [34, 6, 7, 5, 8, 9, 16, 59, 31] and the square-root map [34, 90, 91, 92, 38, 8, 102, 24, 17].

CHAPTER 4

The Piecewise Power Law Maps with Exponent $p > 1$

In this Chapter we extend the work of Chapter 3 to look at superlinear discontinuous maps, which have qualitatively different behaviour from sublinear maps. In particular we are interested in understanding the dynamics that arise in the following map

$$x_{n+1} = \begin{cases} f_L(x_n) & = \lambda x_n + a \quad \text{if } x_n < 0 \\ f_R(x_n) & = -\eta x_n^p + b \quad \text{if } x_n \geq 0 \end{cases} \tag{4.1}$$

where $\lambda \in (-1, 1)$, $a \in \mathbb{R}$, $\eta \in \mathbb{R}$ can be scaled such that $\eta \in \{-1, 0, 1\}$, $p > 1$ and $b \in \mathbb{R}$. We will refer to the map given by (4.1) as the **superlinear piecewise power law map (SPPL map)**. If $a = b$ then the SPPL is continuous. If $a \neq b$ then the SPPL map is discontinuous.

In Chapter 2 we have introduced, and in Chapter 3 we have studied, two types of bifurcation cascades that arise through non-smooth bifurcations, the **period-incrementing cascade** and the **period-adding cascade**. These cascades have been observed in the SPPL map (4.1) with

- $\eta = 0$, $\lambda \in (-1, 1)$, $a \in \mathbb{R}$ and $b \in \mathbb{R}$. Then the SPPL map becomes the piecewise-linear map which has been studied by Avrutin and Schanz in [6].

- $a = b \in \mathbb{R}$, $p \in \{3/2, 2\}$, $\lambda \in (-1, 1)$ and $\eta \in \{-1, 1\}$ in [56]. Halse et al [56] pay particular attention to studying the period-incrementing cascade with a as the bifurcation parameter. For the periodic orbits of this cascade they derive existence and stability conditions. These maps arise in planar piecewise smooth systems where grazing or sliding occurs [34].

Glendinning [51, 52] observed a third cascade in piecewise-smooth superlinear type maps that is unlike the period-doubling or period-adding cascade. Glendinning studied a family of maps where both f_L and f_R are nonlinear, f_L is decreasing and f_R is increasing. We will refer to the maps he studied as f_{Glen} maps. In [51, 52] Glendinning showed that as the bifurcation parameter b decreases the period-N periodic orbits are ordered according to the following sequence of periods N:

$$N = p_1, 2p_1, p_2, 2p_2, \ldots \quad \text{where} \quad p_{k+1} = 2p_k + (-1)^k \quad \text{with} \quad p_0 \in \mathbb{N} \tag{4.2}$$

for $k \in \mathbb{N}_0$. A cascade with such an ordering of bifurcating periodic orbits is termed **anharmonic cascade**. The anharmonic cascade has only been reported in superlinear maps [51, 52], not in sublinear maps, such as those studied in Chapter 3.

Our novel, primary observation is the existence of the anharmonic cascade in the SPPL map (4.1) which is illustrated in Figure 4-1.

Furthermore, Gardini et al. [49] and Tramontana and Gardini [115] show that continuous and discontinuous SPPL type maps arise from economic applications.

Sufficient conditions for a period-incrementing cascades for a one-dimensional map have been presented in [5]. Although the map (4.1) that we study is a special case of the map investigated by Avrutin and Schanz [5], we analyse it differently using similar methods to those described in Chapter 3 and numerically computed bifurcation diagrams.

4.1 The Anharmonic Cascade in the SPPL map

Consider the map (4.1) with the following parameters

$$\lambda \in (-1, 0), \quad a \leq 0, \quad \eta = -1, \quad p > 1 \tag{4.3}$$

where $b \in \mathbb{R}$ is chosen to be the bifurcation parameter.

Fixed Points

We will now consider fixed points of the map (4.1). The map f_L, (4.1), has one fixed point $x = x_L$ (Figure 4-1) given by

$$x_L = \frac{a}{1 - \lambda}.$$

It is admissible, i.e. $x_L < 0$, and stable for all $b \in \mathbb{R}$ given the parameters in (4.3). The map f_R, (4.1), has two fixed points, $x = x_{R1}$ (Figures 4-1 and 4-1c) and $x = x_{R2}$

(Figure 4-1c), which can be obtained by solving the nonlinear equation

$$x^p - x - b = 0.$$

To see that this equation has at most two solutions, and hence two fixed points, $x = x_{R1}$ and $x = x_{R2}$ for $b \leq 0$, solve it for b. Then we obtain the function $b(x)$ given by

$$b(x) = x^p - x.$$

This function has two zeros at $x = 0$ and $x = 1$ and a minimum value at $x = x_F := p^{1/(1-p)}$. Therefore it has at most two solutions for any fixed $b \leq 0$.

The fixed points x_{R1} and x_{R2}, which are created in a smooth fold bifurcation at $b = b_F := (1-p)p^{p/(1-p)} < 0$, exist for $b > b_F$. Let $x_{R1} < x_F$, i.e. the lower fixed point branch, and let $x_{R2} > x_F$, i.e. the upper fixed point branch. Then x_{R2} is unstable for all $b > b_F$ as $|f_R'(x_{R2})| > 1$ and the lower fixed point x_{R1} is stable for all $b > b_F$ as $|f_R'(x_{R1})| < 1$. The fixed point x_{R1} is destroyed in a border-collision (BC) bifurcation at the point $x = 0$, $b = 0$. Hence the stable fixed x_{R1} exists for $b \in (b_F, 0)$.

The Anharmonic Cascade

Numerically, we find that for $b > 0$ the border-collision bifurcation gives rise to a cascade of bifurcating periodic orbits, which is termed anharmonic cascade, Figure 4-1. As the bifurcation parameter increases from $b = 0$, the periods N of the periodic orbits are given by the following sequence:

$$N = p_1, 2p_1, p_2, 2p_2, \ldots \quad \text{where} \quad p_{k+1} = 2p_k + (-1)^k \quad \text{with} \quad p_0 = 1 \tag{4.4}$$

for $k \in \mathbb{N}_0$. We plot two bifurcation diagrams with the parameters $\lambda = -0.9$, $\eta = -1$, $p = 2$ and $a = -0.1$, shown in Figures 4-1a and 4-1b, and $a = 0$, shown in Figure 4-1c. In these Figures 4-1a - 4-1c, the sequence of periods N is

$$2, 4, 3, 6, 7, 14, 13, \ldots .$$

Numerically (Figure 4-1) we find that the mechanism for creation and destruction of periodic orbits, as b increases from $b = 0$, is as follows. Periodic orbits of period-N are created in a border-collision bifurcation at $b = b_{BC,1,N}$ and lose stability in a smooth period-doubling bifurcation at $b = b_{PD,N}$. At $b = b_{PD,N}$ the birth of a period-$2N$ periodic orbit occurs. Increasing b further, it ceases to exist in a second border-collision bifurcation at $b = b_{BC,2,2N}$, Figure 4-1. In Figure 4-1a, for example, the period-2 and period-4 periodic orbits have the following bifurcation values (approximations):

$$b_{BC,1,N} \approx 0.116, \quad b_{PD,N} \approx 1.036, \quad b_{BC,2,2N} = 1.344.$$

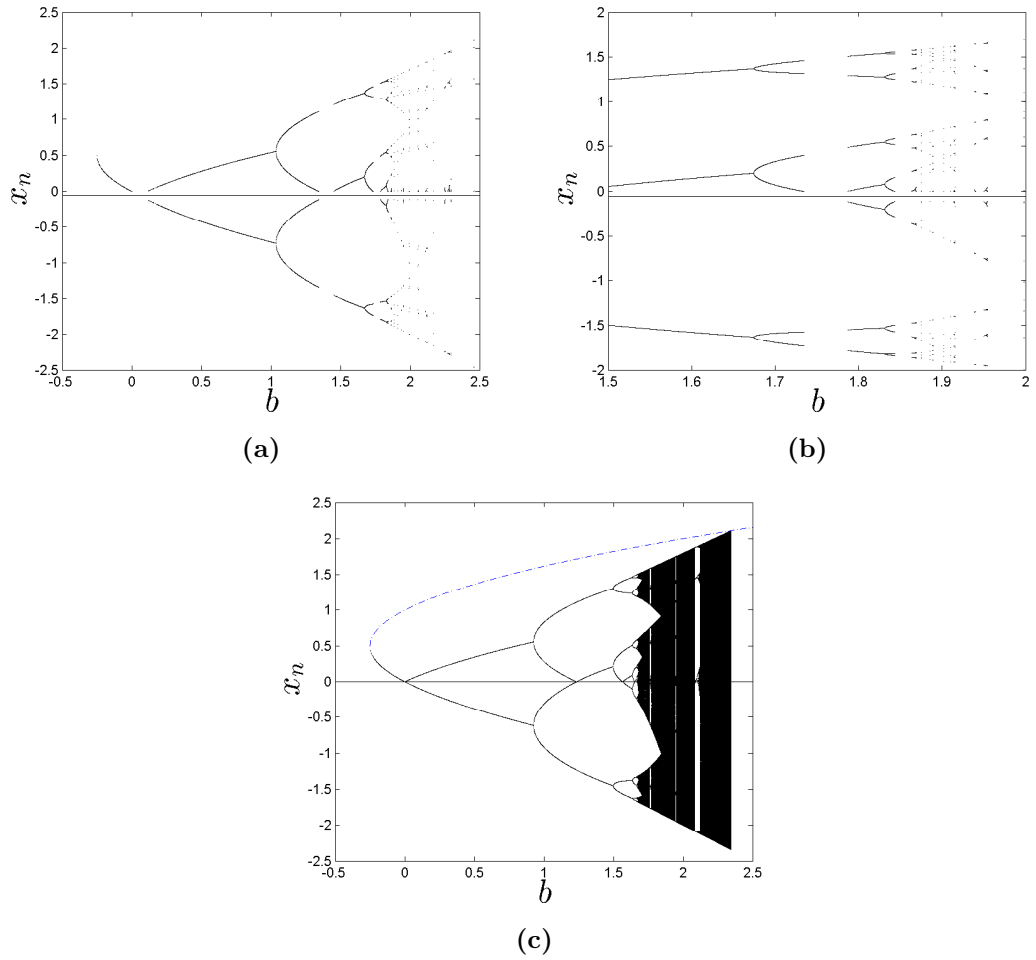

Figure 4-1: *At the BC bifurcation point $x = 0$, $b = 0$, the stable fixed point $x_{R1} > 0$ bifurcates into an anharmonic cascade where $\lambda = -0.9$, $\eta = -1$, $p = 2$ and $a = -0.1$, in Figures 4-1a and 4-1b, and $a = 0$ in Figure 4-1c. Figure 4-1b is a magnification of Figure 4-1a. The stable fixed point $x_L = a/(1-\lambda) = -0.053$ in Figures 4-1a and 4-1b or $x_L = 0$ in Figure 4-1c. In Figure 4-1c at $b = 2.3$ the cascade appears to bifurcate with the unstable fixed point x_{R2} (blue dotted line) and cease to exist as b increases. Chaos is observed for $a = 0$ in Figure 4-1c but not for $a = -0.1$ in Figures 4-1a and 4-1b.*

As b increases, we conjecture that the period N tends to infinity and the quantity $b_{BC,2,2N} - b_{BC,1,N}$ tends to zero. This has been proven for the map f_{Glen} in [51, 52] but not for the SPPL map. Furthermore, in Figures 4-1a and 4-1c we observe that the stable periodic orbits of the anharmonic cascade accumulate at a point of accumulation $b = b_\infty$, much like the logistic map in Chapter 2. However, it is difficult to determine this point numerically as the intervals in which the periodic orbits are stable become very small as b increases towards the point of accumulation. We approximate that in Figure 4-1b the accumulation point is $b_\infty = 1.9$.

Finally, as b increases beyond the point of accumulation b_∞, periodic orbits and chaotic attractors arise for $a = 0$ and only periodic orbits for $a < 0$. For $a = 0$, the cascade appears to be destroyed when it bifurcates with the unstable fixed point x_{R2} at $b \approx 2.35$, Figure 4-1c. We conjecture that the same happens for $a < 0$, however this is harder to see as the existence and stability intervals of stable periodic orbits near that point are much smaller.

4.2 Period-Incrementing and Period-Adding Cascades

Consider the map (4.1)

$$\lambda \in (0, 1), \quad a > 0, \quad \eta = 1, \quad p > 1, \tag{4.5}$$

where $b \in \mathbb{R}$ is chosen to be the bifurcation parameter.

Case $b < 0$: Period-Incrementing Cascade

Let $b < 0$ then we observe a period-incrementing cascade of stable periodic orbits of the form $\mathcal{L}^{N-1}\mathcal{R}$ with $N \geq 2$, which are called **maximal periodic orbits** and were defined in Chapter 3. As we decrease b these orbits are created in a border-collision (BC) bifurcation at $b = b_{BC1,N}$ and are either destroyed in a border-collision at $b = b_{BC2,N}$ (Figure 4-2a) or lose their stability in a period-doubling (PD) bifurcation at $b = b_{PD,N}$ (Figure 4-2b) as b increases. If the latter is the case then the stable periodic orbit of the form $(\mathcal{L}^{N-1}\mathcal{R})^2$, which arises from the period-doubling bifurcation, is destroyed in a border-collision bifurcation at $b = b_{BC4,N}(Figure 4-2b)$. Furthermore, periodic orbits of the form $(\mathcal{L}^{N-1}\mathcal{R})^2$ do not exist for large N. This is the case because the border-collision bifurcation occurs before the period-doubling bifurcation.

We state for what parameter values these scenarios occur in the following Theorem.

Theorem 4.1. *Consider the SPPL map given by* (4.1)*. Let* $N \geq 2$*,* $a > 0$*,* $0 < \lambda < 1$*,*

$b < 0$ and $\eta = 1$. Define the parameters $b_{PD,N}$, $b_{BC1,N}$, $b_{BC2,N}$ and $b_{BC4,N}$ to be

$$\begin{aligned}
b_{PD,N} &= \left(\frac{p+1}{p}\left(\frac{1}{\eta\lambda^{N-1}p}\right)^{\frac{1}{p-1}} - \frac{a(1-\lambda^{N-1})}{1-\lambda}\right)\frac{1}{\lambda^{N-1}},\\
b_{BC1,N} &= -\frac{a(1-\lambda^{N-1})}{\lambda^{N-1}(1-\lambda)},\\
b_{BC2,N} &= \eta a^p - \frac{a(1-\lambda^{N-2})}{\lambda^{N-2}(1-\lambda)},\\
b_{BC4,N} &= \left(\left(\frac{1}{\eta\lambda^{N-1}p}\right)^{\frac{1}{p-1}} - \frac{a(1-\lambda^{N-1})}{1-\lambda}\right)\frac{1}{\lambda^{N-1}},
\end{aligned}$$

respectively. The parameter $b_{BC3,N}$ cannot be defined explicitly but it is the unique solution $b = b_{BC3,N}$ of the order p algebraic equation

$$0 = f_L^{N-1}(f_R(f_L^{N-1}(f_R(0)))). \tag{4.6}$$

Define the parameters a_1 and a_2 to be

$$a_1 = \left(\frac{1}{\eta\lambda^{N-1}p}\right)^{\frac{1}{p-1}}, \tag{4.7}$$

$$a_2 = \frac{p+1}{p}\left(\frac{1}{\eta\lambda^{N-1}p}\right)^{\frac{1}{p-1}}\frac{1-\lambda}{1-\lambda^{N-1}}, \tag{4.8}$$

respectively. Then stable periodic orbits of the form $\mathcal{L}^{N-1}\mathcal{R}$ exist

Case 1 *for $b \in (b_{BC1,N}, b_{BC2,N})$ if $0 < a < a_1$.*

Case 2 *for $b \in (b_{BC1,N}, b_{PD,N})$ if $a > a_1$. Furthermore, stable periodic orbits of the form $(\mathcal{L}^{N-1}\mathcal{R})^2$ are created in a period-doubling bifurcation at $b = b_{PD,N}$ and are destroyed in a border-collision bifurcation at*

- **(a)** *$b = b_{BC3,N}$ if $a_1 < a < a_2$.*
- **(b)** *$b = b_{BC4,N}$ if $a > a_2$.*

Proof. The proof for this Theorem is omitted as it follows the same principles and very similar steps as the proof of Theorem 3.5. □

Let N tend to infinity. Then a_1, given by (4.7), and a_2, given by (4.8), tend to infinity. Thus, only Case 1 holds in Theorem 4.1 for large N. Then, by Theorem 4.1, stable maximal periodic orbits exist for $b \in (b_{BC1,N}, b_{BC2,N})$ but no periodic orbits of the form $(\mathcal{L}^{N-1}\mathcal{R})^2$. This Theorem reveals that for N large enough, the period-incrementing cascade is comprised of maximal periodic orbits. Furthermore, for large enough N when only $\mathcal{L}^{N-1}\mathcal{R}$ are stable, the existence intervals scale with $1/\lambda$ as b decreases.

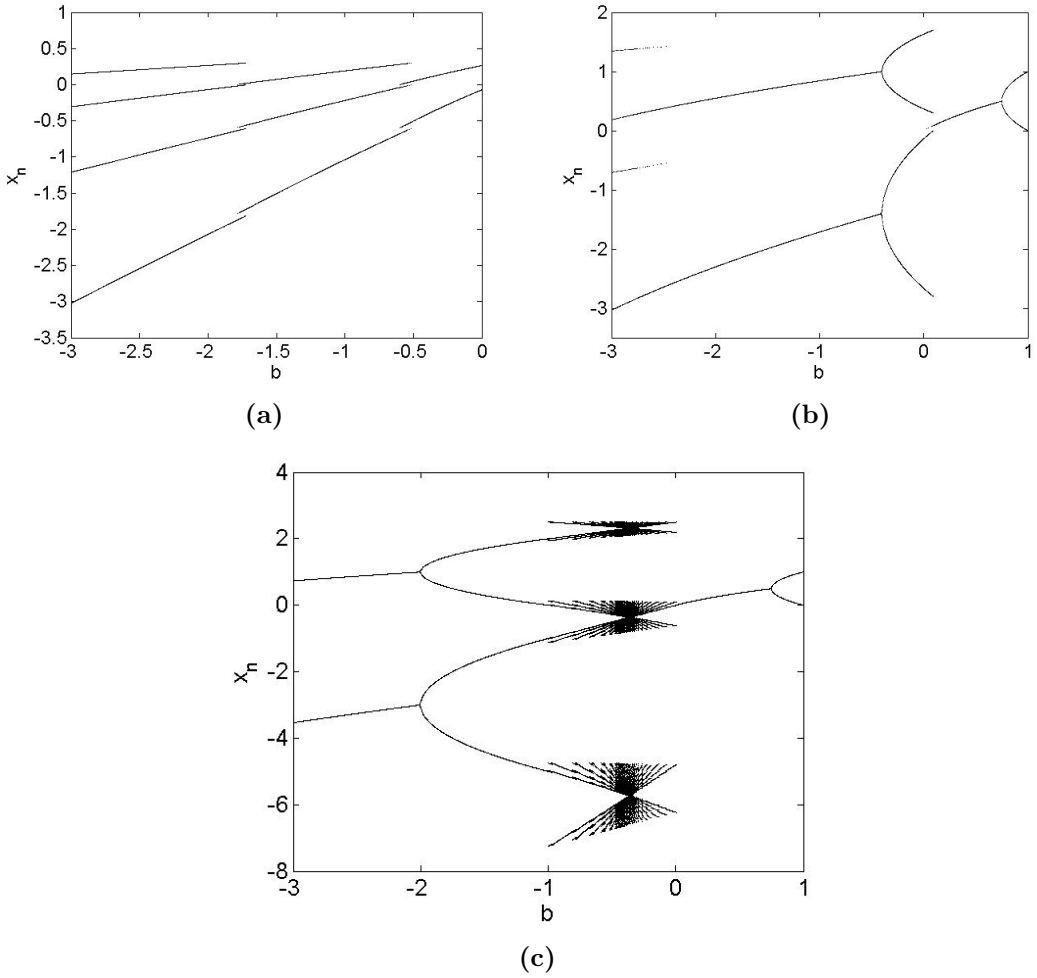

Figure 4-2: *Examples of the dynamics predicted by Theorem 4.1. Figure 4-2a: period-incrementing cascade with maximal periodic orbits only (Case 1), where* $p = 2$, $\eta = 1$, $a = 0.3$ *and* $\lambda = 0.5$. *Figure 4-2b: period-incrementing cascade consisting of maximal periodic orbits and periodic orbits of the form* $(\mathcal{L}^{N-1}\mathcal{R})^2$ *(Case 2(a)) where* $p = 2$, $\eta = 1$, $a = 1.7$ *and* $\lambda = 0.5$. *Figure 4-2c shows an example for Case 2(b) where* $p = 2$, $\eta = 1$, $a = 2.5$ *and* $\lambda = 0.5$. *The birth of a period-adding cascade is observed in the neighbourhood of the border-collision point* $x = 0$, $b = 0$. *Observe the existence of an accumulation point of the period-adding cascade at* $b \approx -0.3$.

Case $b \geq$: Period-Incrementing and Period-Adding Cascade

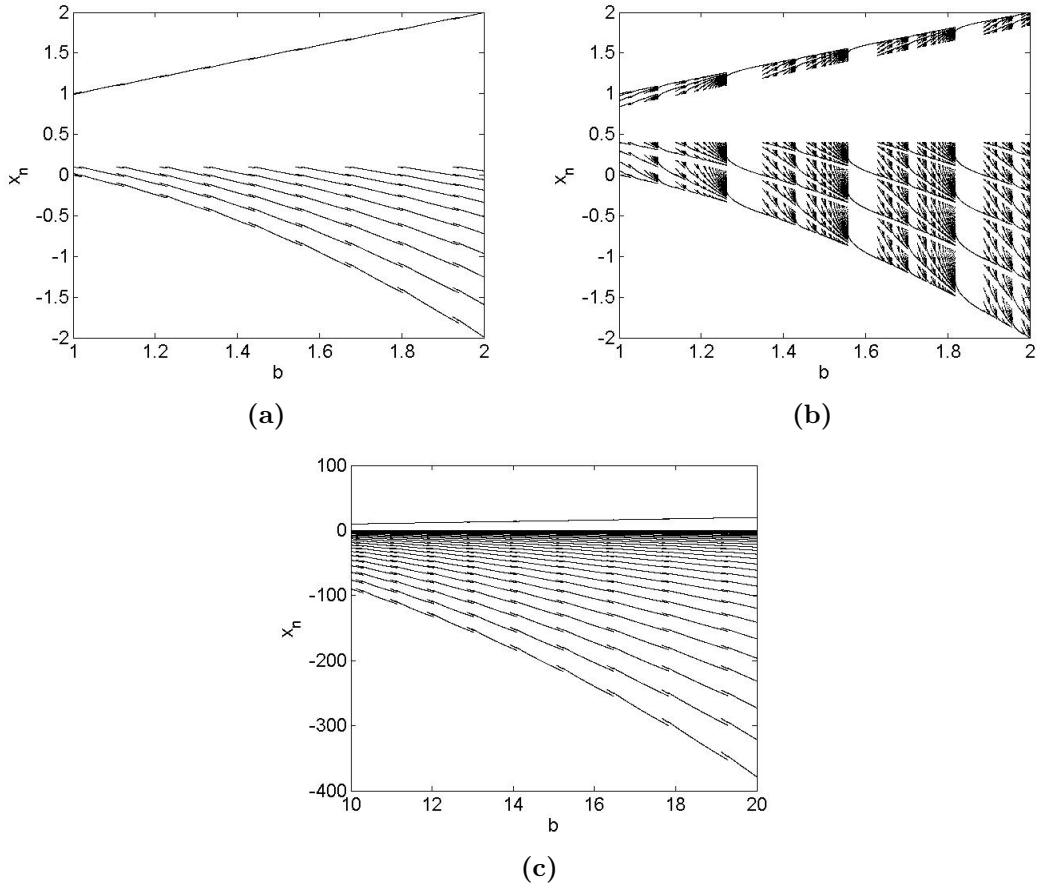

Figure 4-3: *Bifurcation diagram showing the bifurcation cascade of the periodic orbits $\mathcal{L}^{N-2}\mathcal{R}^2$ for $b \geq 0$ with $p = 2$, $\eta = 1$. Figure 4-3a: $\mathcal{L}^{N-2}\mathcal{R}^2$ orbits undergo a border-collision bifurcation and are organised in a period-incrementing cascade where $a = 0.1$ and $\lambda = 0.85$. Figure 4-3b: $\mathcal{L}^{N-2}\mathcal{R}^2$ orbits undergo a fold bifurcation, where $a = 0.4$ and $\lambda = 0.85$. These orbits are organised in a period-adding cascade. Figure 4-3c $\mathcal{L}^{N-2}\mathcal{R}^2$ orbits, which are organised in a period-incrementing cascade, undergo a border-collision bifurcation for $a = 0.4$ and $\lambda = 0.85$.*

We now let $b \geq 0$. Unlike the previous case, the SPPL map (4.1), in particular f_R, has a fixed point $x = x_R$ (Figures 4-2b and 4-2c). This fixed point cannot be defined explicitly but it is the unique solution $x = x_R$ of the order p algebraic equation

$$x = -\eta x^p + b.$$

As b increases it is created in a border-collision bifurcation point at $x = 0$, $b = 0$ and loses its stability in a period-doubling bifurcation at $b = b_{FP,PD}$ which is given by

$$b_{FP,PD} = \frac{p+1}{p}\left(\frac{1}{\eta p}\right)^{\frac{1}{p-1}}.$$

Note that $b_{FP,BC} < b_{FP,PD}$ for all $p > 1$ and $\eta = 1$. Hence, the stable fixed point x_R exist for $b \in (b_{FP,BC}, b_{FP,PD})$.

The notation used in the following paragraph is used for convenience and is only valid in this Section.

Increasing b beyond $b = b_{FP,PD}$, we numerically observe periodic orbits of the form $\mathcal{L}^{N-2}\mathcal{R}^2$ with $N \geq 3$, Figure 4-3. This orbit becomes stable in a fold bifurcation at $b = b_{F,N}$ (Figure 4-3b) or in a border-collision bifurcation at $b = b_{BC1,N}$ (Figure 4-3a) depending on the other parameters λ and a. As b is increased further the periodic orbit is destroyed in a border-collision bifurcation at $b = b_{BC2,N}$ (Figure 4-3). These values can only be obtained explicitly for $p = 2$, except for $b_{F,N}$ which is given by

$$b_{F,N} := \frac{1}{a}\left(\frac{1}{\eta^2\lambda^{N-2}p^2}\right)^{\frac{1}{p-1}} + \eta a^p. \tag{4.9}$$

From numerically computed two-parameter bifurcation diagrams (a, λ) (Figure 4-4a) and (a, b) (Figure 4-4b) we can identify the critical parameter values for which the periodic orbit of the form $\mathcal{L}^{N-2}\mathcal{R}^2$ is stable. The stable orbit $\mathcal{L}^{N-2}\mathcal{R}^2$ exists for $b \in (b_{BC1,N}, b_{BC2,N})$ if λ and a are chosen such that they lie in the region below all blue curves in Figure 4-4a.

Furthermore, for fixed λ the orbits $\mathcal{L}^{N-2}\mathcal{R}^2$ undergo a fold bifurcation only for finitely many N (Figure 4-4a). Thus for large N the existence interval is $(b_{BC1,N}, b_{BC2,N})$ for all λ, a, η and p.

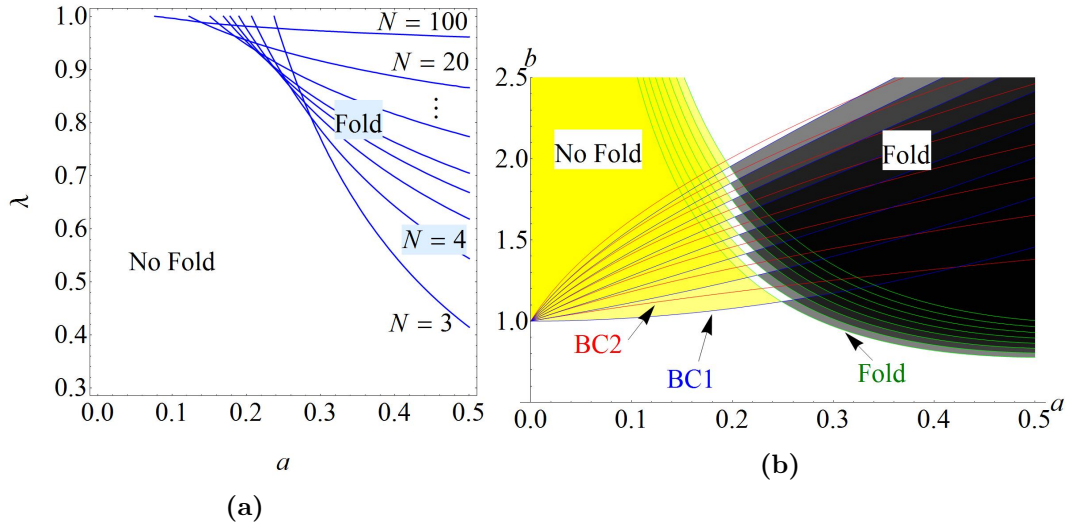

Figure 4-4: *Two-parameter diagram illustrating the bifurcation curves $b_{F,N}$ (blue) in Figure 4-4a (for $p = 2$, $N \in 3, 4, 5, 6, 10, 20, 100$) and $b_{F,N}$ (green), $b_{BC1,N}$ (blue) and $b_{BC2,N}$ (red) in Figure 4-4b (for $p = 2$, $\lambda = 0.85$, $N \in 2, \ldots, 9$). Figure 4-4a: In the parameter region below all blue curves the orbit $\mathcal{L}^{N-2}\mathcal{R}^2$ will not undergo a fold bifurcation, but will do so otherwise. Figure 4-4b: The switch from yellow to dark grey indicates when $b_{F,N} = b_{BC1,N}$.*

4.3 Conclusions

In this Chapter we have shown that the superlinear piecewise-powerlaw map gives rise to bifurcation cascades that have been observed in the sublinear map in Chapter 3 such as the period-incrementing and period-adding cascade. We have also shown that the birth of the anharmonic cascade occurs in the SPPL map for certain parameter values. This cascade has only been reported in maps where both function f_L and f_R are nonlinear [51, 52]. We have shown numerically that the periodic orbits, organised in an anharmonic cascade, are created in a border collision bifurcation and lose stability in a period-doubling bifurcation, which in turn gives rise to a stable periodic orbit that is destroyed in a border-collision bifurcation. The bifurcation diagrams suggested that chaotic attractors are only observed in a special case, i.e. when $a = 0$ but not otherwise.

For a set of parameter values, in particular $b < 0$, we derived the general conditions of existence and stability of maximal periodic orbits. For the same set of parameter values with $b > 0$ we used two-parameter bifurcation diagrams to determine the critical parameter regions in which the periodic orbit of the form $\mathcal{L}^{N-2}\mathcal{R}^2$ is stable and exists.

The SPPL map (4.1) studied in this Chapter does not contain any linear terms in the RHS function which could affect the map's dynamics. Alternatively, to study such effects of linear terms we propose a perturbation of (4.1)

$$x_{n+1} = \begin{cases} f_L(x_n) & = \lambda x_n + a & \text{if } x_n < 0 \\ f_R(x_n) & = -\eta(x_n + \varepsilon)^p + b & \text{if } x_n \geq 0 \end{cases} \tag{4.10}$$

as a possible avenue for future work.

The period-incrementing cascade has been shown to explain impact patterns resulting from grazing bifurcations in mechanical problems. What application would require a more complex cascade, such as the anharmonic cascade?

CHAPTER 5

Non-smooth Hopf Type Bifurcations in Rotating Machinery with Impact and Friction

5.1 Introduction

In rotating machines that are levitated by magnetic bearings, non-smooth events involving impact and friction can occur between a rotor and its housing, the stator. These events are undesirable as they may be destructive and hence costly [104]. An understanding of the resulting dynamics, often characterised by novel types of non-smooth bifurcations, could enable rigorous derivation of possible control strategies. Systems experiencing instantaneous impact and/or friction contact events have been successfully modelled by non-smooth hybrid systems, which model the dynamics of systems with piecewise-smooth flows interrupted by events such as impacts described by maps. These systems experience energy dissipation, which can be modelled by Newton's restitution law and Coulomb's friction law, respectively, [34, 33, 37, 125, 79, 114]. In this Chapter we adopt this formalism to study a simplified rotating machine, i.e. contact events between a disk (rotor) and a rigid circular boundary (stator) modelled by a 2-degree of freedom impact-friction oscillator. Although other energy dissipation models, such as Poisson's kinetic [75] or Stronge's energetic [110, 93] laws, can be adopted all three are equivalent for this system due to the rotor's properties; we will elaborate the details in §5.2. The study of such hybrid systems has led to the identification and classification of many discontinuity induced bifurcations such as the non-smooth fold or persistence boundary equilibrium bifurcation (BEB) [34, 33, 37]. These arise

when the regular equilibrium evolves to lie on the impact surface under a change of the bifurcation parameter. We will demonstrate that, in a suitable rotating frame, such phenomena occur when considering the rotor motion without contact and in continuous contact (synchronous forward rubbing). However, many more non-smooth related phenomena exist [34, 33] such as creation of limit cycles at BEB and we identify them in this Chapter.

In general the behaviour of rotating machines such as these can be very complex. Simplified models that do not take rotor damping and/or stiffness into account have been studied in [77, 78]. Li and Païdoussis [77] focus on numerically investigating continuous contact (rub) and repeated impact motion which yields rich dynamics such as chaos as well as non-smooth bifurcation. While Lu *et al.* [78] analytically derive existence conditions of periodically impacting motion. Our intention in this Chapter is not to give a complete survey of such, but to consider a specific form of motion and the novel Hopf-type bifurcations which lead to this. In particular, Keogh and Cole show [67] that a rotor stator system with damping and friction can exhibit various forms of stable and unstable synchronous single impact limit cycles. We now present a global analysis of the existence of this type of orbit and describe the novel bifurcation of the aforementioned equilibrium states without impact and *two* coexisting limit cycles with different period at the BEB point. This bifurcation has many of the qualitative features of a smooth Hopf bifurcation in that small amplitude impacting limit cycles of non-zero period are created close to the BEB point. For the sake of classification we shall call it a *non-smooth Fold–Hopf bifurcation*. Our analysis of this bifurcation will be general and applicable to many other related problems.

Similar discontinuity induced Hopf bifurcations, exhibiting a bifurcation of the regular equilibrium to one limit cycle, have been observed in planar piecewise-smooth continuous systems [33, 37, 108] with sliding [62] and with biological applications [107]. In vibro-impacting systems of two degrees of freedom non-smooth Hopf bifurcations have been observed and can also be a route to chaos. [79, 125].

In the bifurcation analysis we present in this Chapter, when studying the effects of bearing damping, we find two coexisting smooth fold bifurcations. We also show the existence of orbits which, at the point of impact, have zero normal velocity and lie tangential to the impact surface, called *grazing* orbits [90].

The remainder of this Chapter is laid out as follows. In §5.2, we give a brief introduction to magnetic bearing systems comprising a rotating circular rotor with a disk cross-section impacting with a bearing. We derive the non-dimensionalised equations of the disk in free flight and at impact. In §5.3 we give examples of the rotor motion in the absence of impact and under impact. In §5.4 we study boundary equilibrium bifurcations of synchronous non-impacting states. To do this, the hybrid system approach for modelling systems with instantaneous impact described in [33] is

adopted. This procedure reveals standard non-smooth fold and persistence bifurcation for certain parameters. In §5.5 we apply a Poincaré mapping technique which allows us to determine solutions which are the simplest forms of periodically or quasi-periodically impacting orbit. The resulting global analysis yields interesting and new smooth and non-smooth dynamics described above, including the existence of the non-smooth Hopf-type bifurcations from non-impacting equilibria to periodic orbits with impact. In §5.6 we focus on the local analysis of this Hopf-like bifurcation, looking at a more general class of problems. This analysis allows us to make more a more detailed (local) study of the non-smooth Hopf-type bifurcation and the results can be compared with the calculations in §5.5. Finally, in §5.7 we present our conclusions and suggest some open questions.

5.2 Introduction to Magnetic Bearing Systems and their Associated Dynamics

[1] Rotating machines are prevalent in engineering applications that require power to be generated or utilised. The power rating is determined by the product of the driving or load torque and the rotational speed. In order to operate effectively, a rotor should spin in a stable manner under the support of bearings. The bearings should also be able to cope with inherent rotor imbalance and any fault conditions that may occur during operation of the machine. A number of bearing types are available to designers of machines, commonly including those based on rolling ball or cylindrical elements, and bushings with oil films. Usually, there is a specified maximum operating speed below which it is safe to run the rotor. If this speed is exceeded for any significant period, the bearing is likely to fail due to high mechanical or thermal stresses. Gas bearings may allow higher speed operation, but they are limited in their load carrying capacity and require a continuous flow of pressurised air. Foil/gas bearings are self-acting and do not require a pressurised source, though below a threshold speed the foil element is in rubbing contact with the rotor and is then prone to wear.

Active magnetic bearings have been under development since the 1970s [63] and have seen a growing number of applications including in turbomolecular and vacuum pumps [63], compressors [63], motors [63], generators [63], centrifuges [63], flywheels [63] and beam choppers [63]. An arrangement of electromagnets under feedback control enables a rotor to be levitated. It may then rotate without direct interaction with bearing surfaces or fluids, which has advantages in terms of friction reduction and the elimination of the need for pressurised oil or gas supplies. Higher operating speeds are therefore possible. However, magnetic bearing functionality may be compromised by failure of power supplies, which would lead to rotor delevitation. Also, any external dis-

[1] beginning of Patrick Keogh's first comment

turbance may cause the load capacity of the bearing, which is limited by magnetic flux saturation, to be exceeded. Magnetic bearings may be configured to transmit low forces at a particular operating speed, through use of a notch filter in the feedback control, but high acceleration input disturbances, e.g. shock conditions, would be problematic. For these reasons, magnetic bearings usually contain secondary touchdown bearings to prevent rotor motion from exceeding damaging limits. The design issues for such systems are given in [80].

Although some studies have been made to investigate the nonlinear rotor dynamics that arise from rotor contact with touchdown bearings, the problem is still not completely understood [63]. The condition for backward whirl rubbing, which may involve severe contact forces is understood as the condition in which the rotor is in rolling contact with the touchdown bearing [67]. A number of authors have considered the dynamics of a rotor within a clearance space [11, 13, 20, 21, 25, 39, 40, 64, 69, 74, 88, 87, 121]. With respect to operational magnetic bearing systems, which is in contrast to non-operational delevitation, it is important to gain a full understanding of all nonlinear dynamic issues so that appropriate control action may be designed to recover contact-free levitation. Without this knowledge it is not possible to ensure that normally levitated control is recoverable.[2]

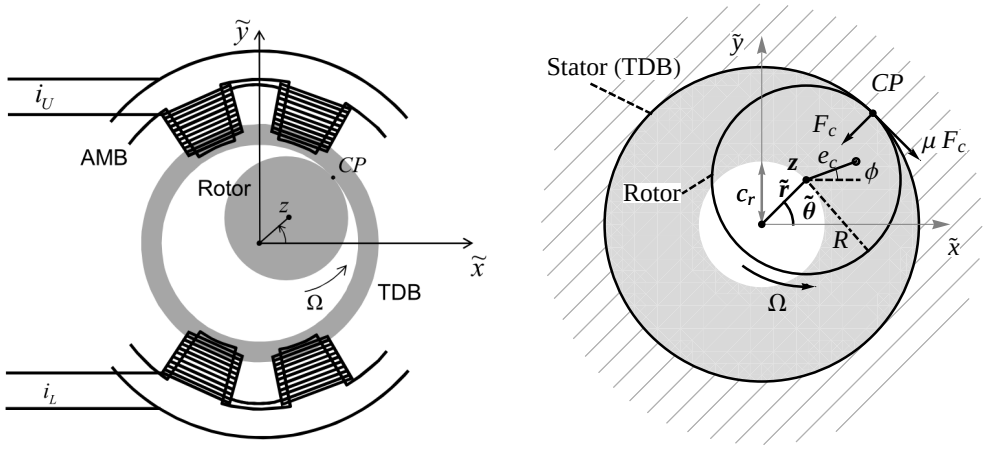

Figure 5-1: *Fixed Frame: (5-1a) The active magnetic bearing (AMB) currents, i_U and i_L, are shown in the vertical axis only. With appropriate control, these determine the AMB stiffness and damping characteristic. (5-1b) The rotor-touchdown bearing (TDB) impact at the contact point CP; contact force F_c and frictional force μF_c are acting. The rotor centre is shown in both complex coordinate z and polar coordinates $(\tilde{r}, \tilde{\theta})$. In free flight its motion is constrained to be within the clearance disk (white). The rotor is affected by mass imbalance with eccentricity e_c and phase angle ϕ.*

The mechanical model, illustrated in Figure 5-1, is adopted from [67]. It comprises a

[2]end of Patrick Keogh's first comment

spinning rotor with disk cross-section of radius R rotating inside a circular touchdown bearing. At the bearing centre lies the origin from which we measure the rotor's position (disk centre) in polar coordinates $(\tilde{r}, \tilde{\theta})$. The rotor comes into contact with the bearing when $\tilde{r} = c_r$. We describe the position of the centre z at time τ using complex coordinates in the form

$$z(\tau) = \tilde{x}(\tau) + i\tilde{y}(\tau) = \tilde{r}(\tau)e^{i\tilde{\theta}(\tau)}.$$

The system under consideration has magnetic bearing supports which are under *proportional-integral-derivative (PID)* control. Then the rotor's motion can be approximated by a linear spring-damper system with stiffness k and damping c, [67]. Further, the rotor, of mass m spinning at constant speed $\Omega > 0$, is affected by mass imbalance. In free flight when the rotor centre, defined by the complex coordinate z, lies within the clearance circle with radius c_r it satisfies a linear constant coefficient complex valued ODE,

$$m\ddot{z}(\tau) + c\dot{z}(\tau) + kz(\tau) = f_u\, e^{i\Omega\tau} \qquad \text{if} \quad |z(\tau)| < c_r \tag{5.1}$$

where m, c and k are real and positive parameters. The forcing term depends on the angular speed Ω as well as the complex imbalance force f_u, which is given by

$$f_u = m\, e_c\, \Omega^2 e^{i\phi}$$

where e is the imbalance eccentricity (distance between geometric centre and centre of mass) and the imbalance phase ϕ, see Figure 5-1.

It is possible to introduce integral control action in equation (5.1). For real machines the integral (I) gain would be typically set at a level that gives rise to a dynamic mode having a very long time constant. Thus, when the magnetic bearing is activated the integral action ensures that the rotor rises slowly to the bearing centre. Thereafter, it is common to set the integral gain to zero and the established control currents will continue to levitate the rotor at the bearing centre. The remaining proportional (P) and derivative (D) gains will then cause the spring-damper terms to be effective when the rotor deviates from levitated equilibrium at the magnetic bearing centre. Hence equation (5.1), without integral control action, is representative of a practically levitated and spinning rotor.

We assume that the system experiences an instantaneous collision at time $\tau_{i,-}$ when the rotor centre z comes into contact with the clearance circle, i.e. $|z| = c_r$, and in that case a *reset law* applies. With $\tau_{i,-}$ we denote the impact time as the rotor is approaching the stator and with $\tau_{i,+}$ as the rotor is leaving the stator. Before stating the reset law we will specify our assumptions. First, the stator is assumed to be infinitely stiff and to behave like a fixed impact surface. Second, as the rotational speed Ω is high, the change of Ω during impact is negligible and hence we presume

that it remains unchanged during impact. Third, at the point of contact, the relative tangential velocity $v_{rel}(\tau_{i,-})$ between the rotor and frame is given by

$$v_{rel}(\tau_{i,-}) = R\Omega + c_r\dot{\tilde{\theta}}(\tau_{i,-}). \tag{5.2}$$

If $\dot{\tilde{\theta}}(\tau_{i,-}) > -R\Omega/c_r$ then the relative tangential velocity does not change sign at impact. In §5.4 and in §5.5 we will show that this condition is satisfied for the periodically impacting limit cycles considered in this Chapter. Hence, it follows that the three coefficient of restitution models, i.e. kinetic, kinematic and energetic, yield the same impact velocity, [110, 93]. It has been shown in [110] that if $v_{rel}(\tau_{i,-})$ is not constant during an instantaneous impact with friction then the kinetic and kinematic models can lead to a non-physical increase in kinetic energy.

Finally, at the impact time $\tau_{i,-}$ the rotor experiences an impulsive normal contact force F_c in the z-direction with an associated impulsive frictional force F_f in the iz-direction. The energy dissipation in the normal contact direction is approximated by Newton's coefficient of restitution d and in the tangential contact direction by Coulomb's coefficient of friction μ. This gives

$$F_f = -\mu\,\mathrm{sgn}(v_{rel}(\tau_{i,-}))F_c = -\mu F_c = -\mu(1+d)m\dot{\tilde{r}}(\tau_{i,-})\delta(\tau-\tau_{i,-}) \tag{5.3}$$

where $\dot{\tilde{r}}(\tau_{i,-})$ is the normal impact velocity and δ is the Dirac delta function.

Under these assumptions the rotor's position is unchanged by the impact:

$$z(\tau_{i,+}) = z(\tau_{i,-}) \equiv z(\tau_i).$$

In contrast its complex velocity changes instantaneously and satisfies a reset law given by

$$\dot{z}(\tau_{i,+}) = \dot{z}(\tau_{i,-}) - q\frac{\mathrm{Re}(z^*\dot{z}(\tau_{i,-}))z}{|z|^2} = \dot{z}(\tau_{i,-}) - q\dot{\tilde{r}}(\tau_{i,-})\frac{z}{|z|}. \tag{5.4}$$

where $q = (1+d)(1+i\mu)$ and z^* is the complex conjugate of z. Note that although the reset law is nonlinear in the $(\tilde{x},\tilde{y})$ Cartesian frame with $z = \tilde{x} + i\tilde{y}$, it is linear in the polar coordinates frame $(\tilde{r},\tilde{\theta})$ and we have

$$\dot{\tilde{r}}(\tau_{i,+}) = -d\dot{\tilde{r}}(\tau_{i,-}) \tag{5.5}$$

$$\dot{\tilde{\theta}}(\tau_{i,+}) = \dot{\tilde{\theta}}(\tau_{i,-}) - \mu(1+d)\frac{\dot{\tilde{r}}(\tau_{i,-})}{c_r}. \tag{5.6}$$

[3] There is a range of designs for practical touchdown bearings, including bushing and rolling element types. These are mounted in housings, either directly as push fits or with some compliant backing material to provide some degree of cushioning. A

[3] beginning of Patrick Keogh's second comment

rotor mounted touchdown sleeve may be included as another component. However, a requirement is that the rotor motion must be constrained sufficiently so as to protect the rotor and magnetic bearing. This necessitates that the radial stiffness associated with a touchdown bearing must be significantly greater that associated with a magnetic bearing [104, 112, 111]. Any contact between a rotor and touchdown bearing will generate a finite region of contact, the size of which will depend on material properties and contact force. The contact mechanics will also determine the level of penetration or relative closure of the touchdown bearing and rotor geometric centres under contact. In the limiting case of zero penetration, or infinite contact stiffness, dynamic contact forces become idealised impulsive approximations to the practically finite contact forces. We also remark that considerable uncertainty of contact conditions may arise from angular misalignment between a rotor and touchdown bearing. The impulsive approximation therefore provides an impact model against which consistent rotor dynamic behaviour may be derived. For this reason, it is adopted in this Chapter. Predicted rotor motions will generally involve sequences of instantaneous impacts involving impulsive normal and tangential forces. In principle, intervals of persistent contact may be regarded as limiting cases when time intervals between impacts tend to zero [67].[4]

However, for most of the analysis, except for the BEB computation in §5.4, it is not appropriate to transform the entire system into the latter frame $(\tilde{r}, \tilde{\theta})$ as in this frame the equation of motion (5.1) is nonlinear. It is convenient for further computations to introduce a complex co-rotating frame with coordinate u so that

$$z = ue^{i\Omega\tau}.$$

As the name indicates, this frame rotates synchronously with the rotor at speed Ω. This will be advantageous when examining synchronous impacting limit cycles. It follows that by substituting into the defining equations and cancelling the factor of $e^{i\Omega\tau}$ we have, in free flight,

$$m\ddot{u} + (c + 2im\Omega)\dot{u} + (k - m\Omega^2 + ic\Omega)u = me_c\Omega^2 e^{i\phi}. \tag{5.7}$$

A general solution of (5.7) may have an impact at a subsequent time τ_i. In this case the reset law (5.4) in the co-rotating frame becomes

$$\dot{u}(\tau_{i,+}) = \dot{u}(\tau_{i,-}) - (1+d)(1+i\mu)\frac{\mathrm{Re}(u(\tau_i)^*\dot{u}(\tau_{i,-}))u(\tau_i)}{|u(\tau_i)|^2}.$$

where u^* is the complex conjugate of u. We now non-dimensionalise the system both to reduce the number of free parameters and also to show that no natural large or small

[4] end of Patrick Keogh's second comment

parameters are present in this system. We introduce a scaled time $t = \Omega\tau$, so

$$\frac{d}{d\tau} = \Omega\frac{d}{dt} \quad \text{and} \quad \frac{d^2}{d\tau^2} = \Omega^2\frac{d^2}{dt^2}.$$

This new term moves through one period in time $t = 2\pi$ if the original time goes through one period of the forcing term, $2\pi/\Omega$. If primes denote differentiation with respect to the scaled time t

$$\ddot{u} = \Omega^2 u'', \quad \dot{u} = \Omega u', \quad \delta(\tau - \tau_{i,-}) = \Omega\delta(t - t_{i,-})$$

then substituting into (5.7) and dividing by $m\Omega^2$ we obtain

$$u'' + \left(\frac{c}{m\Omega} + 2i\right)u' + \left(\frac{k}{m\Omega^2} - 1 + i\frac{c}{m\Omega}\right)u = e_c\, e^{i\phi}. \tag{5.8}$$

Setting the parameters

$$\gamma = \frac{c}{m\Omega}, \quad \omega^2 = \frac{k}{m\Omega^2} \quad \text{and the variable} \quad u = c_r U \tag{5.9}$$

then (5.8) in scaled co-rotating complex coordinate $U := re^{i\theta}$ becomes

$$\ddot{U} + (\gamma + 2i)\,\dot{U} + (\omega^2 - 1 + i\gamma)\,U = \rho\, e^{i\phi} \quad \text{in} \quad |U| \le 1 \tag{5.10}$$

where $\rho = e_c/c_r$. The corresponding inertial complex coordinate $Z := re^{\Theta}$ with $\Theta := \theta + t$. Consequently, the reset law is

$$U(t_+) = U(t_-) \tag{5.11}$$

$$\dot{U}(t_+) - \dot{U}(t_-) = -q\,\dot{r}(t_-)U(t_-) \tag{5.12}$$

where $\dot{r}(t_-)$ is the normal velocity in polar coordinates and $q = (1 + d)(1 + i\mu)$. The choices of parameters (in consistent units) corresponding to the experimental application in [67] are

$$m = 50 \text{ kg}, \quad c = 1400 \text{ N s/m}, \quad k = 9.8 \times 10^5 \text{ N/m}, \quad e_c = 0.3 \times 10^{-3} \text{ m},$$
$$c_r = 0.7 \times 10^{-3}\text{m}, \quad R = 0.4 \times 10^{-1} \text{ m}, \quad \phi = 0.21 \text{ rad}, \quad \Omega = 184.2 \text{ rad/s},$$
$$\mu = 0.15, \quad d = 0.95$$

and the revised parameters, valid in the unit disk after rescaling are

$$\gamma \approx 0.152, \quad \omega \approx 0.76, \quad \rho = 3/7 \approx 0.428, \quad \mu = 0.15, \quad d = 0.95$$

i.e. all the parameters are now order one and there are no privileged small or large parameters. In this Chapter the bearing damping coefficient $\gamma > 0$ will act as the

bifurcation parameter and the remaining parameters will take the values given above unless stated otherwise.

5.3 Basic Solution Types of Synchronous Rotor Dynamics

In this Section we introduce the simplest solution types in the co-rotating frame, and in particular study solutions which are either not in contact, or are in continuous contact, or which have instantaneous impacts. To do this we firstly, we rewrite the scaled equations of motion (5.10) as a first order complex system. This will be helpful in the global and local analysis of a periodically impacting orbit in later Sections. Let the complex vector $\boldsymbol{w}(t) = (U(t), \dot{U}(t))$, then the equation of free motion of the rotor centre U in terms of $\boldsymbol{w}$ is given by

$$\dot{\boldsymbol{w}}(t) = A\boldsymbol{w}(t) + \boldsymbol{b} \quad \text{if} \quad |U| < 1 \tag{5.13}$$

where the matrix A and the vector $\boldsymbol{b}$ are constant and are defined by

$$A = \begin{pmatrix} 0 & 1 \\ 1-\omega^2 - i\gamma & -\gamma - 2i \end{pmatrix} \quad \text{and} \quad \boldsymbol{b} = \begin{pmatrix} 0 \\ \rho e^{i\phi} \end{pmatrix}. \tag{5.14}$$

If $|U| = 1$ an impact occurs and then the rotor position U and velocity $\dot{U}$ obey the reset law given by

$$\boldsymbol{w}_{0,+} = \boldsymbol{w}_{0,-} - \begin{pmatrix} 0 \\ q\dot{r}_{0,-}U_0 \end{pmatrix} \quad \text{if} \quad |U| = 1 \tag{5.15}$$

where $q = (1+d)(1+i\mu)$ and we simplify the notation $\boldsymbol{w}(t_{0,+}) \equiv \boldsymbol{w}_{0,+}$. As the equation of motion (5.13) is linear and the vector $\boldsymbol{b}$ is constant the general solution with initial conditions $\boldsymbol{w}(t_{0,+})$ given by (5.15) can be written as

$$\boldsymbol{w}(t) = \exp(A(t-t_0))\left(\boldsymbol{w}_{0,+} + A^{-1}\boldsymbol{b}\right) - A^{-1}\boldsymbol{b} \quad \text{if} \quad |U| \leq 1. \tag{5.16}$$

The eigenvalues $\lambda_\pm$ of the matrix A are given by

$$\lambda_\pm = \frac{-\gamma + i\left(-2 \pm \sqrt{4\omega^2 - \gamma^2}\right)}{2} \tag{5.17}$$

with real part $\mathrm{Re}(\lambda) = -\gamma/2 < 0$ as we assume (given the experimentally defined values) that $0 < \gamma < 2\omega$. This implies that in the absence of impact there is an asymptotically stable equilibrium solution given by

$$\boldsymbol{w} = -A^{-1}\boldsymbol{b}. \tag{5.18}$$

Depending on the parameters this equilibrium can lie either

1. inside (equilibrium is physically realistic, we denote this steady state *admissible*)
2. on: (continuous contact) or
3. outside: (equilibrium is physically unrealistic, we denote this steady state *virtual*)

the clearance circle. By extension, this nomenclature is implemented for other orbits. In the first case this motion is called non-contacting whirl, Figure 5-2a. The second case describes the critical transition point between physically realistic (case 1) and physically unrealistic orbits (case 3). Due to rotor faults, such as rotor imbalance or mass loss, more complicated rotor trajectories are possible, such as those involving continuous (zero normal velocity and non-negative normal acceleration) or instantaneous rotor-stator contact. When the rotor and stator are in continuous contact, sliding [67] or pure rolling (if relative tangential velocity $v_{rel}(t) = 0$, e.g. [67]), are possible. In the case of sliding, forward rubbing is observed if $\dot{\theta}(t) > -1$ (in the co-rotating frame), and backward rubbing if $\dot{\theta}(t) < -1$ (in the co-rotating frame). In this Chapter we consider only one particular type of continuous contact called synchronous forward rubbing, i.e. in the co-rotating frame the rotor sticks to the stator (tangential velocity $\dot{\theta}(t) = 0$), e.g. [67]. In particular, we will only study the equilibria of this kind of motion and show that standard non-smooth bifurcations with the non-impacting equilibrium occurs in §5.4. Other continuous contact motions are not studied in this Chapter as the reset law is not sufficient to describe such behaviour and how it arises.

When the rotor and stator experience an instantaneous contact it can lead to orbits that impact periodically or quasi-periodically and synchronously in the co-rotating frame, Figures 5-2b, 5-2c. We call these *period-T synchronous impacting limit cycles* as the orbit experiences one impact per period T. The limit cycles with small amplitude (Figure 5-2c) are created in a non-smooth Hopf-type bifurcation, see §5.5. Whereas limit cycles with large amplitude (Figure 5-2b) can lead to grazing events [90], i.e. the trajectory interacts tangentially with the impact surface. A systematic way of analysing such motions with instantaneous impact, is to consider them as orbits of hybrid piecewise-smooth dynamical systems, in which smooth flows between impact are combined with maps describing the impact. Such an approach is very suitable for finding both the existence and the stability of periodic orbits [34] and we will adopt it here.

In addition to periodic [78] or quasi-periodic orbits [77] it has been shown that in similar models the rotor-stator motion can be chaotic [77]. Other types of motion can include an accumulation of infinite number of impacts in finite time [77, 45], often called *chattering*. Chattering can lead to sticking [18] and sliding motion [34] and hence can be used to predict the onset of continuous contact motion without actually computing continuous contact trajectories. Li and Païdoussis [77] have done this to identify for

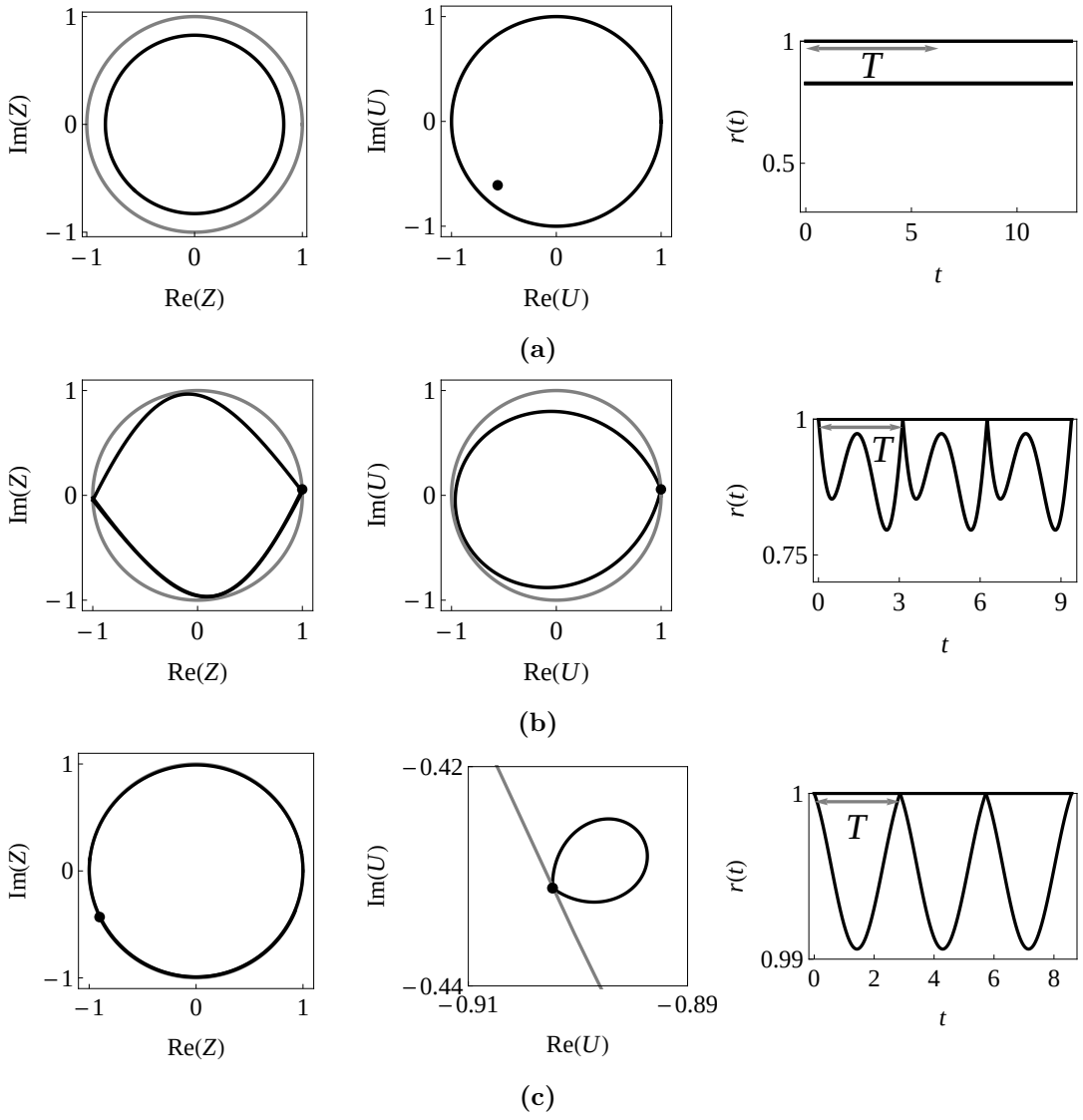

Figure 5-2: *Orbits (black) with period T in the inertial and the rotating frame as well as amplitude $r(t)$ against time t. The clearance circle (grey) has radius 1. (5-2a) Regular equilibrium without impact ($\gamma = 0.3$). (5-2b) Limit cycle $B_{1,d}$ near grazing ($\gamma = 0.065$). (5-2c) Limit cycle $B_{1,a}$ near non-smooth Fold–Hopf Bifurcation, ($\gamma = 0.1$).*

what values of coefficient of friction, μ, and eccentricity, e_c, continuous contact motion occurs. Similarly, the occurrence of chattering sequences and the possibly resulting continuous contact also depends on damping, c, and spring stiffness, k, parameters as we will show in Chapter 6. Such, particle motion can best be systematically described by set valued functions instead of hybrid systems. These types of models, called *differential inclusion* [76] are particularly well suited to analyse problems involving only friction, e.g. sliding and sticking motion of rotating particles. Such a model, a forced rotating pendulum in continuous contact with a circular boundary, shows similar features to ours in that various orbits collapse onto the equilibrium set in finite time [12]. Whilst it is certainly possible that such chattering and sticking motions may arise in a magnetic bearing system, in this Chapter we will restrict or analysis to that of the simpler types of periodic motion described above.

5.4 Boundary Equilibrium Solutions and their Bifurcations

Boundary equilibria are steady states of the form (5.18) that lie on the impact surface, so that $|U| = c_r$. They are important in the bifurcation analysis of non-smooth systems as other equilibria or limit cycles can bifurcate from them. In this Section we focus on the system's equilibria of both motion in free flight and in continuous contact (only sticking), called *regular* and *pseudo* equilibria respectively, in the co-rotating frame. The standard theory developed in [33, 37, 34] and introduced in Chapter 2 will be applied to study their existence and stability and categorise the bifurcation scenarios. Depending on the system's parameters we will observe either *persistence* or a *non-smooth fold*. In the first case a regular equilibrium becomes a pseudo equilibrium as the bifurcation parameter γ is varied. In the second case these two are created in a fold like bifurcation and coexist.

The analysis using the methods mentioned above is much simpler when the reset law is linear; this is the case when the system (5.10) is formulated in polar coordinates. Let the state vector of the rotor centre in polar coordinates $\boldsymbol{x} \in \mathbb{R}^4$ be given by

$$\boldsymbol{x} = (x_1, x_2, x_3, x_4) := (r, \theta, \dot{r}, \dot{\theta}).$$

In contrast, its motion in free flight (5.10) is now given by the nonlinear system

$$\dot{\boldsymbol{x}} = F(\boldsymbol{x}), \quad H(\boldsymbol{x}) := 1 - x_1 > 0 \tag{5.19}$$

where

$$F(\boldsymbol{x}) = \begin{pmatrix} x_3 \\ x_4 \\ x_1\left((1+x_4)^2 - \omega^2\right) - \gamma x_3 + \rho\cos\left(\phi - x_2\right) \\ \left(-(1+x_4)(\gamma x_1 + 2x_3) + \rho\sin\left(\phi - x_2\right)\right)/x_1 \end{pmatrix}.$$

An impact is observed when the state vector $\boldsymbol{x}$ lies on the impact surface Σ defined by

$$\Sigma = \{\boldsymbol{x} : H(\boldsymbol{x}) := 1 - x_1 = 0\} \tag{5.20}$$

in which case the reset law R applies. The state after impact $\boldsymbol{x}^+$ is given by

$$\boldsymbol{x}^+ = R(\boldsymbol{x}^-) = \boldsymbol{x}^- + W(\boldsymbol{x}^-)v(\boldsymbol{x}^-)$$

where the vector $W = (0, 0, 1+d, \mu(1+d))^T$. Let $v(\boldsymbol{x})$ be the velocity of the vector field F relative to H, denoted by

$$v(\boldsymbol{x}) := H_{\boldsymbol{x}}F(\boldsymbol{x}) = -x_3 \tag{5.21}$$

and let $a(\boldsymbol{x})$ be the respective acceleration given by

$$a(\boldsymbol{x}) := (H_{\boldsymbol{x}}F)_{\boldsymbol{x}}F(\boldsymbol{x}) = -\dot{x}_3. \tag{5.22}$$

In the special case when the normal velocity x_3 is zero, the reset law R is the identity mapping.

Next, we will describe the motion in continuous contact. The rotor centre undergoes sticking motion (in the co-rotating frame) when it comes into contact with the boundary, i.e. $H = 0$, and remains there, i.e. when the velocity $v(\boldsymbol{x}) = 0$ and the acceleration $a(\boldsymbol{x}) < 0$, called sticking conditions. The motion, which is degenerate, is maintained along the vector field F_s, as defined by

$$\begin{aligned} F_s(\boldsymbol{x}) &:= F(\boldsymbol{x}) - \eta(\boldsymbol{x})W(\boldsymbol{x}) \\ &= \begin{pmatrix} x_3 \\ x_4 \\ 0 \\ \left(-(1+x_4)(\gamma x_1 + 2x_3) + \rho\sin(\phi - x_2) - \mu(1+d)\,\eta\left(\boldsymbol{x}\right)\right)/x_1 \end{pmatrix} \end{aligned}$$

where η, chosen such that the sticking conditions are satisfied, is given by

$$\eta(\boldsymbol{x}) := \frac{a(\boldsymbol{x})}{(H_{\boldsymbol{x}}F)_{\boldsymbol{x}}W(\boldsymbol{x})} = \frac{-1}{1+d}\left(x_1(\omega^2 - (1+x_4)^2) - \gamma x_3 - \rho\cos(\phi - x_2)\right).$$

As η depends on the acceleration $a(\boldsymbol{x})$ its sign determines when the sticking vector field

is physically realistic, i.e. $\eta(\boldsymbol{x}) > 0$. In an impacting system with these two motions

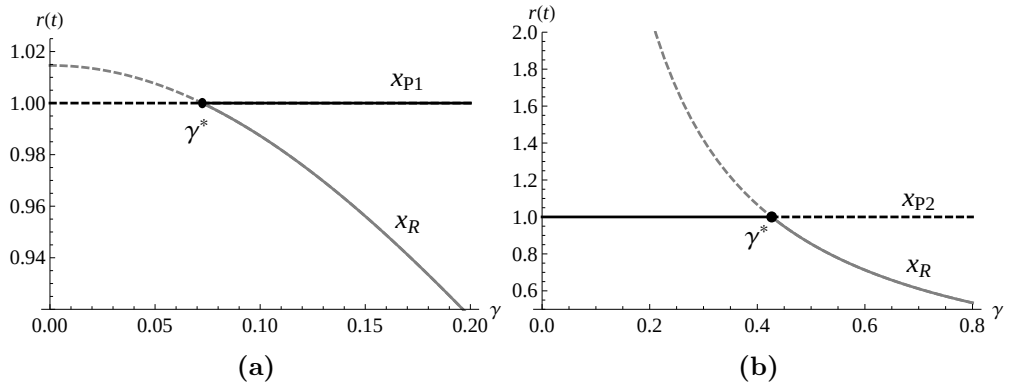

Figure 5-3: *Bifurcation scenario of regular (grey) and pseudo (black) equilibria. (5-3a) Virtual (dashed) regular $\boldsymbol{x}_R$ and pseudo $\boldsymbol{x}_{P1}$ equilibria clash in a non-smooth fold bifurcation at $\gamma^* \approx 0.072$ and become admissible (solid). (5-3b) The admissible pseudo equilibrium x_{P2} and virtual regular equilibrium $\boldsymbol{x}_R$ become virtual and admissible, respectively, in a persistence bifurcation at $\gamma^* \approx 0.428$.*

the following equilibria can be observed; the admissible equilibrium of the steady state:

E1 of free flight motion called *regular equilibrium* $\boldsymbol{x}_R$ if $F(\boldsymbol{x}_R) = 0$ and $H(\boldsymbol{x}_R) > 0$ hold,

E2 of sticking motion called *pseudo equilibrium* $\boldsymbol{x}_P$ if $F_s(\boldsymbol{x}_P) = 0$, $H(\boldsymbol{x}_P) = 0$ and $\eta(\boldsymbol{x}_P) > 0$ hold.

The regular equilibrium is called virtual if it lies outside of the stator boundary, i.e. $H(\boldsymbol{x}_R) < 0$. The pseudo equilibrium is called virtual if the acceleration points away from the stator, i.e. $\eta(\boldsymbol{x}_P) < 0$.

We are interested in when these two equilibria bifurcate. In an impacting system this happens when the regular equilibrium lies on the impacting surface. This is called *boundary equilibrium point* at $\boldsymbol{x} = \boldsymbol{x}_B$ with $\gamma = \gamma^*$ if $F(\boldsymbol{x}_B, \gamma^*) = 0$ and $H(\boldsymbol{x}_B, \gamma^*) = 0$ hold.

We claim that our system has one regular equilibrium (non-impacting whirl) given by

$$\boldsymbol{x}_R = \left(\frac{\rho}{\sqrt{\gamma^2 + (-1+\omega^2)^2}}, \phi - \pi + \arctan\left(\frac{\gamma}{1-\omega^2}\right), 0, 0 \right),$$

but two pseudo equilibria (synchronous forward rubbing)

$$\boldsymbol{x}_{P1,P2} = \left(1, \phi - \pi \mp \arccos\left(\frac{\gamma + \mu(1-\omega^2)}{\rho\sqrt{1+\mu^2}}\right) + \arctan\left(\frac{1}{\mu}\right), 0, 0 \right),$$

with the sticking vector field admissibility condition given by

$$\eta_{1,2} = \frac{1-\omega^2-\gamma\mu \mp \sqrt{\rho^2(1+\mu^2)-(\gamma+\mu(1-\omega^2))^2}}{(1+d)(1+\mu^2)}.$$

Before we state the bifurcation scenario at the boundary equilibrium point

$$\boldsymbol{x}_B = \left(1, \phi-\pi+\arctan\left(\frac{\sqrt{\rho^2-(-1+\omega^2)^2}}{1-\omega^2}\right), 0, 0\right) \quad \text{with} \quad \gamma^* = \sqrt{\rho^2-(-1+\omega^2)^2}$$

of this system we briefly explain the methods developed in [33, 37, 34].

Linearising about the boundary equilibrium point $\boldsymbol{x}_B$ with γ^* yields the conditions which determine how the regular and pseudo equilibrium bifurcate at that point. Assuming that the following conditions hold

$$\begin{aligned}
&\text{(C1)} \quad \det(F_{\boldsymbol{x}}^{-1}(\boldsymbol{x}_B,\gamma^*)) \neq 0\\
&\text{(C2)} \quad H_\gamma(\boldsymbol{x}_B,\gamma^*) - H_{\boldsymbol{x}}(\boldsymbol{x}_B,\gamma^*)\, F_{\boldsymbol{x}}^{-1}(\boldsymbol{x}_B,\gamma^*)\, F_\gamma(\boldsymbol{x}_B,\gamma^*) \neq 0\\
&\text{(C3)} \quad -H_{\boldsymbol{x}}(\boldsymbol{x}_B,\gamma^*)\, F_{\boldsymbol{x}}^{-1}(\boldsymbol{x}_B,\gamma^*)\, W(\boldsymbol{x}_B,\gamma^*) \neq 0
\end{aligned}$$

two bifurcation scenarios can occur. *Persistence* describes the situation when the admissible pseudo equilibrium becomes an admissible regular equilibrium, or vice versa. This is the case when the following inequality holds

$$\text{(C4)} \quad -H_\gamma(\boldsymbol{x}_B,\gamma^*)\, F_{\boldsymbol{x}}^{-1}(\boldsymbol{x}_B,\gamma^*)\, W(\boldsymbol{x}_B,\gamma^*) < 0.$$

A *non-smooth fold* bifurcation takes place when the admissible regular and pseudo equilibrium are created in a fold like bifurcation and coexist as the bifurcation parameter γ is changed in one direction but not the other; they cease to exist in one direction as they are not realisable in a physical sense. Assuming the same conditions as for the previous bifurcation scenario the opposite inequality must hold:

$$\text{(C5)} \quad -H_\gamma(\boldsymbol{x}_B,\gamma^*)\, F_{\boldsymbol{x}}^{-1}(\boldsymbol{x}_B,\gamma^*)\, W(\boldsymbol{x}_B,\gamma^*) > 0.$$

Now, we can state our results and explain all the details of this system's bifurcation scenario. For an example of these scenarios with particular parameters see Figure 5-3. Combining these results we have established the following.

Proposition 5.1. *Assume that the scaled spring constant $\omega \in (0,1)$, scaled imbalance radius $\rho \in (0,1)$, coefficient of restitution $d \in (0,1)$ and friction constant $\mu \in (0,1)$. Then at the boundary equilibrium point $\boldsymbol{x}_B$ with γ^* conditions (C1-3) are satisfied and we observe:*

a non-smooth fold *bifurcation of the regular equilibrium $\boldsymbol{x}_R$ and the pseudo equilib-*

rium $\boldsymbol{x}_{P1}$ *if*

$$\sqrt{1-\rho} < \omega < \sqrt{1 - \frac{\mu\rho}{\sqrt{1+\mu^2}}}. \tag{5.23}$$

The two equilibria, $\boldsymbol{x}_R$ *and* $\boldsymbol{x}_{P1}$*, coexist for* $\gamma \in (\gamma^*, 1)$ *while the second pseudo equilibrium* $\boldsymbol{x}_{P2}$ *exists for all* $\gamma \in (0, 1)$*.*

a persistence *bifurcation of the regular equilibrium* $\boldsymbol{x}_R$ *and the pseudo equilibrium* $\boldsymbol{x}_{P2}$ *if*

$$\sqrt{1 - \frac{\mu\rho}{\sqrt{1+\mu^2}}} < \omega < 1.$$

Then, no equilibrium coexists as the pseudo equilibrium $\boldsymbol{x}_{P1}$ *is virtual and* $\boldsymbol{x}_{P2}$ *exists for* $\gamma \in (0, \gamma^*)$ *while* $\boldsymbol{x}_R$ *exists for* $\gamma \in (\gamma^*, 1)$*.*

Note that $\omega > \sqrt{1-\rho}$ as otherwise the scaled damping parameter γ^* at the boundary equilibrium point is complex. Also, without damping, i.e. if $\gamma = 0$ the rotor in free motion is purely oscillatory.

We complete this Section with the stability analysis of the three equilibria $\boldsymbol{x}_R$, $\boldsymbol{x}_{P1}$ and $\boldsymbol{x}_{P2}$ as well as the boundary equilibrium point $\boldsymbol{x}_B$ with γ^*. The Jacobian matrix at the regular equilibrium $F_{\boldsymbol{x}}(\boldsymbol{x}_R)$ has four distinct eigenvalues Λ given by

$$\Lambda_R = \frac{1}{2}\left(-\gamma \pm 2i \pm i\sqrt{4\omega^2 - \gamma^2}\right).$$

We assume the scaled damping constant γ is positive and hence it follows that the regular equilibrium $\boldsymbol{x}_R$ is stable as $\mathrm{Re}(\Lambda_R) < 0$ for all $\gamma > 0$.

In order to determine the stability of the pseudo equilibria within the sticking set we study the Jacobian of the sticking vector field at the pseudo equilibria $F_{s,\boldsymbol{x}}(\boldsymbol{x}_{P1,P2})$. Two eigenvalues of this matrix are zero as the sticking vector field is degenerate due to the conditions which maintain the motion on the impact surface. But the other two eigenvalues do determine the stability of each pseudo equilibria $\boldsymbol{x}_{P1}$ and $\boldsymbol{x}_{P2}$ which are given by

$$\Lambda_{P1} = \frac{1}{2}\left(\gamma - 2\mu \mp \sqrt{(\gamma+2\mu)^2 + 4\ell_2}\right) \quad \text{and}$$
$$\Lambda_{P2} = \frac{1}{2}\left(\gamma - 2\mu \mp \sqrt{(\gamma+2\mu)^2 - 4\ell_2}\right),$$

respectively. The first pseudo equilibrium $\boldsymbol{x}_{P1}$ is unstable as the real part of the second eigenvalue is positive, whereas the second pseudo equilibrium $\boldsymbol{x}_{P2}$ is stable for $\gamma \in (0, \rho\sqrt{1+\mu^2} - \mu(1-\omega^2)$ but unstable for $\gamma > \rho\sqrt{1+\mu^2} - \mu(1-\omega^2)$.

5.5 Global Analysis of Synchronous Periodically Impacting Limit Cycles

In this Section existence conditions for the simplest type of limit cycles for the full system in which the periodic orbits have one instantaneous impact are derived analytically and are supported by numerical calculations. We show that these invariant sets undergo smooth fold bifurcations and new non-smooth Hopf-like bifurcations, i.e. at the BEB regular and pseudo equilibria as well as two limit cycle bifurcate. In §5.6 we give a local analysis of the latter in a more general setting. We also discuss the stability of these limit cycles in §5.5.1 and codimension-2 bifurcations related to the Hopf-type bifurcation (dependence on the stiffness related parameter ω) in §5.5.2. Having considered equilibrium solutions we now study the simplest type of limit cycle in our system (5.16). These, period-T periodically impacting limit cycles, experience one impact per cycle with identical impact velocity $\dot{U}(t_{i,-})$ at each impact event at time t_i for $i = 0, 1, 2 \ldots$. We further assume that these impacts occur synchronously with respect to the rotating framework. As a consequence the impact position $U(t_i)$ is identical at each impact at time t_i. In summary, we will study the periodically impacting limit cycles which satisfy repeatable initial conditions between consecutive impacts at time t_i and t_{i+1} given by

$$\boldsymbol{w}(t_{i,-}) \equiv \begin{pmatrix} U(t_i) \\ \dot{U}(t_{i,-}) \end{pmatrix} = \begin{pmatrix} U(t_{i+1}) \\ \dot{U}(t_{i+1,-}) \end{pmatrix} \equiv \boldsymbol{w}(t_{i+1,-}) \tag{5.24}$$

where we abbreviate the notation to $U_i = U(t_i)$ and $\dot{U}_{i,-} = \dot{U}(t_{i,-})$. It follows that, in polar coordinates, the normal and tangential velocity components must satisfy $\dot{r}_{i,-} = \dot{r}_{i+1,-}$ and $\dot{\theta}_{i,-} = \dot{\theta}_{i+1,-}$. We will show that for certain values of the damping parameter γ a finite number of such limit cycles coexist with a regular equilibrium. We will then demonstrate that only one set of a pair of physically plausible limit cycles with different period T undergoes a discontinuity induced bifurcation (DIB) at the BEB point $\gamma = \gamma^* =: \gamma_{DIB}$. That bifurcation will be shown to be of *non-smooth Hopf* type as two cycles collide with the boundary equilibrium point as their amplitude shrinks to zero. We conclude with illustrations for cases in which these limit cycles are physically realistic and for which they are stable.

A systematic approach to studying the limit cycles of the hybrid system comprising smooth flows between instantaneous impacts, is to consider the map from one impact event to the next. In particular, to determine the existence and stability of such limit cycles of period $T = t_1 - t_0$ it is equivalent to investigate the fixed points of the impact

map P_I defined by

$$P_I : \Sigma \to \Sigma \tag{5.25}$$

$$\boldsymbol{w}(t_{i,-}) \mapsto P_I\big(\boldsymbol{w}(t_{i,-})\big) = \boldsymbol{w}(t_{i+1,-}). \tag{5.26}$$

Such fixed points ($i = 1$) of period T, $\boldsymbol{w}(t_{0,-})$, satisfy the conditions

$$\boldsymbol{w}(t_{1,-}) = \boldsymbol{w}(t_{0,-}) \quad \text{or equivalently} \quad (t_1, \theta_1, \dot{r}_{1,-}, \dot{\theta}_{1,-}) = (t_0 + T, \theta_0 + 2\pi, \dot{r}_{0,-}, \dot{\theta}_{0,-}).$$

As before $\Sigma \subset \mathbb{R}^n$ denotes the impact surface (5.20). The advantage of this construction is that we can reduce the dimension of the problem by one as the radial coordinate $r = 1$, when the rotor is in contact with the boundary. Note that the set of solutions can include trajectories which are physically implausible in that they exit the interior of the bearing. However, these can be detected numerically once the existence conditions have been obtained.

To find fixed points, $\boldsymbol{w}_{0,-}$, we substitute the repeatable initial condition (5.24) into the general solution of the flow given by (5.16)

$$\boldsymbol{w}_{0,-} = \exp(AT)(\boldsymbol{w}_{0,+} + A^{-1}\boldsymbol{b}) - A^{-1}\boldsymbol{b}$$

where A and $\boldsymbol{b}$ are given in (5.14), and where the real part of the eigenvalues of A, given in (5.17), is negative, i.e. $\mathrm{Re}(\lambda_\pm) = -\gamma/2 < 0$ for $\gamma > 0$. Now, we solve for $\boldsymbol{w}_{0,-}$ to obtain

$$\boldsymbol{w}_{0,-} = -\big(\exp(-AT) - I\big)^{-1} \begin{pmatrix} 0 \\ q\dot{r}_{0,-}U_0 \end{pmatrix} - A^{-1}\boldsymbol{b}. \tag{5.27}$$

The matrix expression can be simplified further by considering the eigendecomposition of $A = VDV^{-1}$. Then

$$\begin{aligned}
&\big(\exp(-AT) - I\big)^{-1} \\
&= \frac{1}{1 - \mathrm{tr}\left(\exp(AT)\right) + \det\left(\exp(AT)\right)} \Big(\exp(AT) - \det\left(\exp(AT)\right) I\Big) \\
&= \frac{1}{1 - \mathrm{tr}\left(\exp(DT)\right) + \exp\left(\mathrm{tr}(AT)\right)} \Big(\exp(AT) - \exp\left(\mathrm{tr}(AT)\right) I\Big)
\end{aligned}$$

by Jacobi's formula. Finally, we can use the eigenvalues of A, λ_+ and λ_-, given in

(5.17), to obtain

$$\begin{aligned}
&\big(\exp(-AT) - I\big)^{-1} \\
&= \kappa \begin{pmatrix} \nu_- e^{\lambda_+ T} - \nu_+ e^{\lambda_- T} - e^{(\lambda_+ + \lambda_-)T} & \nu_+\nu_-(e^{\lambda_- T} - e^{\lambda_+ T}) \\ e^{\lambda_+ T} - e^{\lambda_- T} & \nu_- e^{\lambda_- T} - \nu_+ e^{\lambda_+ T} - e^{(\lambda_+ + \lambda_-)T} \end{pmatrix} \\
&=: \begin{pmatrix} a_{11}(T) & a_{12}(T) \\ a_{21}(T) & a_{22}(T) \end{pmatrix}
\end{aligned}$$

where $\nu_\pm = -\lambda_\pm/(1 - \omega^2 - i\gamma)$ and $\kappa = 1/((1 - e^{\lambda_- T})(1 - e^{\lambda_+ T})(\nu_- - \nu_+))$. Hence substituting this matrix into (5.27) simplifies to

$$\boldsymbol{w}_{0,-} \equiv \begin{pmatrix} U_0 \\ \dot{U}_{0,-} \end{pmatrix} \equiv \begin{pmatrix} e^{i\theta_0} \\ (\dot{r}_{0,-} + i\dot{\theta}_{0,-})U_0 \end{pmatrix} = \begin{pmatrix} -q\, a_{12}(T)\, \dot{r}_{0,-} U_0 + k \\ -q\, a_{22}(T)\, \dot{r}_{0,-} U_0 \end{pmatrix} \tag{5.28}$$

where $k = \rho e^{i\phi}/(\omega^2 - 1 + i\gamma)$. The system (5.28) yields three equations by solving the first row equation for U_0, taking the real part of the second row equation and solving it for $\dot{r}_{0,-}$, and taking the imaginary part of the second row equation, respectively,

$$U_0(1 + a_{12}(T)\, q\, \dot{r}_{0,-}) = k \tag{5.29}$$

$$\dot{r}_{0,-}\big(1 + \mathrm{Re}(q\, a_{22}(T))\big) = 0 \tag{5.30}$$

$$\dot{\theta}_{0,-} = -\,\mathrm{Im}\,\big(q\, a_{22}(T)\big)\dot{r}_{0,-}\,. \tag{5.31}$$

To determine the fixed points $\boldsymbol{w}_{0,-}$ from (5.28), we first find the period T, unknown a priori, from (5.30) and then compute the corresponding values $\dot{r}_{0,-}$ from (5.29), θ_0 from (5.29) and $\dot{\theta}_{0,-}$ from (5.31). Now, (5.30) is satisfied if $\dot{r}_{0,-}$ is zero, which only yields the boundary equilibrium $\boldsymbol{x}_B$, or if the nonlinear term in T, denote it by $F_1(T)$, is zero. Hence the period T can be determined by finding the zeroes of $F_1(T)$, given by

$$F_1(T) := 1 + \mathrm{Re}\left(q\, a_{22}(T)\right) = 1 - \mathrm{Re}\left(\frac{q}{\lambda_+ - \lambda_-}\left(\frac{\lambda_+ e^{\lambda_+ T}}{e^{\lambda_+ T} - 1} - \frac{\lambda_- e^{\lambda_- T}}{e^{\lambda_- T} - 1}\right)\right) \tag{5.32}$$

$$= 1 + \frac{(1+d)e^{-\gamma T/2}}{s_1} \times \tag{5.33}$$

$$\left(\frac{s_2^- e^{\gamma T/2} - 2s_3^- e^{\gamma T}\cos(s_4^- T + \zeta^-)}{2(1 + e^{\gamma T} - 2e^{\gamma T/2}\cos(s_4^- T))} + \frac{-s_2^+ e^{\gamma T/2} + 2s_3^+ e^{\gamma T}\cos(s_4^+ T + \zeta^+)}{2(1 + e^{\gamma T} - 2e^{\gamma T/2}\cos(s_4^+ T))}\right) \tag{5.34}$$

where $s_1 = \sqrt{4\omega^2 - \gamma^2}$, $s_2^\mp = 2 \mp s_1 + \gamma\mu$, $s_3^\mp = \sqrt{(1+\mu^2)(1 + \omega^2 \mp s_1)}$, $s_4^\mp = (\mp 2 + s_1)T/2$, $s_5^\mp = \pm\gamma + (\mp 2 + s_1)\mu$, and $\zeta^\mp = 2\arctan(s_5^\mp/(s_3^\mp + s_2^\mp))$.

We now consider the analytic form of $F_1(T)$. It is evident from (5.32) that it is oscillatory in T. If $\gamma > 0$ then the oscillations have decreasing amplitude as the period T increases and $F_1(T)$ tends to one as T tends to infinity. If T is fixed and $\gamma > 0$

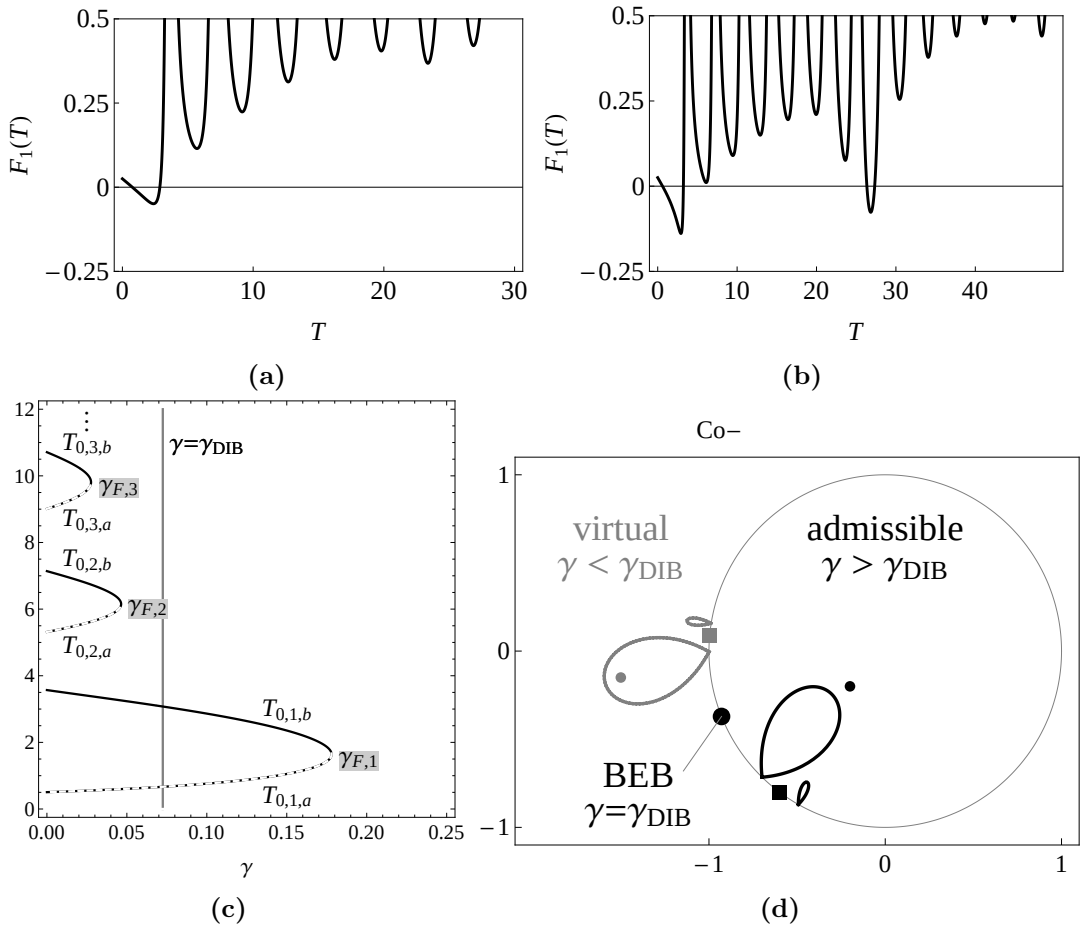

Figure 5-4: *The form of the function $F_1(T)$ for fixed parameters $\omega = 0.76$, $d = 0.95$ and $\mu = 0.15$ with $\gamma = 0.1$ shown in Figure 5-4a and with $\gamma = 0.05$ shown in Figure 5-4b. In (5-4c) we plot the zeros of $F_1(T)$ as the damping coefficient γ is varied ($\omega = 0.76$, $d = 0.95$, $\mu = 0.15$, $\gamma_{F,1} \approx 0.178$, $\gamma_{DIB} \approx 0.072$). In this figure we see, as γ decreases, a smooth fold bifurcation at $\gamma_{F,1}$ creating two fixed point branches. As γ decreases more fixed points are created at γ_2 etc. The symbol $\vdots$ indicates that more fold bifurcation give rise to more fixed points. In (5-4d) we show a schematic of the Non-smooth Fold–Hopf-type Bifurcation of the regular equilibrium $\boldsymbol{x}_R$ (dot), pseudo equilibrium x_{P1} (square) and the two limit cycles $B_{1,a}$ and $B_{1,b}$. These bifurcate at the boundary equilibrium bifurcation point $\gamma = \gamma_{DIB}$. Black indicates physically realistic orbits and grey unphysical orbits.*

increases then the amplitude of the oscillations also decreases to zero. Furthermore, if we fix γ and assume that T is large, then

$$F_1(T) \approx 1 + \frac{(1+d)e^{-\gamma T/2}}{s_1}\big(- s_3^- \cos(s_4^- T + \zeta^-) + s_3^+ \cos(s_4^+ T + \zeta^+)\big) \tag{5.35}$$

and is bounded, i.e. $F_1^-(T) < F_1(T) < F_1^+(T)$ where

$$F_1^\pm(T) = 1 \pm \frac{(1+d)e^{-\gamma T/2}}{s_1}\big(s_3^- + s_3^+\big). \tag{5.36}$$

The upper and lower bounds $F_1^\pm(T)$ are positive for all large T. Therefore, for fixed parameters, and if $\gamma > 0$ the nonlinear function $F_1(T)$ has finitely many zeroes. This is consistent with the plots presented in Figures 5-4a and 5-4b. As γ is decreased and the amplitude of the oscillations of F_1 increase then more zeroes arise pairwise. Moreover, if γ is zero then $F_1(T)$ is purely oscillatory and hence has infinitely many zeroes.

The period T depends on the damping parameter, γ, the stiffness, ω, the coefficient of restitution, d, and the coefficient of friction, μ. Therefore varying imbalance radius ρ, or imbalance angle ϕ will not affect it. We illustrate the period's dependence on γ in a bifurcation plot for fixed parameters $\omega = 0.76$, $d = 0.95$ and $\mu = 0.15$ (Figure 5-4c). This figure not only illustrates the existence of a finite number of zeroes for $\gamma \in (0, \gamma_{F,1} \approx 0.178)$ and hence of fixed points of the map P_I of a period T but also that no such fixed points exist otherwise.

The next variable, normal impact velocity, $\dot{r}_{0,-}$, can now be determined from T by taking the absolute value of (5.29) and solving for $\dot{r}_{0,-}$. Then for each value of the period T, $\dot{r}_{0,-}$ has two solutions $\dot{r}_{0,-,a}$ and $\dot{r}_{0,-,c}$ given by

$$\dot{r}_{0,-,c/a}(T) = \frac{-g(T) \pm \sqrt{g(T)^2 - |q|^2|a_{12}(T)|^2(1-|k|^2)}}{|q|^2|a_{12}(T)|^2} \tag{5.37}$$

where $g(T) = (1+d)\Big(\operatorname{Re}\big(a_{12}(T)\big) - \mu \operatorname{Im}\big(a_{12}(T)\big)\Big)$.

However, we observe that these solutions may themselves coalesce at a fixed bifurcation at $\gamma = \gamma_F^- \approx -0.497$ (Figure 5-5a). But as γ_F^- is negative it has no physical context on the application. As γ is increased these two branches persist under varying stability and admissibility.

A fixed point is potentially *admissible* if the rotor is approaching the impact surface from within the clearance circle, i.e. $\dot{r}_{0,-} > 0$. Otherwise ($\dot{r}_{0,-} < 0$), it is *virtual*. Note that one of the radial velocities (5.37) becomes zero if $1 - |k|^2 = 0$, i.e. when $\gamma = \gamma^*$. In Figure 5-5 it becomes evident that only low normal impact velocity fixed points undergo a sign change in $\dot{r}_{0,-}$.

The angle at impact θ_0 and the tangential impact velocity $\dot{\theta}_{0,-}$, do not need any constraints imposed upon them to ensure admissibility. From (5.29) and (5.31) we

obtain their expressions, respectively,

$$\theta_0(T, \dot{r}_{0,-}) = \mathrm{Arg}\left(\frac{k}{1 + a_{12}(T) q \dot{r}_{0,-}}\right) \tag{5.38}$$

$$\dot{\theta}_{0,-}(T, \dot{r}_{0,-}) = -\,\mathrm{Im}\Big(q\, a_{22}(T)\Big)\dot{r}_{0,-} \tag{5.39}$$

which are determined by T and $\dot{r}_{0,-}$. Note that the imbalance phase ϕ has no effect on the fixed points, i.e. it shifts the angle at impact θ_0 but does not change the nature of the dynamics. In fact, ϕ could have been scaled out of the equation. Furthermore, to satisfy the equivalent scaled condition for the relative tangential velocity, (5.2), the tangential velocity $\dot{\theta}_{0,-}$ would have to be greater than -40 taking pre- and post-impact values into account. This is the case as shown in Figure 5-5c and 5-5d. We can now

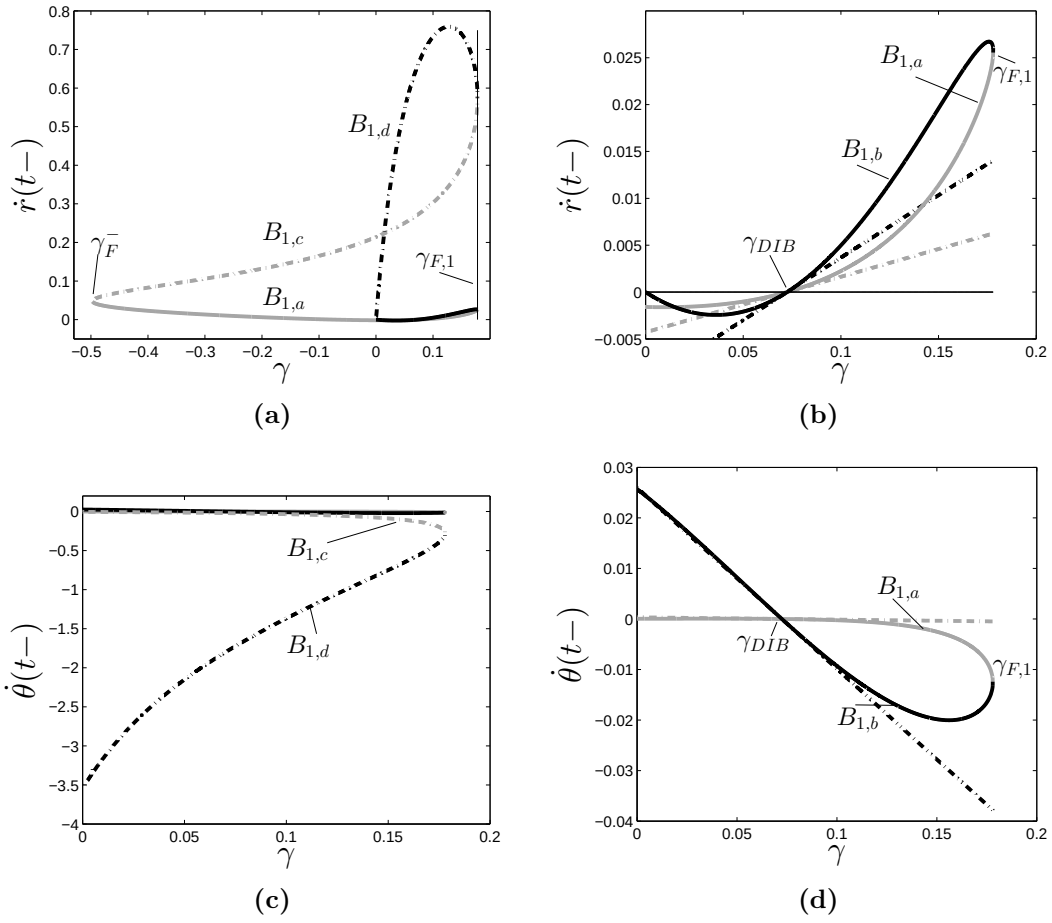

Figure 5-5: *(5-5a) and (5-5b) Normal impact velocity of the four fixed points $B_{1,m}$. (5-5a) The two fixed points $B_{1,a}$ and $B_{1,c}$ coalesce at $\gamma_F^- \approx -0.497$. (5-5b) Enlarged view of (5-5a): the two fixed points $B_{1,a}$ and $B_{1,b}$ including the respective estimate of the fixed points obtained by the local linearisation of the system described in §5.6. ($\gamma_{DIB} \approx 0.072$). (5-5c) and (5-5d) Tangential impact velocity $\dot{\theta}(t-)$ of the four fixed points $B_{1,m}$ with $m = a, b, c, d$. (5-5d) Enlarged view of (5-5c): the two fixed points $B_{1,a}$ and $B_{1,b}$ including the respective estimate of the fixed points obtained by the local linearisation of the system described in §5.6.*

summarise the main result concerning the period T periodic points.

Proposition 5.2. *Let $n \in \{1, \ldots, N\}$ and $m \in \{a, b, c, d\}$.*
If there exists a period $T_{0,n,m}$ such that

$$F_1(T_{0,n,m}) = 0$$

then there are finitely many (up to $2N$), period-T periodic points $B_{n,m}$ given by

$$B_{n,m} = (T_{0,n,m},\, \theta_{0,n,m},\, \dot{r}_{0,-,n,m},\, \dot{\theta}_{0,-,n,m}) \tag{5.40}$$

with $T_{0,n,m}$, $\theta_{0,n,m}$, $\dot{r}_{0,-,n,m}$ and $\theta_{0,-,n,m}$ determined by the equations (5.32), (5.38), (5.37) and (5.39), respectively. Two pairs of fixed points, $B_{n,a}$ and $B_{n,c}$, and $B_{n,b}$ and $B_{n,d}$, have the same period, i.e.

$$T_{0,n,a} \equiv T_{0,n,c} \quad \textit{and} \quad T_{0,n,b} \equiv T_{0,n,d}.$$

If $\gamma \in (0, \gamma^*)$ then half of the fixed points, $B_{n,a}$ and $B_{n,b}$, are virtual and the other half, $B_{n,c}$ and $B_{n,d}$, are admissible.

Proof. If the damping coefficient $\gamma > 0$ then, as stated above, $F_1(T)$ has finitely many zeroes $T_{0,n,m}$. Now, let $n \in \{1, \ldots, N\}$ and $m \in \{a, b, c, d\}$. Then for each $T_{0,n,a}$ two normal impact velocities, $\dot{r}_{0,-,n,a}$ and $\dot{r}_{0,-,n,c}$ can be computed from (5.37) and hence $\theta_{0,n,a}$ and $\theta_{0,n,c}$ from (5.38) and $\dot{\theta}_{0,-,n,a}$ and $\dot{\theta}_{0,-,n,c}$ (5.39). Thus we obtain two different periodic points, $B_{n,a}$ and $B_{n,c}$ given by (5.40), with the period $T_{0,n,a}$. For the purpose of nomenclature set $T_{0,n,c} = T_{0,n,a}$. Due to the oscillatory character of $F_1(T)$ its zeros arise pairwise, i.e. there exists a second zero $T_{0,n,b}$. Assume that $T_{0,n,b} \neq T_{0,n,a}$ then the equivalent result follows for $B_{n,b}$ and $B_{n,d}$.

Assume $\gamma \in (0, \gamma^*)$ then $|k|^2 > 1$. Assume further that there exists a period $T_{0,n,a}$. Consider

$$\dot{r}_{0,-,n,a} := \dot{r}_{0,-}(T_{0,n,a}) = \frac{-g - \sqrt{g^2 - |q|^2|a_{12}|^2(1 - |k|^2)}}{|q|^2|a_{12}|^2} < \frac{-g - |g|}{|q|^2|a_{12}|^2} \leqslant 0.$$

Similarly,

$$\dot{r}_{0,-,n,c} := \dot{r}_{0,-}(T_{0,n,a}) = \frac{-g + \sqrt{g^2 - |q|^2|a_{12}|^2(1 - |k|^2)}}{|q|^2|a_{12}|^2} > \frac{-g + |g|}{|q|^2|a_{12}|^2} \geqslant 0.$$

The same holds for the period $T_{0,n,b}$. Therefore the fixed points $B_{n,a}$ and $B_{n,b}$ are virtual but $B_{n,c}$ and $B_{n,d}$ are admissible. □

Proposition 5.3. *Let $n \in \{1, \ldots, N\}$ and assume that the fixed points $B_{n,m}$ exist for all $m \in \{a, b, c, d\}$. Then at $\gamma = \gamma_{F,n}$ for fixed n there are two simultaneous smooth*

fold bifurcations to which the fixed points coalesce, i.e. $B_{n,a}$ and $B_{n,b}$ meet at the first fold and $B_{n,c}$ and $B_{n,d}$ at the other.

Proof. As stated above, the function F_1 has finitely many zeros for any $\gamma > 0$ and an infinite number as $\gamma \to 0$. Furthermore, F_1 is a smooth function of γ and has regular quadratic minima. It follows, that as γ decreases, then zeros arise pairwise at regular fold bifurcations at points $\gamma_{F,n}$. Let $n \in \{1, \ldots, N\}$ and $m \in \{a, b, c, d\}$. Assume $0 < \gamma < \gamma_{F,n}$ and that the fixed points $B_{n,m}$ exists. Then there exist γ, $T_{0,n,a} \equiv T_{0,n,c}$ and $T_{0,n,b} \equiv T_{0,n,d}$ with $T_{0,n,a} \neq T_{0,n,b}$ such that

$$F_1(T_{0,n,a}, \gamma) = F_1(T_{0,n,b}, \gamma) = 0.$$

as $F_1(T)$ is oscillatory with decreasing amplitude due to $\gamma > 0$. By the continuity of $F_1(T, \gamma)$ there exists $\gamma = \gamma_{F,n}$ such that

$$T_{0,n,a} = T_{0,n,b} =: T_{0,n,F}.$$

Then for each n and $T = T_{0,n,F}$ there exist two fixed points $B_{n,a}$ and $B_{n,c}$. For $\gamma > \gamma_{F,n}$ the nonlinear function $F_1(T)$ has no zeroes. Hence for each n two pairs of fixed points coincide at $\gamma = \gamma_{F,n}$, i.e. $B_{n,a}$ and $B_{n,b}$ bifurcate in a smooth fold bifurcation and so do $B_{n,c}$ and $B_{n,d}$. □

A numerical example of the this bifurcation at $\gamma = \gamma_{F,n}$ is depicted in Figures 5-4c and 5-5a.

Now let us turn to the question of admissibility. If $0 < \gamma_{F,N} < \gamma^*$ then the low impact velocity branches $B_{n,a}$ and $B_{n,b}$ are virtual for all n whereas the other two, $B_{n,c}$ and $B_{n,d}$ are admissible by Proposition 5.2. However, in the other case, $\gamma_{F,N} > \gamma^*$, further information about $\dot{r}_{0,-,n,m}$ is required. If $\dot{r}_{0,-,n,m}$ is increasing as γ is increasing then all four fixed point sets are admissible. Otherwise they are virtual.

In either case the normal velocity $\dot{r}_{0,-}$ of a pair of fixed points, $m = a, b$ or c, d, changes sign, Figure 5-5b, leading one to anticipate a discontinuity-induced bifurcation, setting the scene for the main result of this Chapter. We call this a sub-critical non-smooth *Fold–Hopf bifurcation* (NSFH).

Proposition 5.4. *Let $n \in \{1, \ldots, N\}$ and assume that the fixed points $B_{n,m}$ exist $\forall m = a, b, c, d$. Assume further that $\gamma_{F,1} > \gamma^*$, ω satisfies the non-smooth fold condition* (5.23) *and that $\dot{r}_{0,-,1,m}$ is increasing as the damping parameter γ is increasing. Then at the BEB point*

$$\gamma = \gamma^* \equiv \gamma_{DIB}$$

a more general discontinuity-induced bifurcation occurs. The fixed point pairs, $B_{n,a}$ and $B_{n,b}$, clash with the regular non-impacting equilibrium $\boldsymbol{x}_R$ and the pseudo equilibrium

$\boldsymbol{x}_{P1}$. *As* γ *decreases through* γ_{DIB} *the four invariant sets switch from being admissible to virtual.*

Proof. Let $\gamma = \gamma^*$. Then either $\dot{r}_{0,-,n,a} = 0$ or $\dot{r}_{0,-,n,c} = 0$ by (5.37). Consequently, by (5.27), it follows that

$$\boldsymbol{w}_{0,-} = -A^{-1}\boldsymbol{b} = \begin{pmatrix} k \\ 0 \end{pmatrix} = \boldsymbol{w}_{0,+}\,.$$

Therefore the fixed point corresponds to the equilibrium solution $\boldsymbol{w}(t) = -A^{-1}\boldsymbol{b}$, which is the boundary equilibrium $\boldsymbol{x}_B$. Hence as the impact velocity $\dot{r}_{0,-,n,a} = 0$ increases through $\gamma = \gamma^*$ it undergoes a sign change corresponding to the limit cycle transitioning from physically implausible to plausible. Taking Proposition 5.1 into consideration it follows that a clash of two limits cycles $B_{n,a}$ and $B_{n,b}$ and two equilibria $\boldsymbol{x}_R$ and $\boldsymbol{x}_{P1}$ occurs. □

A schematic of this phenomenon in (r, θ) phase space is illustrated in Figure 5-4d. Our statement is further supported by numerical examples such as Figure 5-7a where the limit cycles corresponding to fixed points $B_{1,a}$ and $B_{1,b}$ are depicted. Their amplitudes, $\min(r(t))$ between impacts at times t_i and t_{i+1}, increase as γ decreases and clash with the boundary, the regular equilibrium $\boldsymbol{x}_R$, and pseudo equilibrium $\boldsymbol{x}_{P1}$.

Although we have identified under what conditions pairs of fixed points $B_{n,m}$ are admissible, their physical plausibility is not guaranteed as it is possible that between impacts the corresponding limit cycle trajectory has a further impact, Figure 5-2b. Therefore, whilst in our global analysis we have derived the necessary existence condition for such limit cycles further sufficient conditions are necessary as large amplitude limit cycles can undergo a grazing event, [90].

In order to demonstrate whether such an impact occurs we present the numerical analysis for our model example. We compute the trajectories of the corresponding fixed points $B_{1,m}$ and plot all local extrema of $r(t)$ between impacts $t \in (t_i, t_{i+1})$, Figure 5-7. The branches, $B_{1,a}$, $B_{1,b}$ and $B_{1,c}$ are not affected by this phenomenon unlike the limit cycle corresponding to the fixed point $B_{1,d}$. As γ is decreased a grazing event [90] (orbit lies tangential to Σ with zero normal impact velocity) occurs, i.e. amplitude $r(t)$ crosses the impact surface at $\gamma = \gamma_{\text{graze}} \approx 0.0636$, Figure 5-7b.

Furthermore, these numerical calculations indicate that fixed point pairs with high normal impact velocity, $B_{n,c}$ and $B_{n,d}$ with $n > 1$, are virtual. We believe this to be the case as these pairs only exist for $\gamma \in (0, \gamma_{\text{graze}})$, where the orbit of the corresponding limit cycle exceeds the boundary [86] (Chapter 6). In §5.6 we extend this result using a local linearised system to give more precise results.

5.5.1 Stability Analysis

In the following we present the stability analysis of the fixed points of the impact map P_I. In particular, we focus on the first pair of fixed points, i.e. $B_{1,m}$ with $m = a, b, c, d$, as these appear to be the only physically plausible ones, as shown in the previous Section. Their stability is determined by the eigenvalues $\tilde{\lambda}$ of the Jacobian matrix

$$J(B_{1,m}) = \frac{\partial(t_1, \theta_1, \dot{r}_{1,-}, \dot{\theta}_{1,-})}{\partial(t_0, \theta_0, \dot{r}_{0,-}, \dot{\theta}_{0,-})}.$$

It is evident that determining this matrix analytically is difficult as the general solution to (5.16) in polar coordinates is a complicated nonlinear function. But we can compute the Jacobian eigenvalues numerically. In Figure 5-6b we present $\max(|\tilde{\lambda}|)$ of the four fixed points illustrating that $B_{1,a}$, $B_{1,b}$ and $B_{1,c}$ are unstable for all γ and that $B_{1,d}$ is quasi-periodically stable for $\gamma \in (0.083, \gamma_{\mathrm{F},1})$ but unstable otherwise. Taking into account the results from the previous Section it is evident that as γ decreases from $\gamma_{\mathrm{F},1}$ the fixed point $B_{1,d}$ becomes unstable before it undergoes grazing.

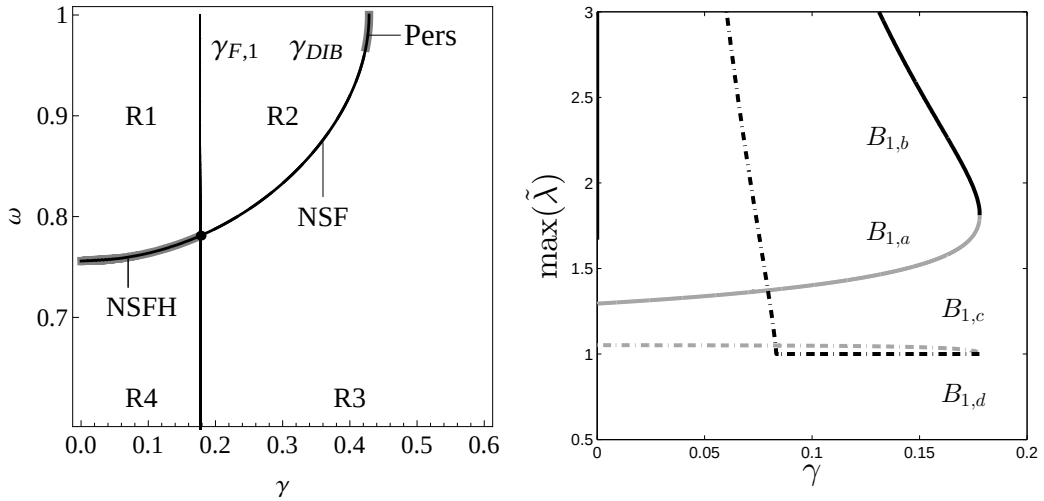

Figure 5-6: *(5-6a) Co-dimension-2 bifurcation by varying damping γ and stiffness ω. (5-6b) Eigenvalue analysis yields only one stable fixed point $B_{1,d}$ for $\gamma > 0.0834$.*

5.5.2 Codimension-2 Bifurcation

We complete this Section with a codimension-2 bifurcation analysis studying the coalescence of various bifurcation points. Of interest is the influence of other parameters on the NSFH bifurcation. Certain magnetic bearing parameters are constrained due to the system's characteristics such as coefficient of friction, μ, or restitution, d, which are governed by material properties. Stiffness, however, can be more easily adjusted

through the PID control. Hence we have chosen ω to be the second bifurcation parameter.

For our particular example, $\mu = 0.15$, $d = 0.95$ and $\rho = 3/7$, we analyse the smooth fold at $\gamma_{F,1}$ of the first fixed point set $B_{1,m}$ and the DIB point, $\gamma_{DIB} = \sqrt{\rho^2 - (1-\omega^2)^2}$, as we vary γ and ω (Figure 5-6a). This shows that $\gamma_{F,1}$ and γ_{DIB} coincide at $\gamma \approx 0.178$ and $\omega \approx 0.781$, and that four critical regions can be identified (not taking pseudo-equilibria into account):

R1: The three invariant sets $\boldsymbol{x}_R$, $B_{1,a}$ and $B_{1,b}$ are virtual, whereas $B_{1,c}$ and $B_{1,d}$ are admissible.

R2: No fixed points exist and the regular equilibrium $\boldsymbol{x}_R$ is virtual.

R3: No fixed points exist and $\boldsymbol{x}_R$ is admissible.

R4: All invariant sets $B_{1,m}$ and $\boldsymbol{x}_R$ are admissible.

This demonstrates that three types of non-smooth bifurcation between equilibria and/or period-T limit cycles occurs, i.e. the already known NSF and persistence (Pers) bifurcations and the new NSFH bifurcation, on the boundary of regions **R1** and **R2**. We observe that the limit cycle corresponding to $B_{1,d}$ undergoes a grazing event in regions **R1** and **R2**. Identifying this grazing set is part of future work.

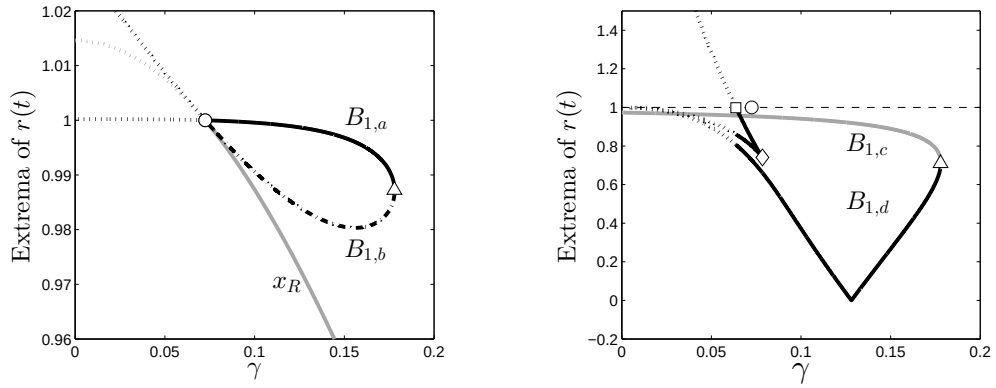

Figure 5-7: *Bifurcation diagram of γ against local extrema of $r(t)$ for $t \in (t_i, t_{i+1})$ for fixed point pairs (5-7a) $B_{1,a}$ and $B_{1,b}$ and (5-7b) $B_{1,c}$ and $B_{1,d}$. ($\gamma_{F,1} \approx 0.178$ ($\triangle$)). In (5-7a) we also plot the regular equilibrium $\boldsymbol{x}_R$ to illustrate the non-smooth Fold–Hopf bifurcation at $\gamma_{DIB} \approx 0.072$ ($\circ$). Fig. (5-7b) depicts a grazing bifurcation at $\gamma \approx 0.0636$ ($\square$) after an increase in the number of local extrema of $r(t)$ at $\gamma = 0.0785$ ($\Diamond$).*

5.6 Generalised Local Analysis of the Hopf-type Bifurcation

[5] The global analysis of this specific nonlinear system implies that limit cycles bifurcate in pairs at a non-smooth Fold–Hopf-type bifurcation from a boundary equilibrium point. We now examine this bifurcation in more detail locally by considering a locally linearisation of the system described earlier close to the bifurcation point. This allows us to perform the local analysis for a more general system which includes the one discussed in Section 5. The purpose of this Section is two fold. On the one hand we can establish the conditions for the existence of two fixed point solutions of the impact map P_I with period T given by the solutions of the equation (5.44). On the other hand we also obtain a more precise description of the local behaviour of the periodic solutions. We find that the estimates obtained by this analysis agree well with the calculations given in §5.5. To do this local analysis we consider the complex linear differential equation in $\boldsymbol{w} = (z, \dot{z})$

$$\dot{\boldsymbol{w}} = A\boldsymbol{w} + \boldsymbol{b} \quad \text{in } |z| < \sigma \tag{5.41}$$

with a reset law applying at $|z| = \sigma$

$$\dot{z}_+ - \dot{z}_- = -(1+d)(1+i\mu)\,\mathrm{Re}(z^* \dot{z_-})\frac{z}{|z|^2} \tag{5.42}$$

where

$$A = \begin{pmatrix} 0 & 1 \\ -\beta & -\alpha \end{pmatrix} \quad \text{and} \quad \boldsymbol{b} = \begin{pmatrix} 0 \\ \Gamma \end{pmatrix}.$$

Our basic assumptions are that there exist parameters α_0, β_0 and Γ_0 such that $|\Gamma_0/\beta_0| = \sigma$ and that the eigenvalues of the matrix A have negative real part. These conditions imply that at the critical parameters there is a stable boundary equilibrium as is the case for the bearing problem.

We now consider the dynamical behaviour of solutions which are small perturbations to this situation. To do this we introduce a small real parameter ε and consider the perturbed system coefficients (5.41) with

$$\alpha \sim \alpha_0 + \varepsilon\alpha_1,\ \beta \sim \beta_0 + \varepsilon\beta_1 \quad \text{and} \quad \Gamma \sim \Gamma_0 + \varepsilon\Gamma_1$$

and the same reset law (5.42). From here onwards we use the symbol $\sim$ to denote equality up to the stated order in ε. We pose the asymptotic solution

$$z(t) \sim z_0 + \varepsilon z_1(t), \quad \text{or} \quad \boldsymbol{w}(t) = \boldsymbol{w}_0 + \varepsilon \boldsymbol{w}_1(t)$$

[5] This section is work done in collaboration with Prof. Paul Glendinning

with $z_0 = \Gamma_0/\beta_0 = \sigma e^{i\Psi}$ defining the phase Ψ of z_0 and $z_1(t) = r_1(t)e^{i\theta_1(t)}$. At order ε, i.e. ignoring terms higher than ε,

$$\dot{\boldsymbol{w}}_1 \sim A_0 \boldsymbol{w}_1 + \boldsymbol{b}_1 \text{ in } |z| < \sigma$$

where

$$A_0 = \begin{pmatrix} 0 & 1 \\ -\beta_0 & -\alpha_0 \end{pmatrix} \quad \text{and} \quad \boldsymbol{b}_1 = \begin{pmatrix} 0 \\ \Gamma_1 - \beta_1 z0 \end{pmatrix}$$

and $|z| < \sigma$ becomes $|\sigma + \varepsilon r_1(t)e^{i(\theta_1(t)-\Psi)}|$ or

$$\varepsilon r_1(t)\cos(\theta_1(t) - \Psi) < 0.$$

There is an equilibrium at $z_0 = \Gamma_0/\beta_0$, $z_1 = (\Gamma_1 - \beta_1 z_0)/\beta_0$. Defining real constants c and ψ by

$$z_1 = \frac{\Gamma_1\beta_0 - \beta_1\Gamma_0}{\beta_0^2} = ce^{i\psi}$$

the equilibrium lies in $|z| < \sigma$ if

$$\varepsilon c\cos(\psi - \Psi) < 0.$$

In order to find a choice for ε we look at the magnetic bearing example $\beta_0 = \omega^2 - 1 + i\gamma^*$, $\beta_1 = i$, $\Gamma_0 = \rho e^{i\phi}$ and $\Gamma_1 = 0$. Then the expression above becomes

$$-2\varepsilon\gamma^* < 0.$$

As γ^* is positive the equilibrium lies within the clearance circle if ε is negative. By choice of the sign of ε (and hence of Γ_1 and β_0) we may assume that

$$\cos(\psi - \Psi) < 0$$

and hence the stable equilibrium lies inside the clearance circle if $\varepsilon > 0$ but not otherwise. The question we wish to answer is what happens if $\varepsilon > 0$ in this case.

The general solution in $|z| < \sigma$ at order ε is

$$\boldsymbol{w}_1(t) = \exp\Big(A(t - t_0)\Big)(\boldsymbol{w}_{1,0,+} + A_0^{-1}\boldsymbol{b}_1) - A_0^{-1}\boldsymbol{b}_1 \tag{5.43}$$

where $\boldsymbol{w}_{1,0,+} = \boldsymbol{w}_1(t_0+)$ denotes the post impact initial condition. Next we need to find the reset law at order ε and hence consider the impact position first

$$|z(t_0)| = |\sigma e^{i\Psi} + cr_{1,0}e^{i\theta_{1,0}}| = \sigma.$$

This yields a constraint on the angle at impact

$$\varepsilon c r_{1,0} \cos(\theta_{1,0} - \Psi) = 0$$

or $\theta_{1,0} = \Psi + \pi/2$. Deriving the reset law for the impact velocity components requires a few more computations and we shall derive them in stages. Consider the RHS of (5.42)

$$\mathrm{Re}\left(z^*(t_0)\dot{z}(t_{0,-})\right)\frac{z_0}{|z_0|^2} = -\frac{\varepsilon r_{1,0}\dot{\theta}_{1,0,-}}{\sigma}(\sigma e^{i\Psi} + \varepsilon r_{1,0} e^{i\theta_{1,0}}) = -\varepsilon r_{1,0}\dot{\theta}_{1,0,-}e^{i\Psi}$$

where we have substituted for $\theta_{1,0}$. As the LHS of (5.42) can be expressed in the form of

$$\varepsilon\left(i(\dot{r}_{1,0,+} - \dot{r}_{1,0,-}) - r_1(\dot{\theta}_{1,0,+} - \dot{\theta}_{1,0,-})\right)$$

we can now equate the real and imaginary parts of (5.42) to find the reset law at order ε

$$\dot{z}_{1,0,+} = \dot{z}_{1,0,-} + (1+d)(1+i\mu)\, r_{1,0}\, \dot{\theta}_{1,0,-}\, e^{i\theta_{1,0}}.$$

As in the problem considered earlier, this system may have a variety of motions, possibly including chattering behaviour. However, for the purposes of our analysis, we seek solutions which comprise a simple periodic orbit with a single impact. Thus we look for a time of impact $t_1 = t_0 + T$ depending on the previous impact time t_0 and the limit cycle period T. As described in previous Sections, such limit cycles satisfy repeatability conditions for position and velocity, given by $z(t_0) = z(t_1)$ and $\dot{z}(t_0-) = \dot{z}(t_1-)$ respectively. The equivalent conditions at order ε are

$$z_1(t_0) = z_1(t_1) \quad \text{and} \quad \dot{z}_1(t_0-) = \dot{z}_1(t_1-).$$

Substituting these into the general solution (5.43) we can obtain the impact maps P_I for the perturbed orbit by solving for the initial conditions $\boldsymbol{w}_{1,0,-} = (z_{1,0}, \dot{z}_{1,0,-})$ that yield period-T limit cycles,

$$\boldsymbol{w}_{1,0,-} = -A_0^{-1}\boldsymbol{b} - \begin{pmatrix} a_{11}(T) & a_{12}(T) \\ a_{21}(T) & a_{22}(T) \end{pmatrix}\begin{pmatrix} 0 \\ i(1+d)(1+i\mu)\, r_{1,0}\, \dot{\theta}_{1,0,-} \end{pmatrix} e^{i\theta_{1,0}}$$

where

$$\begin{pmatrix} a_{11}(T) & a_{12}(T) \\ a_{21}(T) & a_{22}(T) \end{pmatrix} := \left(\exp(-A_0 T) - I\right)^{-1}.$$

By methods similar to those used in §5.5 we can find the period T by solving the nonlinear equation

$$F_1(T) := 1 - (1+d)\,\mathrm{Re}\left((1+i\mu)a_{22}(T)\right) = 0. \tag{5.44}$$

A necessary condition for the existence of such periodic orbits is then given by the requirement that the nonlinear problem (5.44) has a solution T. Note, that such a solution will then describe a family of periodic orbits, parametrised by ε close to the bifurcation point. The period T of the limit cycle only depends on the parameters at the BEB, i.e. α_0 and β_0, and the impact parameters μ and d. Then the other unknowns determined by T are given by

$$\begin{aligned} r_{1,0} &= \frac{c\big(\ell_3\cos(\psi-\Psi)-\ell_4\sin(\psi-\Psi)\big)}{-\ell_4},\\ \dot\theta_{1,0,-} &= \frac{\cos(\psi-\Psi)}{(1+d)\big(\ell_3\cos(\psi-\Psi)-\ell_4\sin(\psi-\Psi)\big)},\\ \dot r_{1,0,-} &= \frac{c\cos(\psi-\Psi)\,\mathrm{Im}\,\big((1+i\mu)a_{22}(T)\big)}{\ell_4}, \end{aligned}$$

where $\ell_3 := \mu\,\mathrm{Re}\,\big(a_{12}(T)\big)+\mathrm{Im}\,\big(a_{12}(T)\big)$ and $\ell_4 := \mathrm{Re}\,\big(a_{12}(T)\big)-\mu\,\mathrm{Im}\,\big(a_{12}(T)\big)$. Hence it follows that the linearised impact map P_I is given by

$$\theta(t_0) := \arg\big(z(t_0)\big) = \Psi + \frac{r_{1,0}}{\sigma}\,\varepsilon, \quad \dot r(t_0-) = -\varepsilon r_{1,0}\,\dot\theta_{1,0,-}, \quad \text{and} \quad \dot\theta(t_0-) = \varepsilon\dot r_{1,0,-}$$

where the period $T = t_1 - t_0$ is a constant and does not depend ε. If we let ε tend to zero then $\theta(t_0)$ tends to Ψ and both $\dot r(t_0-)$ and $\dot\theta(t_0-)$ tend to zero, clearly indicating that the limit cycle resulting from this impact map tends to the boundary equilibrium. Depending on the signs of the parameters, the normal impact velocity switches sign and hence demonstrates the transition from admissible to virtual limit cycle or vice versa giving rise to the NSFH bifurcation. This linearisation agrees with the global analysis from the previous Section we illustrate, Figure 5-5b. Furthermore, this is evidence that the NSFH bifurcation can be approximated by a linear impact map in general.

5.7 Conclusions

In this chapter we used impacting hybrid systems to model magnetic bearing systems. We studied analytically and numerically the simplest dynamics, equilibria and periodic orbits that experience one impact per cycle.

In the first part we studied regular equilibria (no impact), boundary equilibria (on impact surface) and pseudo equilibria (sticking motion). We determined existence and stability conditions for these three type of equilibria. Furthermore, we derived the conditions that give rise to standard boundary equilibrium bifurcations, such as the non-smooth fold and persistence.

In the second part we studied periodic orbits of the hybrid system that experience one impact per period. To discretise the system and reduce its dimensions we computed the impact map P_I. We derived global existence conditions for the fixed points of the

impact map, which are associated with the periodic orbits of the piecewise-smooth flow. We showed that for certain damping related parameter values γ there exists a large but finite number of fixed points. Numerical simulations suggested that at most four of the fixed points are associate with orbits that are physically realisable, i.e. orbits that do not cross the impact surface. Furthermore, the computation of the eigenvalues showed that only one of these fixed points is stable.

To study qualitatively different dynamics we set γ to be the bifurcation parameter. A discontinuity induced Hopf–type bifurcation has been shown to exist in the impacting hybrid system. We have shown that in a sub-critical non-smooth Fold–Hopf bifurcation two unstable periodic orbits, a stable equilibrium without impact and a stable pseudo–equilibrium, are created and coexist. This type of bifurcation has not been reported in literature to our knowledge. Thus, we believe this result contributes to the classification of discontinuity induced bifurcation in higher dimensional systems.

For a general linear complex system the local analysis revealed that the impact map is linear in the bifurcation parameter in the neighbourhood of the non-smooth Fold–Hopf bifurcation, indicating that this phenomenon can be expected in higher-dimensional impacting systems.

Other typical impact dynamics such as grazing have been observed which will be studied in more detail in the following Chapter. One avenue for further research is use the stroboscopic map to see if grazing bifurcation are a route to chaos via a period-incrementing cascade, which has been observed in the $1D$ impact oscillators. Furthermore, we conjecture that other Hopf-type bifurcations leading, for example, to torus doubling as in [79, 125] could be observed in this system.

The rich dynamics studied in this Chapter also revealed co-existing smooth fold bifurcations, which to our knowledge have not been reported in impacting systems.

Finally, future work could include the comparison of this simplified model to experimental data from rigid magnetic bearing systems and determine how much of the qualitative dynamics discussed in this Chapter can be observed.

CHAPTER 6

Numerical Investigation of Magnetic Bearing Systems

6.1 Overview

In this Chapter we continue our study of the magnetic bearing system of Chapter 5. In particular we use numerical methods to extend the bifurcation results of Chapter 5 and look at a wider class of the dynamics of the magnetic bearing system. To be specific, we study the same impacting hybrid system (5.13), (5.14) with reset law (5.15) and general solution (5.16) as in Chapter 5. We will show that in magnetic bearing systems, rich and intricate dynamics and smooth and non-smooth bifurcations exist. In particular, we will show that grazing bifurcations, as described in Chapter 2.2.1, can indeed occur for certain parameter values leading to the creation of a wide range of different and complex behaviours. A part of our investigation is dedicated to identifying when chattering, as described in Chapter 2, occurs as this behaviour can lead to damaging interactions between rotor and stator.

For convenience we now state the scaled equation of motion of the rotor centre again. As before, we consider the motion of a rotor in the co-rotating frame, i.e. the frame rotates synchronously with the rotor at scaled rate 1. Let the complex variable $U(t) = x(t) + iy(t) = r(t)e^{i\theta(t)}$ denote the position of the rotor centre at time t in the co-rotating frame. Then the complex velocity $\dot{U}(t) = \dot{x} + i\dot{y} = (\dot{r}(t) + ir(t)\dot{\theta}(t))e^{i\theta(t)}$. Note that the angle $\theta(t)$ in the co-rotating frame can be expressed in terms of the angle in the fixed frame with complex position vector $Z(t) = r(t)e^{\Theta(t)}$, i.e. $\theta(t) = \Theta(t) - t$.

Let the complex vector $\boldsymbol{w} = (U, \dot{U})$ then the rotor's free motion can be modelled

by the linear ODE (identical to (5.13))

$$\dot{\boldsymbol{w}}(t) = A\boldsymbol{w}(t) + \boldsymbol{b} \quad \text{for} \quad |U| < 1 \tag{6.1}$$

where the matrix A and the vector $\boldsymbol{b}$ are constant (identical to (5.14)) and are defined by

$$A = \begin{pmatrix} 0 & 1 \\ 1-\omega^2 - i\gamma & -\gamma - 2i \end{pmatrix} \quad \text{and} \quad \boldsymbol{b} = \begin{pmatrix} 0 \\ \rho e^{i\phi} \end{pmatrix}.$$

Recall that the scaled parameter γ, defined in (5.9), depends on damping c and that the parameter ω, defined in (5.9), depends on stiffness k.

An impact between rotor and stator occurs at t_0 if $|U| = 1$ in which case the energy dissipation during impact is modelled by a reset law. Before impact $(-)$ and after impact $(+)$ the position remains the same, $U(t_{0,-}) = U(t_{0,+}) =: U_0$, but the normal impact velocity $\dot{r}(t_{0,+}) = -d\dot{r}(t_{0,-})$ and the tangential velocity $\dot{\theta}(t_{0,+}) = \dot{\theta}(t_{0,-}) - \mu(1+d)\dot{r}(t_{0,-})$, where d is the coefficient of restitution and μ is the coefficient of friction. In terms of the complex vector $\boldsymbol{w}$, the reset law (identical to (5.15)) is given by

$$\boldsymbol{w}_{0,+} = \boldsymbol{w}_{0,-} - \begin{pmatrix} 0 \\ q\dot{r}_{0,-}U_0 \end{pmatrix} \quad \text{if} \quad |U| = 1, \tag{6.2}$$

where $q = (1+d)(1+i\mu)$ and we simplify the notation $\boldsymbol{w}(t_{0,+}) \equiv \boldsymbol{w}_{0,+}$. In the fixed frame, the tangential velocity at impact $\dot{\Theta}_{0,-}$ will later be used to indicate if the rotor moves in a forward sense, i.e. anticlockwise $\dot{\Theta}_{0,-} > 0$, or in a backward sense, i.e. clockwise $\dot{\Theta}_{0,-} < 0$.

Throughout this Chapter we will numerically investigate how the system's dynamics changes as the parameter γ (damping) is varied. We will fix the other scaled parameters, which correspond to the experimental application in [67], i.e.

$$\omega \approx 0.76, \quad \rho = 3/7 \approx 0.428, \quad \phi = 0.21, \quad \mu = 0.15, \quad d = 0.95, \tag{6.3}$$

where ρ is the scaled imbalance radius and ϕ is the imbalance angle. In Section 6.5 the stiffness related parameter ω will become the second bifurcation parameter for a numerically computed two-parameter bifurcation diagram.

6.2 Numerical Simulation

The balanced rotor is said to be in normal operating mode if the rotor centre U is positioned at the origin with zero angular and tangential velocity in the co-rotating frame, i.e. $\dot{U} = 0$. In the fixed frame this motion corresponds to a rotor, rotating at rate 1, with centre Z positioned at the origin. Due to rotor faults, such as those

described in Chapter 2.4, a mass imbalance can arise and the rotor will deviate from the origin. From an engineer's point of view it is important to know for what damping related parameter value γ an impact can occur and what motion can result from this impact. Hence the numerical simulations forthwith will be prescribed with the initial condition $\boldsymbol{w} = (0, 0)$ at initial time $t = 0$. This means that for both the one- and two-parameter bifurcation diagrams the Monte Carlo method, described in Chapter 2, was not used here. However, this could be an avenue for future work.

In a typical simulation, the system (6.1), (6.2) was evolved from the steady state until it settled into either an asymptotic state or exhibited some other behaviour, such as chattering. As described in Chapter 2, chattering (Figure 6-1b) is an infinite sequence of impacts that occurs in finite time. As the sequence tends towards a point of accumulation, the impact velocity decreases and so does the time between impacts.

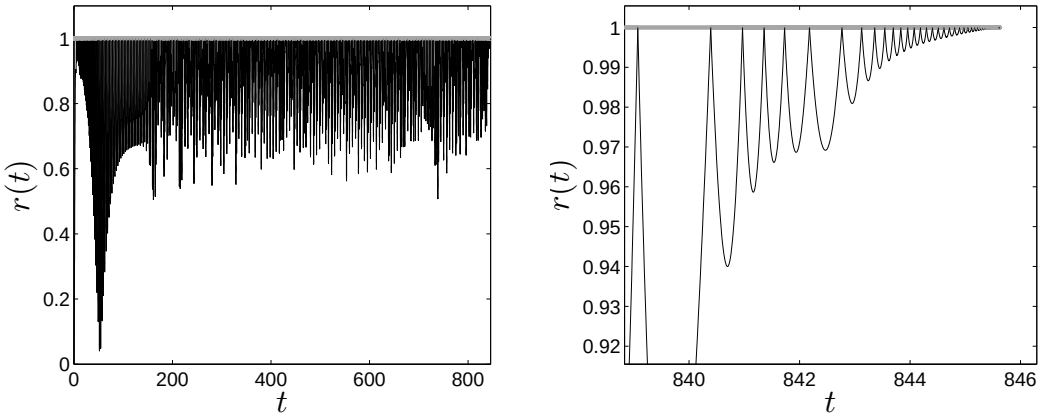

Figure 6-1: *A sequence of impacts for $t \in [0, 846]$ that leads to chattering where $\gamma = 0.077$ and $\omega = 0.76$. In Figure (a) we observe the transient behaviour that leads to chattering for $t \in [0, 840]$ and in Figure (b) we observe the chattering sequence for $t \in [840, 846]$.*

The solution of the magnetic bearing system (6.1) was obtained by using standard numerical integration techniques such as the subroutines provided by MATLAB® [84]. To compute the impact, MATLAB®'s [84] *event* detection function was used. For a repeatedly impacting orbit, 1200 impacts were computed and the last 200 stored for plotting. We dismissed the first 1000 impacts as transient behaviour is not the focus of our analysis. When chattering occurred then the complete sequence was not computed. Instead we used an error bound to ensure that the impact time t_i and the normal impact velocity $\dot{r}_{i,-} > 0$ were decreasing similar to those introduced in [94].

In Section 6.4 we use these simulations to plot one-parameter bifurcation diagrams and two-parameter bifurcation diagrams. By that we mean that we plot the asymptotic state as one parameter γ is varied or two parameters γ and ω are varied, respectively.

6.3 Dynamics Observed

The most prominent form of the behaviour of the magnetic bearing system (6.1), (6.2) is periodic motion. In Chapter 5 and [86] we saw such behaviour. Our analytical and numerical studies then followed this behaviour as parameters varied.

In particular, in Chapter 5.5 we have shown analytically and numerically that there exists a stable period-T orbit which experiences one impact per cycle. It was associated with the fixed point $B_{1,d}$ of the impact map P_I (5.25). This periodic orbit can also be computed using the simulation method introduced in Section 6.2, see Figure 6-2, which agrees with numerical calculations in Chapter 5.5.

Periodic orbits experiencing several impacts per period in the co-rotating frame are also found in these systems, e.g. 2 impacts per period, Figures 6-3 and 6-4, and 11 impacts per period, Figure 6-5. These periodic orbits will be referred to as N-**impact periodic orbits**, where $N \in \mathbb{N}$. In addition we observe chaotic attractors (with Lyapunov exponent greater than zero), Figure 6-6. Note that in the delay plots of Figures 6-3 and 6-5 we observe blobs rather than clear dots. This is due to remaining transient behaviour. This effect is not observed when simulating these periodic orbits for a total of 3000 impacts and plotting the last 200 impacts.

The transition between these states will be discussed in Section 6.4 and is illustrated in Figure 6-7.

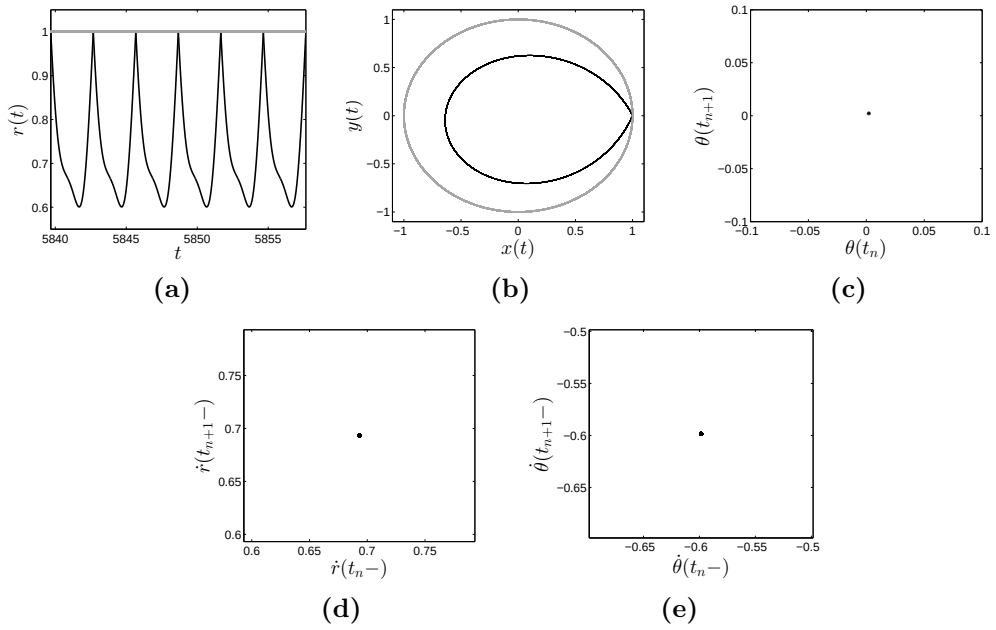

Figure 6-2: *Periodic orbit with one impact per period where $\omega = 0.76$ and $\gamma = 0.0834$. Figure (a) $r(t)$ against t. Figure (b) Rotor trajectory in the rotating complex frame (x, y) with one impact at $(x, y) = (1, 0)$ on the impact surface (grey). Delay plots for angle at impact $\theta(t_n)$ in Figure (c), and pre-impact normal velocity $\dot{r}(t_n-)$ in Figure (d) and tangential impact velocity $\dot{\theta}(t_n-)$ in Figure (e).*

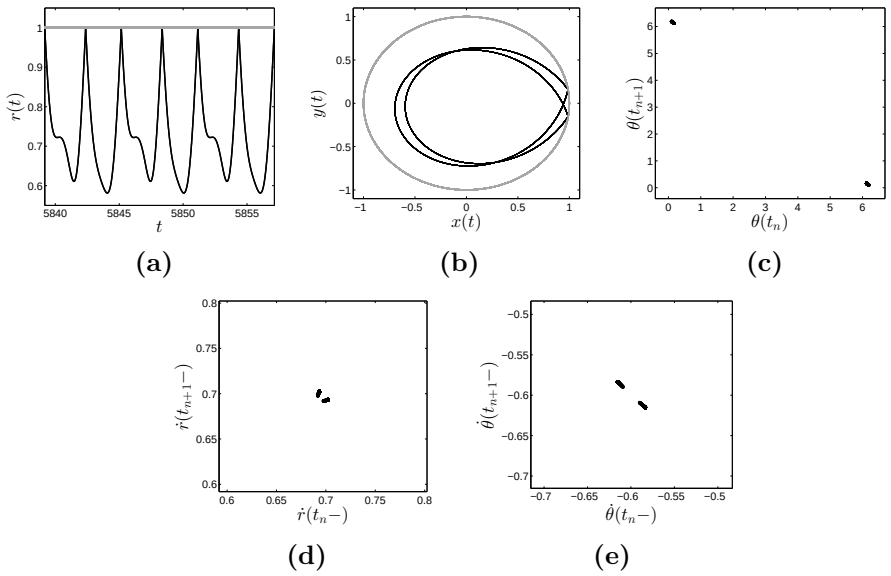

Figure 6-3: *Periodic orbit with* 2 *impacts per period where* $\omega = 0.76$ *and* $\gamma = 0.0833$. *This orbit is created in a non-smooth period-doubling bifurcation from a* 1*-impact periodic orbit. Figure (a)* $r(t)$ *against* t. *Figure (b) Rotor trajectory in the rotating complex frame* (x, y) *(black) with impact surface (grey). Delay plots for angle at impact* $\theta(t_n)$ *in Figure (c), and pre-impact normal velocity* $\dot{r}(t_n-)$ *in Figure (d) and tangential impact velocity* $\dot{\theta}(t_n-)$ *in Figure (e).*

6.4 One-parameter Bifurcation Analysis

In this Section we explore the dynamics reported in Chapter 5.5 in much more detail. We will use the numerical simulation method introduced in Section 6.2 to compute bifurcation diagrams where the bifurcation parameter is γ. We assume that the other parameters are fixed and their values are given in (6.3). The resulting diagrams are presented in Figure 6-7, where Figure 6-7a is the main bifurcation diagram, and Figures 6-7b, 6-7c and 6-7d are magnifications of 6-7a. These clearly show that rich dynamics exist in the magnetic bearing system (6.1), (6.2).

In [86] and Chapter 5 we have shown that a periodic orbit, experiencing one impact per period, exists and is stable within a certain damping parameter interval $\gamma \in (0.08335, 0.178)$. At both boundaries of this interval this periodic orbit loses stability. When $\gamma \approx 0.178$ it does so in a fold bifurcation (Figure 5-6b). When $\gamma \approx 0.0824$ the equations that determine existence and stability of the 1-impact periodic orbit are not suited to investigate the progression of the dynamics as γ decreases beyond the lower limit.

Now, the bifurcation diagrams (Figure 6-7) computed from numerical simulations, as described in Section 6.2, will provide insight into the dynamics of (6.1), (6.2) as γ is decreased beyond $\gamma = 0.08335$. In Figure 6-7a we observe that the periodic orbit with one impact per period (Figure 6-2) loses stability at $\gamma \approx 0.08335$ and bifurcates into a

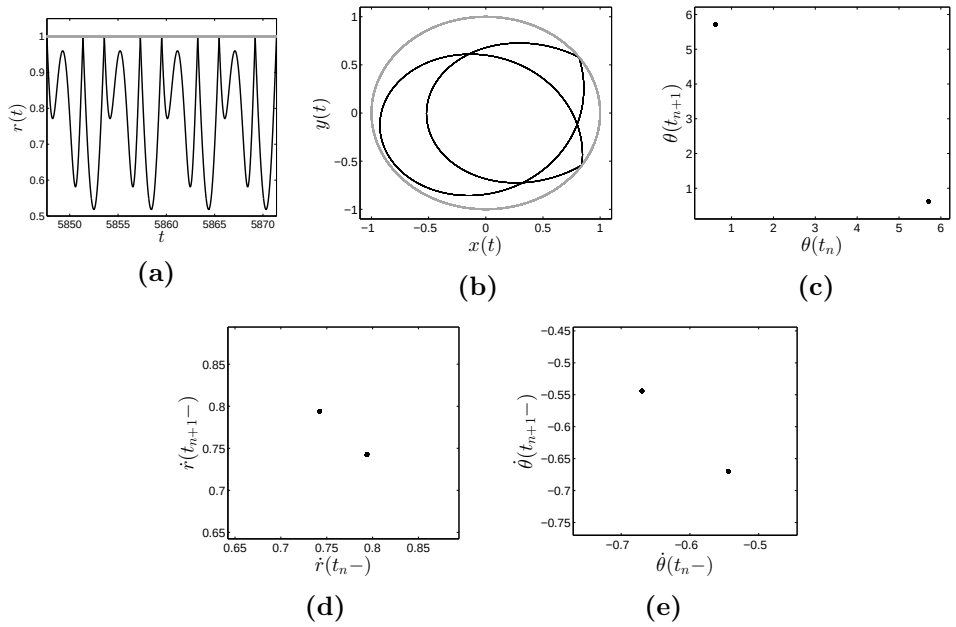

Figure 6-4: *Periodic orbit with two impacts per period near a grazing event* $\omega = 0.76$ *and* $\gamma = 0.0827$. *Figure (a)* $r(t)$ *against* t. *Figure (b) Rotor trajectory in the rotating complex frame* (x, y) *(black) with impact surface (grey). Delay plots for angle at impact* $\theta(t_n)$ *in Figure (c), and pre-impact normal velocity* $\dot{r}(t_n-)$ *in Figure (d) and tangential impact velocity* $\dot{\theta}(t_n-)$ *in Figure (e).*

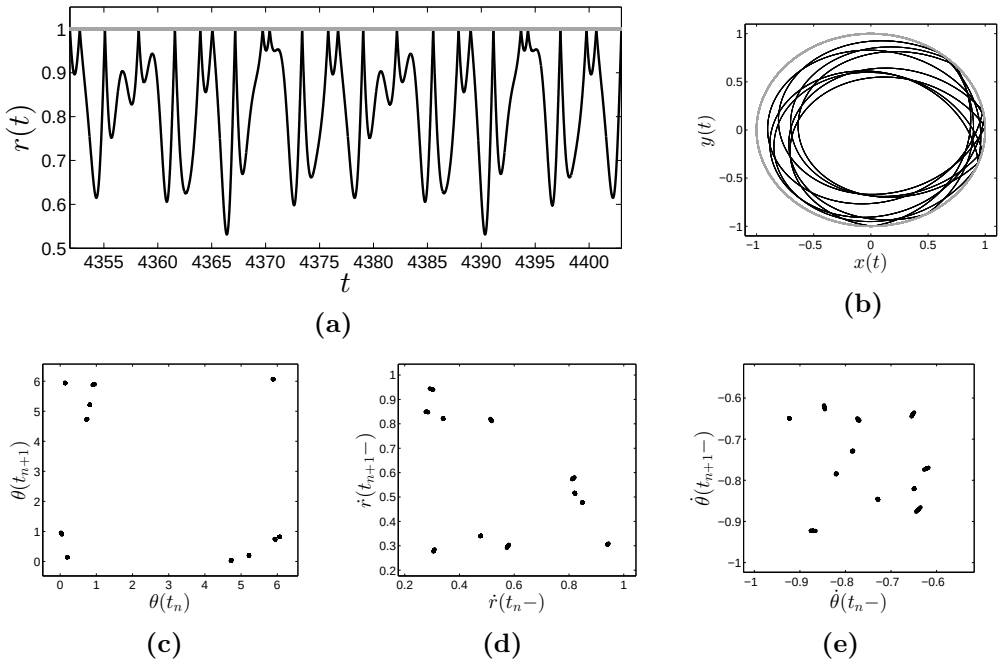

Figure 6-5: *Periodic orbit with* 11 *impacts per period where* $\omega = 0.76$ *and* $\gamma = 0.08156$. *Figure (a)* $r(t)$ *against* t. *Figure (b) Rotor trajectory in the rotating complex frame* (x, y) *(black) with impact surface (grey). Delay plots for angle at impact* $\theta(t_n)$ *in Figure (c), and pre-impact normal velocity* $\dot{r}(t_n-)$ *in Figure (d) and tangential impact velocity* $\dot{\theta}(t_n-)$ *in Figure (e).*

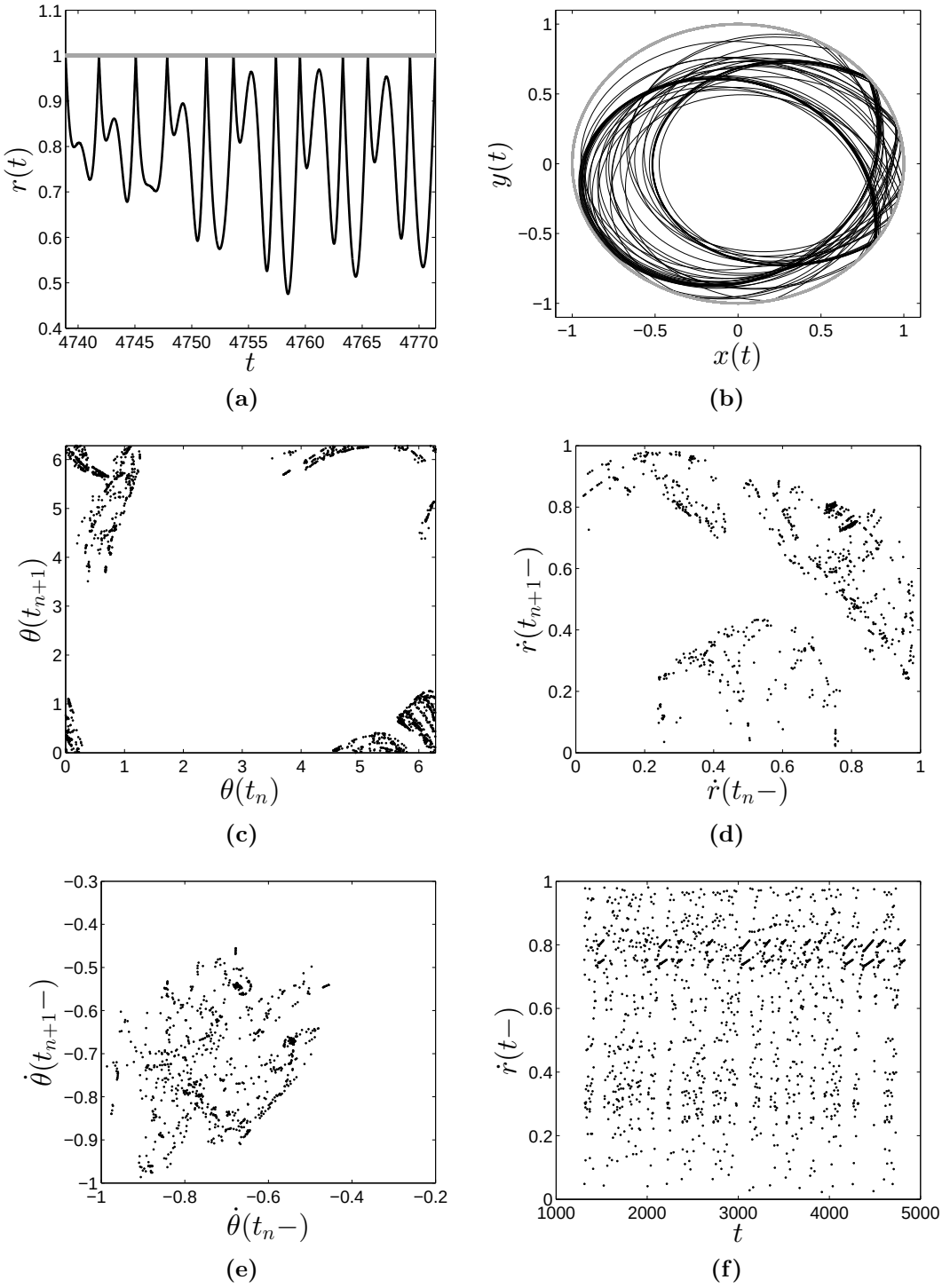

Figure 6-6: *Chaotic attractor (with Lyapunov exponent greater than zero) with* $\omega = 0.76$ *and* $\gamma = 0.0823$. *Figure (a)* $r(t)$ *against* t. *Figure (b) Rotor trajectory in the rotating complex frame* (x, y) *(black) with impact surface (grey). Delay plots for angle at impact* $\theta(t_n)$ *in Figure (c), and pre-impact normal velocity* $\dot{r}(t_n-)$ *in Figure (d) and tangential impact velocity* $\dot{\theta}(t_n-)$ *in Figure (e).*

2-impact periodic orbit (Figure 6-3e). We conjecture that this is a non-smooth period-doubling bifurcation as both branches of the periodic orbit increase as γ decreases (Figure 6-7b), which is unlike a smooth period-doubling bifurcation. Furthermore, the maximum eigenvalue computed numerically in Chapter 5.5 was not -1 for the 1-impact periodic orbit. Determining the bifurcation type is a possibility for future work. Note that in Figure 6-7b we do not observe straight lines due to remaining transient behaviour as discussed in Section 6.3.

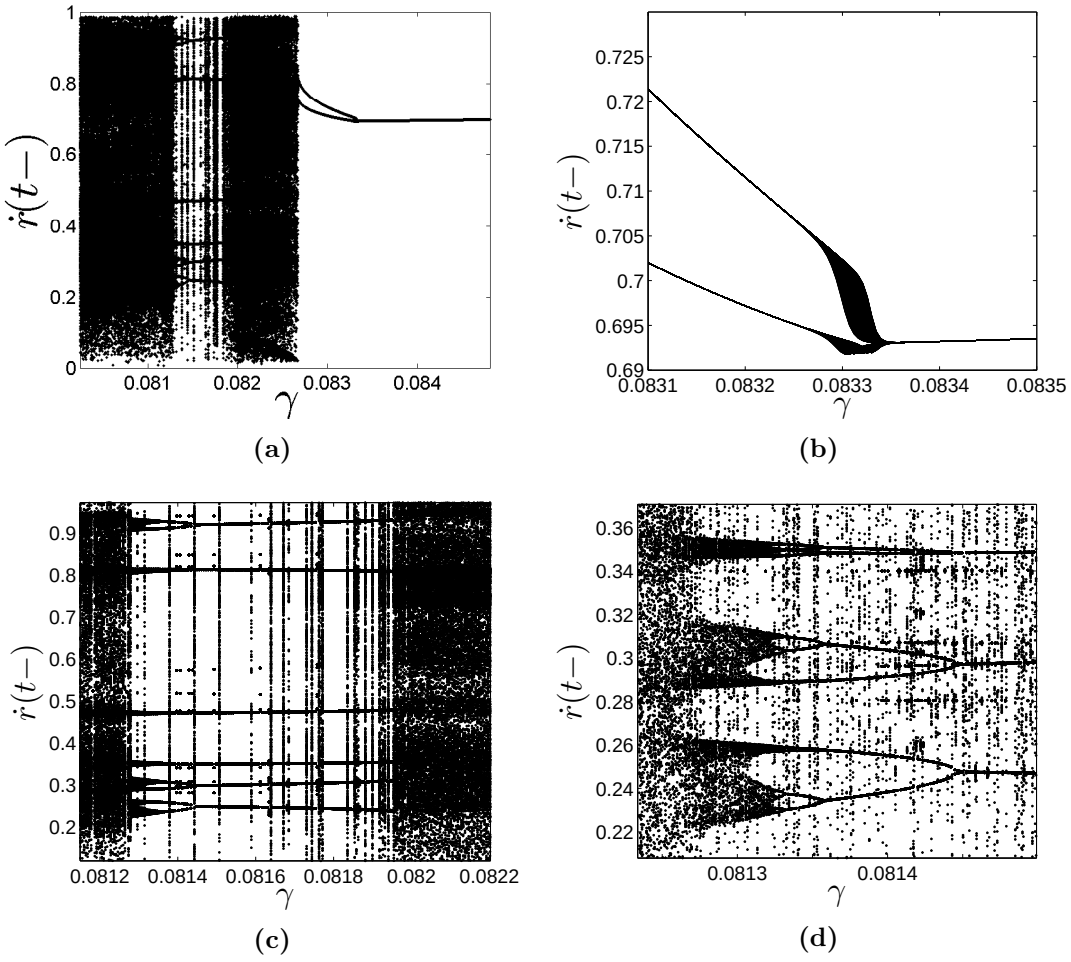

Figure 6-7: *Bifurcation diagram with bifurcation parameter γ. Figures 6-7b, 6-7c and 6-7d are magnifications of the main diagram Figure 6-7a. In all diagrams we see a number of different types of behaviour. Figures 6-7a and 6-7b: As γ decreases from $\gamma = 0.085$ the stable 1-impact periodic orbit bifurcation into a 2-impact periodic orbit in a non-smooth period-doubling bifurcation at $\gamma \approx 0.08335$. The 2-impact periodic orbit bifurcates into a chaotic attractor at $\gamma \approx 0.08265$ (Figure 6-7a). In Figures 6-7a, 6-7c and 6-7d, for $\gamma \in (0.08195, 0.08126)$ coexisting many-impact periodic orbits and possibly chaos and quasi-periodic orbits are observed. In Figure 6-7d we see a smooth period-doubling cascade for $\gamma \in (0.08128, 0.08145)$.*

Decreasing the parameter γ further in Figure 6-7 we observe a sudden bifurcation to a chaotic attractor at $\gamma \approx 0.08265$. This bifurcation, called a **grazing bifurcation**

and defined in Chapter 2, can be classified when looking at the 2-impact periodic orbit in Figure 6-4. In Figure 6-4 we see that the trajectory of the 2-impact periodic orbit is close to the boundary at $(x, y) \approx (-0.55, -0.85)$. As γ is further decreased, the periodic orbit will graze the impact surface with zero normal velocity $\dot{r}$, i.e. a grazing event, also defined in Chapter 2. From the grazing bifurcation complex orbits can arise. Investigating the chaotic orbit in more detail in Figure 6-6, where $\gamma = 0.0823$, we observe that characteristics of the 2-impact periodic orbit seem to irregularly emerge for a few impacts, Figure 6-6f.

Further decreasing the bifurcation parameter in Figures 6-7a and 6-7c, we observe for $\gamma \in (0.08195, 0.08126)$ coexisting, many-impact periodic orbits and perhaps even small chaotic intervals or quasi periodic orbits. As γ decreases, the birth of a 6-impact periodic orbit is observed at $\gamma \approx 0.08195$ in what appears to be another grazing bifurcation, which needs further investigation. This orbit loses stability in a smooth period-doubling bifurcation at $\gamma \approx 0.08145$ which gives rise to a smooth period-doubling cascade for $\gamma \in (0.08128, 0.08145)$, Figures 6-7a, 6-7c and 6-7d. Eventually this cascade becomes chaotic in what appears to be another grazing bifurcation at $\gamma \approx 0.08145$ as γ decreases.

6.5 Two-parameter Bifurcation Analysis

Essentially, chattering arises when the bearing is forced towards the stator and comes into contact, leading to a theoretically infinite number of impacts with it. A chattering sequence (Figure 6-1) can be very damaging to the rotor as a large number of impacts occur on a small surface area. Consequently thermal issues arise [68] and ultimately material deterioration is inevitable. Furthermore, it can lead to continuous contact between rotor and stator [18, 77], such as sticking [67, 26], sliding [67, 26] or rolling [67, 26]. It is crucial to identify for what parameter values chattering can occur.

In this Section we present a crude two-parameter bifurcation diagram, Figure 6-8, that distinguishes between four types of motions:

Type 1 trajectories that after no or a few impacts settle into a non-impacting orbit.

Type 2 trajectories that lead to chattering with tangential impact velocity $\Theta_{0,-} > 0$ (in the fixed frame), which are referred to as **forward chattering**.

Type 3 trajectories that lead to chattering with tangential impact velocity $\Theta_{0,-} < 0$ (in the fixed frame), which are referred to as **backward chattering**.

Type 4 trajectories that will repeatedly impact the stator, but do not include chattering.

The rotor motion with Type 1 trajectories is classed as *not damaging* if no impacts occur, or the *least damaging* if a few impacts occur. Some examples of such motion have been discussed in Chapter 5, in particular Chapters 5.3 and 5.4, as well as Figure 5-2a.

Type 4 motion has been analysed in Chapter 5 and Sections 6.4, where a detailed numerical bifurcation analysis has been presented. Repeated instantaneous contact between rotor and stator is viewed as *damaging* [67, 26].

Both Type 2 and 3 motion can result in continuous contact [77], called rub or rubbing (Chapter 2). More specifically, Type 3 motion can lead to forward rub, a sliding motion (Chapter 2). Type 4 motion can lead to either backward rub, a sliding motion possibly mixed with rolling motion (Chapter 2), or backward whirl rub, a pure rolling motion (Chapter 2). These motions have been observed in magnetic bearing models simpler than the one studied in this Thesis (6.1), (6.2), [77]. Both Type 2 and 3 motions are very damaging [67, 26, 103]. However, backward whirl rub has been described as the most damaging, [67, 26, 103], due to the large contact forces. In such cases, no control is possible, i.e. the rotor cannot be returned to a non-contacting operating state [103].

We present a two-parameter bifurcation diagram (Figure 6-8) where we vary the damping parameter γ and stiffness ω to determine for what values Type 1-4 motion occurs. We vary γ and ω as these are easily controllable in experiments [67, 26, 103], whereas the impact parameters, coefficient of restitution d and friction μ, are dictated by material properties that are usually fixed [80]. The unbalance properties can suddenly vary during an experiment [22, 41, 89, 50].

We have found that for γ large enough (Figure 6-8a: dotted area) the orbits do not experience impact, which corresponds to Type 1 motion. Type 4 motion is mainly confined to the parameter area where $\gamma \in (0.1, 0.2)$. By comparison, Type 2 (Figure 6-8a: black $*$) motion seems more distributed and very intertwined with Type 3 motion (Figure 6-8a: grey $*$) provided that $\gamma < 0.1$. In particular, low damping and high stiffness yields mainly Type 3 motion, the potentially most damaging type. Under magnification, the delineation of these regions is not clear (Figure 6-8b). In fact, a complex distribution of Type 2, 3 and 4 motion is found, Figure 6-8b, which could be fractal. This is not unusual for impacting hybrid system [34]. Generally, it appears that the damping related parameter has a larger effect on the dynamics of the magnetic bearing system (6.1), (6.2). By that we mean that if ω is fixed and γ is varied, all four motion types can be observed in the system (6.1), (6.2), but not vice versa, i.e. if γ is fixed and ω is varied.

From an engineer's point of view the magnetic bearing system will operate normally, if the damping related parameter $\gamma > 0.4$, for the prescribed parameter values given in (6.3).

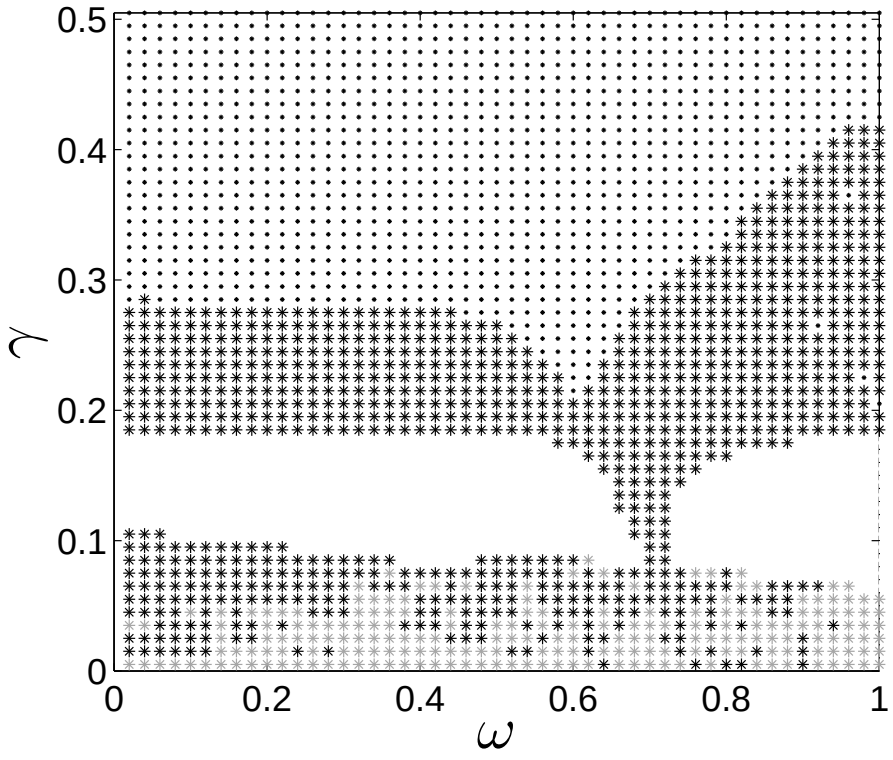

(a)

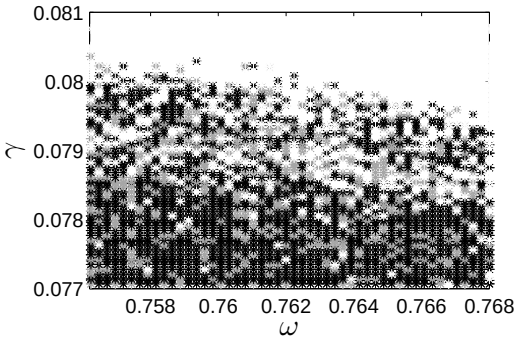

(b)

Figure 6-8: *Numerically computed two-parameter bifurcation diagram depicting orbits with no impact (.), forward chattering (black ∗), backward chattering (grey ∗), continuously impacting orbit without chattering (white space). Figure 6-8b displays a magnified section of the bifurcation diagram in Figure 6-8a. In Figure 6-8b we see that the boundary between continuously impacting orbits and chattering orbits is very complex, perhaps fractal.*

6.6 Conclusions

In this Chapter we were able to complete the bifurcation analysis of the 1-impact periodic orbit, which was extensively studied in Chapter 5. We showed numerically that this periodic orbit loses stability in a non-smooth period doubling bifurcation, which gives rise to a 2-impact periodic orbit. We were able to demonstrate that in addition to the 1-impact periodic orbit other, more complex, attractors are found in magnetic bearing systems. These include many-impact periodic orbits, chaos and possibly quasi-periodic orbits.

Moreover, we have illustrated that for certain parameter values

- smooth bifurcations, such as smooth period-doubling and period-doubling bifurcation cascades, and
- non-smooth bifurcations, such as grazing bifurcation and non-smooth period-doubling bifurcation

can arise in magnetic bearing systems. However, a more detailed analysis for a larger interval of the damping related parameter is necessary for a better understanding and classification of other non-smooth bifurcation phenomena. This could be numerically analysed by computing a Monte Carlo bifurcation diagram (defined in Chapter 2).

Furthermore, we have identified critical regions in the (ω, γ)-parameter space, that can lead to damaging rotor-stator contact motion. In future work this analysis could be used to assess the thermal effects [68] resulting from the rotor dynamics and thus not only identify possible damage but also predict the longevity of magnetic bearing components.

An important issue that needs addressing is how to resolve the infinite chattering sequence, i.e. what motion occurs after the accumulation point? There are several possibilities: sticking, sliding, a combination of sliding and rolling, or pure rolling. The simple model studied in this Thesis is not suited for such an investigation; other models are probably more appropriate [93].

CHAPTER 7

Conclusions

In this Thesis we have demonstrated that the theory of piecewise-smooth dynamical systems can provide a mathematical framework which enables the study of impacting systems, such as magnetic bearing systems, and the study of non-smooth phenomena arising in such applications. These applications are of great interest to mechanical engineers. We have also studied piecewise-smooth dynamical systems in their own right. Throughout the Chapters, the piecewise-smooth continuous or discrete systems were shown to give rise to intricate and interesting dynamics and bifurcations. A diverse set of analytical tools and numerical methods were utilised to show how these arise.

In the first part of this work we focused on studying the dynamics and bifurcations of one-dimensional piecewise-smooth maps. These maps can arise from many applications such as the impact oscillator [90]. We introduced the piecewise power law map which contains a nonlinear term with exponent p,

$$x_{n+1} = \begin{cases} \lambda x_n + \mu, & \text{if } x_n < 0 \\ -\eta x_n^p + \mu - \ell, & \text{if } x_n > 0. \end{cases} \tag{7.1}$$

We have studied the dynamics and bifurcations of the map when $p \in [0, 1]$ in Chapter 3 and when $p > 1$ in Chapter 4.

Chapter 3 concerned the border-collision bifurcation of the negative stable fixed point and the resulting bifurcation scenarios for the bifurcation parameter $\mu > 0$. For the continuous map (7.1), i.e. $\ell = 0$, we proved, utilising an induced map, that the three characteristic scenarios (robust chaos, period-incrementing cascade with chaotic windows and period-incrementing cascade with coexisting periodic orbits) depend on the exponent p. We derived the necessary and sufficient conditions for these scenarios to arise. However, the exponent p does not introduce new dynamics or bifurcations.

For the discontinuous map (7.1) with $\ell > 0$ we derived the general conditions required for the breakdown of the period-incrementing cascade for $\mu > 0$, i.e. some of the periodic orbits in the cascade lose stability and give rise to a chaotic attractor. These conditions were then utilised to conclude that a chaotic attractor will never exist in the neighbourhood of small $\mu > 0$, unlike in the continuous piecewise power law map. Instead, a period-incrementing cascade is observed. To obtain these results we studied the maximal periodic orbits of which the period-incrementing cascade is composed. These results agreed with the dynamics of the maps, which represent special cases of (7.1) (continuous/discontinuous piecewise linear or square-root map) presented in literature.

Finally, when considering the discontinuous map (7.1) with $\ell < 0$, we proved that stable maximal periodic orbits with large periods do not exist, i.e. as $N \to \infty$ maximal periodic orbits cease to exist. Numerically, we demonstrated that the negative fixed point bifurcates into a period-adding cascade. Period-incrementing cascades and chaos have also been observed. However, a detailed analysis, similar to the one in the first part of this Chapter, is required to fully understand how the bifurcation structures, period-adding and period-incrementing cascade, arise. It also remains to show what parameter conditions are required to observe chaotic attractors are robust chaos.

In Chapter 4 we considered the border-collision bifurcations of the positive stable fixed point. Numerically, we illustrated that as $b := \mu - \ell < 0$ decreases through zero this fixed point can bifurcate into a range of invariant sets such as period-2, period-4 and large period periodic orbits. The main organising structure for this map is the period-incrementing cascade for $b < 0$ and the period-adding cascade for $b > 0$. However, increasing μ introduces a period-adding cascade for large $b < 0$ in the neighbourhood of the border collision bifurcation. For certain parameter values the fixed point also bifurcates into a chaotic attractor in the neighbourhood of the border-collision bifurcation point. In the final part of this chapter we chose a new bifurcation parameter μ. For the parameter region $\mu > 0$ we showed that the anharmonic cascade, which was first discovered by Glendinning [51, 52], also arises in the piecewise power law map. However, this last result throws up more questions than it answers. Glendinning was able to show, using renormalisation methods and kneading theory, that the period of the periodic orbits in the anharmonic cascade tends to zero as b tends to a point of accumulation. Is this the case for the piecewise power law map? Is it possible to compute or at least approximate the point of accumulation? A two parameter bifurcation analysis of b and μ could yield how the mechanism of the period-adding scenario and the anharmonic cascade are connected.

Chapters 3 and 4 clearly illustrate the richness of non-smooth dynamics in piecewise power law maps. As briefly explained in Chapter 2, this map can arise from the study of non-smooth events in the impact oscillator that impacts with a repelling wall. A

variety of motions, including grazing events, of such an impact system are currently being investigated numerically and experimentally by Virgin [124]. A comparison of the predictions in this Thesis with experimental data would indicate how realistic the repulsive reset law is. Although certain dynamics of the impact oscillator can be approximated by a one-dimensional map, the Poincaré map, near grazing or elsewhere, is two-dimensional. This indicates the necessity for extending these results to two- or higher-dimensional maps as part of future work to contribute to the current but sparse literature [35, 85, 101, 125].

In Chapters 5 and 6 the theory of impacting hybrid dynamical systems was used to model and study magnetic bearing systems. In Chapter 5, boundary equilibrium bifurcations of regular equilibria in the co-rotating frame were shown to exist in this system and the conditions for persistence and non-smooth fold bifurcation scenarios were derived. The impact map, a type of Poincaré map, was calculated reducing the system's dimension to investigate fixed points associated with limit cycles that experience one impact per period T in the co-rotating frame. The fixed points' global existence conditions were derived mostly analytically and it was revealed that there can exist a large but finite number of fixed points for certain damping parameter values. However, at most four fixed points give rise to physically realistic limit cycles. The stability and bifurcation analysis, which were performed numerically, showed that, as the damping parameter is varied, at most one fixed point is stable and that it loses stability before it undergoes a grazing event. The key finding was that a more complex bifurcation scenario than the non-smooth fold scenario is taking place at the boundary equilibrium bifurcation point. In fact, we have proved that a novel Hopf-like bifurcation occurs, which we termed non-smooth Fold-Hopf bifurcation, where a regular equilibrium, a virtual equilibrium and two limit cycles (experiencing an impact) bifurcate. This bifurcation is unlike any other reported in literature and is, we believe, an important contribution to the classification of bifurcation scenarios in higher dimensional piecewise-smooth dynamical systems. Finally, we showed that local to the bifurcation point the impact map associated with the limit cycle (one impact per period T) is linear. From the analysis of this map the same non-smooth Fold-Hopf bifurcation was deduced.

In Chapter 6 the numerical investigation gave an insight into other intricate dynamics and bifurcations that occur in the magnetic bearing systems. As the magnetic bearing system is four-dimensional in phase space we have observed a range of attracting invariant sets such as periodic orbits, quasi-periodic orbits, chaotic orbits and chattering motion. It was essential, in particular from an engineer's point of view, to identify for what damping and stiffness values damaging motion occurs; chattering motion is very damaging as it can lead to continuous contact. We defined four categories of motion: impacts that lead to a non-impacting orbit (least damaging),

orbits which experience repeated impacts (no chattering, damaging), forward chattering (very damaging) and backward chattering motion (most damaging). We concluded that these types of motion are largely influenced by the damping parameter, whereas the influence of the stiffness parameter is minor. The unbalanced rotor starting from the origin settles into a non-impacting orbit provided damping is large enough (scaled parameter $\gamma > 0.3$). Orbits experiencing repeated impacts are most likely to occur for $\gamma \in (0.1, 0.2)$. If $\gamma \in (0.2, 0.3)$ forward chattering can occur, whereas for $\gamma \in (0, 0.1)$ both forward and backward chattering is possible. The boundaries between these regions were intricate and appeared fractal. Furthermore, from this analysis we concluded that large enough damping could prevent rotor-stator interaction and thus avoid severe damage to both rotor and stator. Finally, the numerical bifurcation analysis obtained from varying the damping parameter yielded smooth and non-smooth bifurcation, such as grazing.

One avenue for future work could be to compare experimental data to the motion predicted in this work. However, great care would have to be taken for three reasons. Firstly, we assumed that the stator (impact surface) behaves rigidly during impact. Yet even for a very stiff experimental set up, the stator is not completely rigid and thus could affect the rotor dynamics. Secondly, the rotor motion is not only influenced by impacts but also by other rotor behaviour that occurs at high speeds, such a shaft bending. Thirdly, experimental data is notorious for its noise. In all cases, small scale dynamics predicted analytically and numerically might be missed in experimental data, e.g. small amplitude limit cycles. Major non-smooth phenomena such as sudden transitions from periodic to chaotic motion should be detectable.

The hybrid system model studied in this work has stringent limitations on predicting the transition into continuous contact motion and is unsuitable for modelling the continuous contact motion itself. However, there are more capable formalisms for that purpose such as the altered reset law suggested by Stronge [110]. He suggests an energetic coefficient of restitution and a breakdown of the impact event into distinct phases of stick and slip. An altered impacting hybrid dynamical system implementing Stronge's reset laws has been suggested in [93]. Modelling magnetic bearing systems with the altered impacting hybrid system [93] could be another avenue for future work. We suspect that this model is better suited to study the rotor motion following grazing events, which can lead to continuous contact.

The study of the impact oscillator near grazing via the discontinuous square-root map, a special case of the piecewise power law map (7.1), showed that the repulsing impact surface (i.e. the discontinuity ℓ) introduced stable periodic orbits near the grazing event. If a magnetic bearing system could implement the idea of a repelling impact surface, would it enable less damaging motion?

In conclusion, our study of magnetic bearing systems in Chapters 5 and 6 certainly

contributes to the wider understanding of higher dimensional piecewise-smooth systems, continuous and discrete. At the same time it is clear that even this simple model of a magnetic bearing system gives rise to an abundance of interesting and intricate dynamics and bifurcations which need further investigation from a mathematical and an engineering point of view.

Bibliography

[1] V. Acary, O. Bonnefon, and B. Brogliato, *Nonsmooth modeling and simulation for switched circuits*, vol. 69, Springer, 2011.

[2] V. Acary and B. Brogliato, *Numerical methods for nonsmooth dynamical systems: applications in mechanics and electronics*, vol. 35, Springer, 2008.

[3] M. A. Aizerman and F. R. Gantmakher, *On the stability of periodic motions*, Journal of Applied Mathematics and Mechanics, 22 (1958), pp. 1065 – 1078.

[4] R. Alzate, M. Di Bernardo, U. Montanaro, and S. Santini, *Experimental and numerical verification of bifurcations and chaos in cam-follower impacting systems*, Nonlinear Dynamics, 50 (2007), pp. 409–429.

[5] V. Avrutin, A. Granados, and M. Schanz, *Sufficient conditions for a period incrementing big bang bifurcation in one-dimensional maps*, Nonlinearity, 24 (2011), p. 2575.

[6] V. Avrutin and M. Schanz, *On the scaling properties of the period-increment scenario in dynamical systems*, Chaos, Solitons & Fractals, 11 (2000), pp. 1949 – 1955.

[7] ——, *On multi-parametric bifurcations in a scalar piecewise-linear map*, Nonlinearity, 19 (2006), p. 531.

[8] V. Avrutin, M. Schanz, and B. Schenke, *Breaking the continuity of a piecewise linear map*, in ESAIM: Proceedings, vol. 36, EDP Sciences, 2012, pp. 73–105.

[9] V. Avrutin, I. Sushko, and L. Gardini, *Cyclicity of chaotic attractors in one-dimensional discontinuous maps*, Mathematics and Computers in Simulation, 95

(2014), pp. 126 – 136. Discontinuous Differential Systems : Theory and Numerical Methods.

[10] S. Banerjee, J. A. Yorke, and C. Grebogi, *Robust Chaos*, Physical Review Letters, 80 (1998), pp. 3049–3052.

[11] A. R. Bartha, *Dry friction backward whirl of rotors*, PhD thesis, ETH. Zürich, Switzerland, 2000.

[12] J. J. B. Biemond, A. P. S. de Moura, C. Grebogi, N. van de Wouw, and H. Nijmeijer, *Dynamical collapse of trajectories*, EPL Europhys. Lett., 98 (2012), p. 20001.

[13] H. F. Black, *Interaction of a whirling rotor with a vibrating stator across a clearance annulus*, J. Mech. Eng. Sci., 10 (1968), pp. 1–12.

[14] V. Botella-Soler, J. A. Oteo, and J. Ros, *Dynamics of a map with a power-law tail*, Journal of Physics A: Mathematical and Theoretical, 42 (2009), p. 385101.

[15] ——, *Coexistence of periods in a bifurcation*, Chaos, Solitons & Fractals, 45 (2012), pp. 681 – 686.

[16] P. C. Bressloff and J. Stark, *Neuronal dynamics based on discontinuous circle maps*, Physics Letters A, 150 (1990), pp. 187–195.

[17] C. J. Budd, *Non-smooth dynamical systems and the grazing bifurcation*, Nonlinear mathematics and its applications, (1996), pp. 219–235. ed. Aston P.

[18] C. J. Budd and F. Dux, *Chattering and related behaviour in impact oscillators*, Phil. Trans. R. Soc. A, 347 (1994), pp. 365–389.

[19] R. Casey, H. De Jong, and J.-L. Gouzé, *Piecewise-linear models of genetic regulatory networks: Equilibria and their stability*, Journal of mathematical biology, 52 (2006), pp. 27–56.

[20] D. W. Childs, *Rub-induced parametric excitation in rotors*, ASME J. Mech. Des., 101 (1979), pp. 640–644.

[21] ——, *Fractional–frequency rotor motion due to nonsymmetric clearance effects*, ASME. J. Eng. Power, 104 (1982), pp. 533–541.

[22] ——, *Turbomachinery – Rotordynamics – Phenomena, Modeling, and Analysis*, John Wiley & Sons, New York, NY, 1993.

[23] D. R. J. Chillingworth, *Dynamics of an impact oscillator near a degenerate graze*, Nonlinearity, 23 (2010), p. 2723.

[24] W. Chin, E. Ott, H. E. Nusse, and C. Grebogi, *Grazing bifurcations in impact oscillators*, Physical Review E, 50 (1994), p. 4427.

[25] M. O. T. Cole, *On stability of rotordynamic systems with rotor–stator contact interaction*, Proc. R. Soc. A, 464 (2008), pp. 3353–3375.

[26] M. O. T. Cole and P. S. Keogh, *Asynchronous periodic contact modes for rotor vibration within an annular clearance*, Proceedings of the Institution of Mechanical Engineers, Part C: Journal of Mechanical Engineering Science, 217 (2003), pp. 1101–1115.

[27] S. Coombes and S. H. Doole, *Neuronal population dynamics with post inhibitory rebound: a reduction to piecewise linear discontinuous circle maps*, Dynam. Stability Systems, 11 (1996), pp. 193–217.

[28] S. Coombes and A. H. Osbaldestin, *Period-adding bifurcations and chaos in a periodically stimulated excitable neural relaxation oscillator*, Phys. Rev. E, 62 (2000), pp. 4057–4066.

[29] S. Coombes, R. Thul, and K. C. A. Wedgwood, *Nonsmooth dynamics in spiking neuron models*, Phys. D, 241 (2012), pp. 2042–2057.

[30] R. B. Davis and L. N. Virgin, *Non-linear behavior in a discretely forced oscillator*, International Journal of Non-Linear Mechanics, 42 (2007), pp. 744–753.

[31] H. De Jong, J.-L. Gouzé, C. Hernandez, M. Page, T. Sari, and J. Geiselmann, *Qualitative simulation of genetic regulatory networks using piecewise-linear models*, Bulletin of mathematical biology, 66 (2004), pp. 301–340.

[32] M. di Bernardo, C. J. Budd, and A. Champneys, *Grazing, skipping and sliding: Analysis of the non-smooth dynamics of the DC/DC buck converter*, Nonlinearity, 11 (1998), p. 859.

[33] M. di Bernardo, C. J. Budd, A. Champneys, P. Kowalczyk, A. B. Nordmark, G. Tost, and P. Piiroinen, *Bifurcations in nonsmooth dynamical systems*, SIAM Rev., 50 (2008), pp. 629–701.

[34] M. di Bernardo, C. J. Budd, A. R. Champneys, and P. Kowalczyk, *Piecewise-smooth dynamical systems: theory and applications*, Springer-Verlag, London, 2008.

[35] M. Di Bernardo, M. I. Feigin, S. J. Hogan, and M. E. Homer, *Local analysis of C-bifurcations in n-dimensional piecewise-smooth dynamical systems*, Chaos, Solitons & Fractals, 10 (1999), pp. 1881–1908.

[36] M. di Bernardo, F. Garefalo, L. Glielmo, and F. Vasca, *Switchings, bifurcations, and chaos in DC/DC converters*, Circuits and Systems I: Fundamental Theory and Applications, IEEE Transactions on, 45 (1998), pp. 133–141.

[37] M. di Bernardo, A. B. Nordmark, and G. Olivar, *Discontinuity-induced bifurcations of equilibria in piecewise-smooth and impacting dynamical systems*, Phys. D, 237 (2008), pp. 119–136.

[38] P. S. Dutta and S. Banerjee, *Period increment cascades in a discontinuous map with square-root singularity*, Discrete Contin. Dyn. Syst. Ser. B, 14 (2010), pp. 961–976.

[39] F. F. Ehrich, *Bistable vibration of rotors in bearing clearance*, in ASME, Winter Annual Meeting, Chicago, ILL, ASME 65-WA/MD-1, 1965.

[40] ——, *High order subharmonic response of high speed rotors in bearing clearance*, ASME J. Vib. Acoust. Stress Reliab. Des., 110 (1988), pp. 9–16.

[41] ——, *Handbook of rotordynamics*, McGraw-Hill, New York, 1992.

[42] E. Farcot and J.-L. Gouzé, *Limit cycles in piecewise-affine gene network models with multiple interaction loops*, International Journal of Control, 41 (2010), pp. 119–130.

[43] M. I. Feigin, *On the structure of c-bifurcation boundaries of piecewise-continuous systems: PMM vol. 42, no. 5, 1978, pp. 820–829*, Journal of Applied Mathematics and Mechanics, 42 (1978), pp. 885 – 895.

[44] ——, *The increasingly complex structure of the bifurcation tree of a piecewise-smooth system*, Journal of Applied Mathematics and Mechanics, 59 (1995), pp. 853 – 863.

[45] Z. C. Feng and X. Z. Zhang, *Rubbing phenomena in rotor-stator contact*, Chaos, Solitons Fract., 14 (2002), pp. 257 – 267.

[46] S. Foale, *Analytical determination of bifurcations in an impact oscillator*, Philosophical Transactions of the Royal Society of London. Series A: Physical and Engineering Sciences, 347 (1994), pp. 353–364.

[47] S. Foale and S. R. Bishop, *Dynamical complexities of forced impacting systems*, Philos. Trans. Roy. Soc. London Ser. A, 338 (1992), pp. 547–556.

[48] ——, *Bifurcations in impact oscillations*, Nonlinear Dynamics, 6 (1994), pp. 285–299.

[49] L. Gardini, I. Sushko, and A. K. Naimzada, *Growing through chaotic intervals*, Journal of Economic Theory, 143 (2008), pp. 541 – 557.

[50] G. Genta, *Dynamics of Rotating Systems*, Springer, 2005.

[51] P. Glendinning, *Robust new routes to chaos in differential equations*, Physics Letters A, 168 (1992), pp. 40 – 46.

[52] ——, *The anharmonic route to chaos: kneading theory*, Nonlinearity, 6 (1993), p. 349.

[53] ——, *Stability, instability and chaos: an introduction to the theory of nonlinear differential equations*, Cambridge Texts in Applied Mathematics, Cambridge University Press, Cambridge, 1994.

[54] ——, *Routes to chaos*, in Encyclopedia of nonlinear science, A. Scott, ed., Routledge, New York, 2005, pp. xliv+1053.

[55] J. Guckenheimer and P. J. Holmes, *Nonlinear oscillations, dynamical systems, and bifurcations of vector fields*, vol. 42 of Applied Mathematical Sciences, Springer-Verlag, New York, 1990. Revised and corrected reprint of the 1983 original.

[56] C. Halse, M. Homer, and M. di Bernardo, *C-bifurcations and period-adding in one-dimensional piecewise-smooth maps*, Chaos, Solitons & Fractals, 18 (2003), pp. 953–976.

[57] M. P. Hassell, *Density-dependence in single-species populations*, J. anim. Ecol, 44 (1975), pp. 283–295.

[58] S. J. Hogan, *On the dynamics of rigid-block motion under harmonic forcing*, Proceedings of the Royal Society of London. A. Mathematical and Physical Sciences, 425 (1989), pp. 441–476.

[59] S. J. Hogan, L. Higham, and T. C. L. Griffin, *Dynamics of a piecewise linear map with a gap*, Proceedings of the Royal Society A: Mathematical, Physical and Engineering Science, 463 (2007), pp. 49–65.

[60] J. Ing, E. Pavlovskaia, M. Wiercigroch, and S. Banerjee, *Experimental study of impact oscillator with one-sided elastic constraint*, Philosophical Transactions of the Royal Society A: Mathematical, Physical and Engineering Sciences, 366 (2008), pp. 679–705.

[61] P. Jain and S. Banerjee, *Border-collision bifurcations in one-dimensional discontinuous maps*, International Journal of Bifurcation and Chaos, 13 (2003), pp. 3341–3351.

[62] M. R. Jeffrey, *Three discontinuity-induced bifurcations to destroy self-sustained oscillations in a superconducting resonator*, Physica D: Nonlinear Phenomena, 241 (2012), pp. 2077 – 2082. Dynamics and Bifurcations of Nonsmooth Systems.

[63] J.-C. Ji, C. H. Hansen, and A. C. Zander, *Nonlinear dynamics of magnetic bearing systems*, Journal of Intelligent Material Systems and Structures, 19 (2008), pp. 1471–1491.

[64] D. C. Johnson, *Synchronous whirl of a vertical shaft having clearance in one bearing*, J. Mech. Eng. Sci., 4 (1962), pp. 85–93.

[65] A. Katok and B. Hasselblatt, *Introduction to the modern theory of dynamical systems*, vol. 54 of Encyclopedia of Mathematics and its Applications, Cambridge University Press, Cambridge, 1995. With a supplementary chapter by Katok and Leonardo Mendoza.

[66] J. Keener and J. Sneyd, *Mathematical physiology*, vol. 8 of Interdisciplinary Applied Mathematics, Springer-Verlag, New York, 1998.

[67] P. S. Keogh and M. O. T. Cole, *Rotor vibration with auxiliary bearing contact in magnetic bearing systems part 1: Synchronous dynamics*, Proc. Inst. Mech. Eng. C J. Mech. Eng. Sci., 217 (2003), pp. 377–392.

[68] P. S. Keogh and Y. Y. Woon, *Thermal assessment of dynamic rotor/auxiliary bearing contact events*, Journal of tribology, 129 (2007), pp. 143–152.

[69] R. G. Kirk, *Evaluation of AMB turbomachinery auxiliary bearings*, ASME J. Vib. Acoust., 121 (1999), pp. 156–161.

[70] T. Küpper, H. A. Hosham, and K. Dudtschenko, *The dynamics of bells as impacting system*, Proceedings of the Institution of Mechanical Engineers, Part C: Journal of Mechanical Engineering Science, 225 (2011), pp. 2436–2443.

[71] Y. A. Kuznetsov, *Elements of applied bifurcation theory*, vol. 112 of Applied Mathematical Sciences, Springer-Verlag, New York, second ed., 1998.

[72] H. Lamba, *Impacting oscillators and nonsmooth dynamical systems*, PhD thesis, 1993.

[73] ——, *Chaotic, regular and unbounded behaviour in the elastic impact oscillator*, Physica D: Nonlinear Phenomena, 82 (1995), pp. 117 – 135.

[74] J. L. Lawen and G. T. Flowers, *Synchronous dynamics of a coupled shaft bearing housing system with auxiliary support from a clearance bearing: Analysis and experiment*, ASME J. Eng. Gas Turb. Power, 119 (1997), pp. 430–435.

[75] R. I. Leine and D. H. Van Campen, *Bifurcation phenomena in non-smooth dynamical systems*, Eur. J. Mech. A-Solid, 25 (2006), pp. 595–616.

[76] R. I. Leine and N. v. d. Wouw, *Stability and convergence of mechanical systems with unilateral constraints*, vol. 36, Springer-Verlag Berlin Heidelberg, 2008.

[77] G. X. Li and M. P. Païdoussis, *Impact phenomena of rotor-casing dynamical systems*, Nonlinear Dynam., 5 (1994), pp. 53–70.

[78] Q. S. Lu, Q. H. Li, and E. H. Twizell, *The existence of periodic motions in rub-impact rotor systems*, J. Sound Vib., 264 (2003), pp. 1127–1137.

[79] G. W. Luo and J. H. Xie, *Hopf bifurcation of a two-degree-of-freedom vibro-impact system*, J. Sound Vib., 213 (1998), pp. 391–408.

[80] E. H. Maslen and G. Schweitzer, *Magnetic Bearings: Theory, Design, and Application to Rotating Machinery*, Springer, 2009.

[81] J. F. Mason, N. Humphries, and P. T. Piiroinen, *Numerical analysis of codimension-one, -two and -three bifurcations in a periodically-forced impact oscillator with two discontinuity surfaces*, Mathematics and Computers in Simulation, 95 (2014), pp. 98–110. Discontinuous Differential Systems: Theory and Numerical Methods.

[82] J. F. Mason and P. T. Piiroinen, *Saddle-point solutions and grazing bifurcations in an impacting system*, Chaos: An Interdisciplinary Journal of Nonlinear Science, 22 (2012), pp. 013106–013106.

[83] J. F. Mason, P. T. Piiroinen, R. E. Wilson, and M. E. Homer, *Basins of attraction in nonsmooth models of gear rattle*, International Journal of Bifurcation and Chaos, 19 (2009), pp. 203–224.

[84] MATLAB, *version 7.14 (R2012a)*, The MathWorks Inc., Natick, Massachusetts, United States of America, 2012.

[85] J. Molenaar, J. G. de Weger, and W. van de Water, *Mappings of grazing-impact oscillators*, Nonlinearity, 14 (2001), p. 301.

[86] K. Mora, C. J. Budd, P. Glendinning, and P. S. Keogh, *Piecewise-smooth hopf-type bifurcations arising from impact/friction contact events in rotating machinery.* submitted (2013).

[87] A. Muszynska, *Partial lateral rotor to stator rubs*, in International Conference on Vibrations in Rotating Machinery, 3rd, Heslington, England, 1984, pp. 327–335.

[88] ——, *Rotor-to-stationary part full annular contact modelling*, in Proc. of 9th International Symposium on Transport Phenomena and Dynamics of Rotating Machinery, Hawaii, 2002.

[89] ——, *Rotordynamics*, Boca Raton, London, Taylor & Francis, 2005.

[90] A. B. Nordmark, *Non-periodic motion caused by grazing incidence in an impact oscillator*, J. Sound Vib., 145 (1991), pp. 279–297.

[91] ——, *Universal limit mapping in grazing bifurcations*, Physical Review E, 55 (1997), p. 266.

[92] ——, *Existence of periodic orbits in grazing bifurcations of impacting mechanical oscillators*, Nonlinearity, 14 (2001), pp. 1517–1542.

[93] A. B. Nordmark, H. Dankowicz, and A. Champneys, *Discontinuity-induced bifurcations in systems with impacts and friction: Discontinuities in the impact law*, Int. J. Nonlinear Mech., 44 (2009), pp. 1011–1023.

[94] A. B. Nordmark and P. T. Piiroinen, *Simulation and stability analysis of impacting systems with complete chattering*, Nonlinear Dynam., 58 (2009), pp. 85–106.

[95] H. E. Nusse and J. A. Yorke, *Border-collsion bifurcations for piecewise smooth one-dimensional maps*, International Journal of Bifurcation and Chaos, 05 (1995), pp. 189–207.

[96] M. Oestreich, N. Hinrichs, K. Popp, and C. J. Budd, *Analytical and experimental investigation of an impact oscillator*, in Proc. ASME 16th Biennal Conf. Mech. Vibrations and Noise, Sacramento, California, DETC97VIB-3907, 1997, pp. 1–11.

[97] F. Peterka, *Analysis of the periodic motion of impact dampers (impact dampers with spring connection of masses, analyzing periodic motion)*, Revue Roumaine des Sciences Techniques, Série de Mécanique Appliquée, 16 (1971), pp. 875–886.

[98] A. J. K. Phillips and P. A. Robinson, *A quantitative model of sleep-wake dynamics based on the physiology of the brainstem ascending arousal system*, Journal of Biological Rhythms, 22 (2007), pp. 167–179.

[99] P. T. Piiroinen, L. N. Virgin, and A. R. Champneys, *Chaos and period-adding; experimental and numerical verification of the grazing bifurcation*, Journal of Nonlinear Science, 14 (2004), pp. 383–404.

[100] S. H. Piltz, M. A. Porter, and P. K. Maini, *Prey switching with a linear preference trade-off*, arXiv preprint arXiv:1302.6197, (2013).

[101] S. R. Pring, *Discontinuous maps with applications to impacting systems*, PhD thesis, 2009.

[102] S. R. Pring and C. J. Budd, *The dynamics of a simplified pinball machine*, IMA Journal of Applied Mathematics, 76 (2011), pp. 67–84.

[103] M. N. Sahinkaya, A. Abulrub, P. S. Keogh, and C. R. Burrows, *Multiple sliding and rolling contact dynamics for a flexible rotor/magnetic bearing system*, Mechatronics, IEEE/ASME Transactions on, 12 (2007), pp. 179–189.

[104] G. Schweitzer, *Safety and reliability aspects for active magnetic bearing applications-a survey*, P. I. Mech. Eng. I–J. Sys., 219 (2005), pp. 383–392.

[105] S. W. Shaw and P. J. Holmes, *A periodically forced impact oscillator with large dissipation*, Journal of Applied Mechanics, 50 (1983), pp. 849–857.

[106] ——, *A periodically forced piecewise linear oscillator*, Journal of Sound and Vibration, 90 (1983), pp. 129–155.

[107] D. J. W. Simpson, D. S. Kompala, and J. D. Meiss, *Discontinuity induced bifurcations in a model of saccharomyces cerevisiae*, Math. Biosci., 218 (2009), pp. 40–49.

[108] D. J. W. Simpson and J. D. Meiss, *Andronov–hopf bifurcations in planar, piecewise-smooth, continuous flows*, Phys. Lett. A, 371 (2007), pp. 213–220.

[109] A. Skeldon, *The fast-slow dynamics of sleep.* Private communication at the PANDA meeting Aug. 2013, A two day joint meeting with the London Dynamical Systems Group, University of Surrey, unpublished.

[110] W. J. Stronge, *Impact mechanics*, Cambridge University Press, 2004.

[111] G. Sun, A. B. Palazzolo, A. Provenza, and G. Montague, *Detailed ball bearing model for magnetic suspension auxiliary service*, J. Sound Vib., 269 (2004), pp. 933–963.

[112] L. P. Tessier, *The development of an auxiliary bearing landing system for a flexible AMB–supported hydrogen process compressor rotor*, 1997, pp. 120–128.

[113] J. M. T. Thompson and R. Ghaffari, *Chaotic dynamics of an impact oscillator*, Phys. Rev. A, 27 (1983), pp. 1741–1743.

[114] J. M. T. Thompson and H. B. Stewart, *Nonlinear Dynamics and Chaos*, Wiley, 2002.

[115] F. Tramontana and L. Gardini, *Border collision bifurcations in discontinuous one-dimensional linear-hyperbolic maps*, Communications in Nonlinear Science and Numerical Simulation, 16 (2011), pp. 1414 – 1423.

[116] F. Tramontana, L. Gardini, V. Avrutin, and M. Schanz, *Period adding in piecewise linear maps with two discontinuities*, International Journal of Bifurcation and Chaos, 22 (2012), p. 1250068 (30 pages).

[117] A. van der Schaft and H. Schumacher, *An introduction to hybrid dynamical systems*, vol. 251 of Lecture Notes in Control and Information Sciences, Springer-Verlag London, Ltd., London, 2000.

[118] G. C. Varley, G. R. Gradwell, and M. P. Hassell, *Insect population ecology: an analytical approach*, Univiversity of California Press, 1974.

[119] L. N. Virgin, W. T. Fielder, and R. H. Plaut, *Transient motion and overturning of a rocking block on a seesawing foundation*, Journal of Sound and Vibration, 191 (1996), pp. 177–187.

[120] L. N. Virgin and R. H. Plaut, *Some non-smooth dynamical systems in offshore mechanics*, in Vibro-Impact Dynamics of Ocean Systems and Related Problems, Springer, 2009, pp. 259–268.

[121] X. Wang and S. Noah, *Nonlinear dynamics of a magnetically supported rotor on safety auxiliary bearings*, ASME J. Vib. Acoust., 120 (1998), pp. 596–606.

[122] G. S. Whiston, *Impacting under harmonic excitation*, Journal of Sound and Vibration, 67 (1979), pp. 179 – 186.

[123] ——, *Global dynamics of a vibro-impacting linear oscillator*, Journal of Sound and Vibration, 118 (1987), pp. 395 – 424.

[124] T. Witelski, L. N. Virgin, and C. George, *A driven system of impacting pendulums: Experiments and simulations*, Journal of Sound and Vibration, 333 (2014), pp. 1734–1753.

[125] J. Xie, W. Ding, E. H. Dowell, and L. N. Virgin, *Hopf–flip bifurcation of high dimensional maps and application to vibro–impact systems*, Acta Mech. Sin., 21 (2005), pp. 402–410.

[126] G. Yuan, S. Banerjee, E. Ott, and J. A. Yorke, *Border-collision bifurcations in the buck converter*, IEEE Trans. Circuits Systems I Fund. Theory Appl., 45 (1998), pp. 707–716.